POLITECNICO
MILANO 1863

SCUOLA DI INGEGNERIA INDUSTRIALE
E DELL'INFORMAZIONE

# Manufacturing and characterization of fiber reinforced polymers with natural fibers and recyclable matrix

Tesi di Laurea Magistrale in
Materials Engineering and Nanotechnology - Ingegneria dei Materiali e delle Nanotecnologie

Author: **Francesco Pastormerlo**

Student ID: 249220
Advisor: Prof. Valter Carvelli
Co-advisors: Prof. Tatsuya Tanaka - Doshisha University, Kyoto, Japan
Academic Year: 2024-2025

# Abstract

This Master's thesis, carried out during the research period at Doshisha University (Kyoto, Japan), investigates the manufacturing and characterization of sustainable fiber reinforced thermoplastic composites based on natural fibers and recyclable matrices. The work focuses on polypropylene (PP) composites reinforced with pineapple leaf fibers (PF) and jute fibers (JF), also considering hybrid PF/JF systems, with the aim of supporting solutions for industrial applications. A systematic experimental campaign was performed on both virgin and recycled material streams to quantify the effect of reprocessing on microstructure and properties. The materials were characterized through physical and mechanical testing. Scanning electron microscopy on fracture surfaces was used to link mechanical trends to fiber dispersion, interfacial quality and void content, highlighting a marked reduction of porosity after recycling. Overall, the results show how processing affects the structure and properties of natural-fiber PP composites, and highlight the main benefits and limits of reprocessing.

**Keywords:** Polypropylene, pineapple and jute fibers, natural fiber reinforced composites, manufacturing, characterization, recycling.

# Abstract in lingua italiana

Questa tesi di laurea magistrale, svolta durante il periodo di ricerca presso la Doshisha University (Kyoto, Giappone), indaga la produzione e la caratterizzazione di compositi termoplastici sostenibili rinforzati con fibre naturali e matrici riciclabili. Il lavoro si concentra su compositi di polipropilene (PP) rinforzati con fibre di foglia di ananas (PF) e fibre di juta (JF), considerando anche sistemi ibridi PF/JF, con l'obiettivo di supportare soluzioni per applicazioni industriali. È stata condotta una campagna sperimentale sistematica sia su materiali vergini sia su materiali riciclati, per quantificare l'effetto del riprocessamento su microstruttura e proprietà. I materiali sono stati caratterizzati tramite prove fisiche e meccaniche. La microscopia elettronica a scansione (SEM) delle superfici di frattura è stata utilizzata per collegare gli andamenti meccanici a dispersione delle fibre, qualità dell'interfaccia e contenuto di vuoti, evidenziando una marcata riduzione della porosità dopo il riciclo. Nel complesso, i risultati mostrano come il processo influenzi struttura e proprietà dei compositi in PP con fibre naturali e mettono in evidenza i principali benefici e limiti del riciclo.

**Parole chiave:** Polipropilene, fibre di ananas e di juta, compositi rinforzati con fibre naturali, produzione, caratterizzazione, riciclo.

# Contents

# 1 | Introduction

## 1.1. Background and motivation

In recent years, the increasing demand for sustainable materials has led to a growing interest in fiber-reinforced polymers (FRPs) that incorporate natural fibers and recyclable matrices. Conventional FRPs, typically composed of synthetic fibers such as glass or carbon embedded in thermoset or thermoplastic polymers, offer excellent mechanical performance but pose significant environmental challenges due to their high embodied energy and limited recyclability [1, 2].

In response, research has intensified around more sustainable composite solutions, especially those combining natural fibers (e.g., flax, hemp, jute, pineapple leaf fiber) with recyclable thermoplastic or biodegradable polymer matrices. These materials can reduce the environmental impact of composites production while still meeting functional requirements for a wide range of applications, particularly in automotive and transportation, construction, and consumer goods [3, 4]. Recent polypropilene (PP)-based studies also confirm that natural reinforcements such as jute and pineapple leaf fiber can provide competitive tensile and flexural properties, with performance influenced by processing and microstructural quality [5].

Compared to synthetic FRPs, natural fiber-reinforced composites (NFRCs) offer key advantages including low density, low cost, reduced $CO_2$ emissions, renewability, and energy-efficient production [1]. However, they also present well-known challenges, such as variability in fiber properties, moisture sensitivity, and suboptimal interfacial bonding with polymer matrices, particularly when using hydrophobic thermoplastics [6, 7]. In PP systems, interfacial tailoring through compatibilization and formulation strategies is therefore critical, as widely documented for short jute fiber reinforced PP composites [8].

## 1.2. Research gap and objectives

Among thermoplastics, polypropylene (PP) is particularly attractive for scalable NFRC production due to its low density, cost-effectiveness, and compatibility with industrial processing routes such as extrusion and injection molding. From a circularity perspective, the use of recycled PP and/or the reprocessing of composites can further reduce environmental burden, but repeated processing may affect matrix integrity, fiber length and damage, and interfacial conditions, with consequent changes in mechanical performance [9, 10].

Within this framework, this thesis focuses on PP-based composites reinforced with pineapple leaf fibers (PF) and jute fibers (JF), including hybrid formulations. Hybridization means combination of two different reinforcements within the same matrix system, and it is a promising strategy to balance stiffness/strength and toughness by exploiting complementary fiber attributes [11].

Despite the extensive literature on NFRCs, direct comparisons across studies are often complicated by differences in fiber morphology and treatments, compounding strategies, compatibilizers, fiber length distributions, and specimen preparation. As a consequence, the literature on PP-based natural fiber systems still shows three main limitations:

- limited direct comparisons of PF, JF and PF/JF hybrids under identical processing and testing conditions;;
- incomplete understanding of how hybridization affects the balance between stiffness/strength and impact resistance;
- scarce evidence linking recycling to changes in mechanical properties, microstructure and moisture absorption behavior.

The overall aim of this thesis is to manufacture and characterize PP-based natural fiber composites reinforced with PF and JF, including hybrid formulations, and to quantify the effect of recycling by comparing virgin and recycled counterparts. Accordingly, the main research questions are:

1. How does increasing fiber content (e.g., 15 to 30 wt%) influence tensile, flexural, and impact properties for PF-, JF-, and hybrid-reinforced PP composites?
2. Do PF and JF exhibit distinct mechanical trends under identical processing and testing conditions, or are differences mainly driven by microstructural quality and process variability?

3. Does hybridization provide measurable benefits in terms of stiffness/strength versus toughness and dynamic fracture resistance?
4. What is the effect of recycling on composite performance, and which mechanisms are most likely responsible (e.g., matrix degradation, fiber damage/shortening, and/or changes in interfacial conditions)?

## 1.3. Scope and methodology

The scope of this thesis is limited to PP-based composites reinforced with PF and JF, produced by melt compounding using a twin-screw extruder, followed by injection molding. Mechanical characterization includes tensile, flexural, and impact testing, complemented by density measurements, water-uptake at different temperatures, and microstructural observations (SEM fracture surfaces). The study does not aim to provide a full life-cycle assessment (LCA) or an industrial process optimization; moreover, time-dependent such as creep, and high-frequency characterizations such as fatigue and dynamic mechanical analysis (DMA) are not included and are proposed as future work.

The experimental workflow can be summarized as:

1. selection and preparation of raw materials (PP matrix and natural fibers);
2. melt compounding by twin-screw extrusion to produce composite pellets;
3. injection molding of standardized specimens;
4. mechanical testing (tensile, flexural, impact) and physical characterization (density);
5. moisture uptake testing through water absorption at different temperatures;
6. microstructural analysis to support the interpretation of macroscopic properties.

## 1.4. Thesis outline

The remainder of this thesis is organized as follows. Chapter 2 summarizes the literature on NFRCs, highlighting PP matrices, interface engineering, hybridization concepts, mechanical response, and application areas. Chapter 3 describes the materials and manufacturing processes adopted. Chapter 4 details the experimental methods and testing standards. Chapter 5 presents and discusses the results, highlighting comparisons across formulations and the effect of recycling. Finally, Chapter 6 summarizes the main conclusions and proposes future research directions.

# 2 | Literature review

This chapter reviews the state of the art on natural fiber-reinforced composites (NFRCs). In particular, it summarizes the main classes of natural fibers and their key properties, the polymer matrices commonly adopted, the manufacturing routes for thermoplastic NFRCs (including twin-screw extrusion and injection molding) together with recycling and reprocessing aspects, surface treatment and compatibilization strategies to improve fiber–matrix adhesion, typical mechanical and durability trends, and representative applications across engineering sectors. This background provides the context for the experimental chapters, where pineapple leaf fiber (PF) and jute fiber (JF) reinforced PP systems, including hybrid and reprocessed variants, are investigated.

In composite materials, the structure typically consists of two main phases: the continuous phase and the dispersed phase. The continuous phase usually forms the matrix, which is responsible for transferring loads and providing the overall shape of the material, while the dispersed phase, often the reinforcing element, enhances the composite's mechanical behavior [1, 4]. In fiber-reinforced composites (FRCs), the fibers serve as the dispersed phase, imparting strength, stiffness, and other desired mechanical properties to the composite. The effectiveness of the composite largely depends on the interaction between the continuous matrix phase and the dispersed natural fibers, as well as the compatibility between these two phases. Proper fiber–matrix adhesion and dispersion are crucial for optimizing the performance of the resulting material [12].

## 2.1. Natural fibers

Natural fibers, particularly those derived from plants, have gained significant attention. They are light, renewable, biodegradable, low-cost, and have a significantly lower environmental impact than conventional fibers (e.g., glass or carbon) [12].

The basic structure of natural fibers consists primarily of cellulose, hemicellulose, lignin, and pectin. Cellulose provides rigidity and tensile strength, hemicellulose contributes to flexibility and moisture affinity, lignin acts as a structural binder enhancing stiffness

and microbial resistance, while pectin supports cell wall adhesion [11]. This biochemical composition gives plant fibers useful mechanical properties; nonetheless, it also presents challenges, especially in terms of moisture sensitivity and poor interfacial bonding with hydrophobic matrices [3, 6]. These fibers, often referred to as plant-based fibers, are typically sourced from various parts of the plant, including stems, leaves, seeds, and fruits [2].

A classification of common plant fibers includes [1]:

| | Examples | Source | Key characteristics |
|---|---|---|---|
| **Blast fibers** | Flax, hemp, jute | Outer stem (phloem) | High tensile strength and stiffness; suitable for structural applications |
| **Leaf fibers** | Sisal, abaca, pineapple | Vascular bundles in leaves | Coarse and durable; used in mats, ropes |
| **Seed/fruit fibers** | Coir, cotton | Seed surface or fruit husk | Soft, moisture-absorbent; used in insulation and cushioning |
| **Stalk fibers** | Wheat straw, rice straw | Stem residues | Agricultural by-products; low-cost reinforcement |
| **Grass fibers** | Bamboo, elephant grass | Entire plant/stalk | Fast-growing; good mechanical properties |
| **Wood fibers** | Softwood, hardwood | Wood pulp | Fine fibers used in WPC and panels |

Table 2.1: Classification of plant fibers.

Recent experimental studies report distinct mechanical behaviors of various fibers, which will be discussed later. Several plant-based fibers are commonly used in composite materials. Among the most widely investigated are flax, hemp, jute, sisal, kenaf, and bamboo, examples of which are visually presented in Figure 2.1:


Figure 2.1: Commonly used natural fibers [3]: (a) jute; (b) hemp; (c) sisal; (d) kenaf; (e) bamboo; (f) banana.

To provide a clearer understanding of their origins, properties, and typical applications, Table 2.2 summarizes the key characteristics of the most relevant plant-based fibers employed in NFRCs, including pineapple leaf fibers and jute fibers, which are introduced here and will be the reinforcement systems investigated in this thesis in the following experimental chapters.

| Fiber | Type | Key characteristics |
|---|---|---|
| **Flax** | Bast fiber | High cellulose, high strength/stiffness; automotive, construction [1, 2, 13] |
| **Hemp** | Bast fiber | High strength; good water resistance; glass-fiber-like; textiles, pulp/paper, medical [2, 14, 15] |
| **Jute** | Bast fiber | Low-cost, widely available; good tensile properties (low density); thermal/acoustic insulation; packaging, automotive interiors. Limits: moisture uptake and property variability → treatments for adhesion / lower water uptake [1, 2] |
| **Kenaf** | Bast fiber | Low density; balanced properties; eco-friendly/recyclable; competitive cost; automotive [2, 7] |
| **Ramie** | Bast fiber | High thermal conductivity; high tensile strength/specific modulus; costly processing/pretreatment [2] |
| **Sisal** | Leaf fiber | High tenacity; saltwater resistance; ropes/mats [1, 2] |
| **Pineapple** | Leaf fiber | High cellulose; excellent specific tensile properties (high strength/stiffness, low density); lightweight composites (automotive/structural). Limits: hydrophilic → treatments for better adhesion [1, 2, 16, 17] |
| **Oil palm** | Fruit fiber | Low cost/weight; good biocompatibility; low density; good strength (moderate-high cellulose) [2, 18] |
| **Coire** | Fruit fiber | Cheap, renewable, biodegradable; thick, coarse; highest elongation (microfibrillar angle 30°-45°); wear and water resistance; insulation [1, 2] |
| **Rice husk** | Grain husk | Abrasive; low bulk density; tough; weathering resistant; construction filler and composites (bricks, frames, decks, panels) [1] |
| **Sugar cane** | Grass fiber | Moderate strength (below flax/hemp); low-mid performance composites; cost-sensitive uses [19] |

Table 2.2: Key characteristics of plant fibers.

A critical limitation of plant fibers in composites is their intrinsic moisture sensitivity, which stems from the hydrophilic nature of lignocellulosic constituents. In particular, cel-

lulose and hemicellulose expose abundant hydroxyl groups that form hydrogen bonds with water, while the hierarchical microstructure (from cell wall to lumen) provides additional pathways and storage sites for moisture [1, 3, 20]. Cai et al. [20] distinguish two main moisture populations: bound water, which is strongly associated with polar sites within the cell wall, and free water, which is physically trapped within microvoids and lumens or transported through capillary pathways. During the early stages of exposure, moisture is mainly present as bound water and the fiber-matrix interface may remain largely intact; as exposure progresses, damage at the fiber, matrix, and interface level increases the fraction of free water and promotes faster uptake through newly formed pathways [20].

In composites, moisture transport is controlled not only by the fiber itself but also by microstructural features such as voids, incomplete wetting, and interfacial defects. Water can preferentially penetrate along the fiber-matrix interface and through void networks, accelerating ingress compared with the neat matrix [2, 20]. As fibers absorb water, cell-wall swelling can generate local stresses at the interface, potentially leading to interfacial debonding and microcrack formation; this, in turn, increases permeability and may degrade mechanical performance under service conditions [12, 20]. A representative experimental example is provided by Yildizhan et al. [21], who reported a maximum water absorption of about 5.98% for woven jute/epoxy composites, reaching equilibrium after approximately 120 h of water soaking; moisture exposure was associated with marked reductions in tensile and impact properties.

Hybridization can mitigate moisture uptake by reducing the effective exposure of the hydrophilic phase and limiting transport pathways. Massou et al. [22] showed that jute–carbon/epoxy hybrid laminates exhibit lower equilibrium moisture content than a laminate reinforced only with jute plies (four jute layers). In their results, the all-jute laminate reached 9.3% equilibrium moisture content, whereas the hybrid layups reached 6.55% and 5.69%, indicating improved hydrothermal resistance due to the hybrid architecture. Overall, these findings highlight that moisture behavior in NFRCs is a coupled outcome of fiber chemistry, hierarchical porosity, and interface integrity, and that both processing quality (void control, wetting) and design strategies (compatibilization and hybridization) are key to improving durability [1, 2, 20].

Accordingly, the experimental chapters of this thesis include water uptake tests at different temperatures to quantify moisture kinetics and equilibrium uptake, and to relate durability trends to the underlying microstructural and interfacial mechanisms discussed above.

## 2.2. Polymer matrix

The matrix material in natural fiber composites plays a crucial role in binding the fibers together and transferring stress between them. In sustainable composite development, increasing attention is paid to using recyclable or bio-based matrices alongside natural fibers [4, 12]. The choice of matrix significantly affects moisture resistance, thermal stability, mechanical integrity, and environmental impact. Good fiber-matrix compatibility is essential for optimal load transfer, which is often improved through chemical treatments or compatibilizers like maleated polypropylene (MAPP) [1, 7].

Based on their chemical structure and recyclability, polymer matrices commonly used in NFRCs can be broadly categorized into thermoplastics, thermosets, and bio-based polymers [2], each offering distinct advantages and limitations that will be discussed in the following sections:

- Thermoplastic matrices, such as polypropylene (PP), polyethylene (PE), polylactic acid (PLA), and polycarbonate (PC) are widely used. Among these, PP is the most common, valued for its low cost, easy processability, and recyclability, and it is also the thermoplastic matrix selected and used throughout this thesis. However, its non-biodegradable nature has driven interest toward PLA, a biodegradable polyester [7, 12, 23].
- Thermosets such as epoxy, unsaturated polyester (UP), and phenolic resins provide high thermal stability, chemical resistance, and dimensional accuracy. These properties make thermosets ideal for load-bearing and structural applications. However, their cross-linked molecular structure prevents melting and reshaping, limiting recyclability [4, 8]. Research is increasingly focusing on partially bio-based thermosets, such as epoxidized soybean oil and modified linseed oil, which attempt to merge structural performance with sustainability [12].
- Bio-based matrices are increasingly gaining attention due to their renewable origin and lower environmental impact. Polymers like polylactic acid (PLA), polyhydroxyalkanoates (PHA), and polybutylene succinate (PBS) are derived from biomass sources such as corn starch, sugarcane, or bacterial fermentation [4, 12]. These matrices are often biodegradable, allowing for end-of-life composting or safe environmental disposal. For example, jute fabric reinforced PLA exhibited better impact strength compared to PP-based composites due to higher matrix stiffness [24]. PLA has been widely used in NFRCs for its balance of stiffness and environmental performance, as well as for its good compatibility with various natural fibers. Its mi-

crostructural behavior when combined with different hemp fiber forms is illustrated in Figure 2.2, showing how the morphology of the reinforcing phase (e.g., pulp, shives, dust) affects dispersion and interfacial bonding. In contrast, PHA offers excellent biodegradability, making it suitable for packaging and agricultural films. PBS shows higher toughness and thermal stability than PLA, and when combined with fibers like jute or coir, it enables the production of fully bio-based composites with enhanced mechanical behavior [1, 2]. The main challenge remains the cost and industrial scalability of these polymers, although advancements in fermentation and compounding technologies are making them increasingly viable for commercial use.

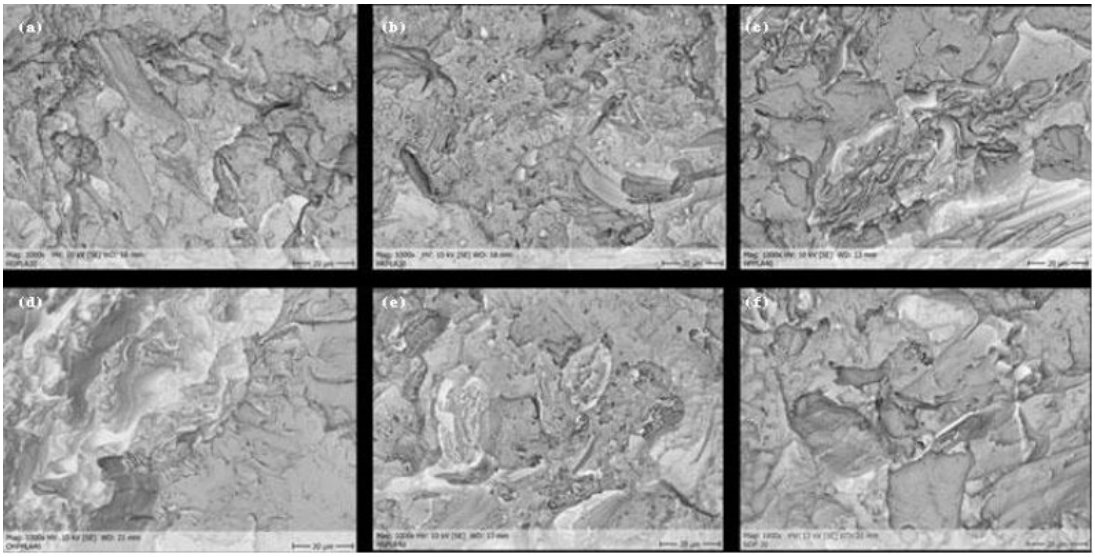


Figure 2.2: SEM pictures of injection molded PLA-composites [14]: (a) Jute; (b) hemp; (c) sisal; (d) kenaf; (e) bamboo; (f) banana

Thus, selecting appropriate fiber–matrix combinations is important to achieving high-performance and sustainable composite materials.

## 2.3. Fiber surface treatments techniques and mechanisms

Although no fiber surface treatments were applied in this thesis, this overview is included to clarify why such modifications are widely employed in NFRCs and how they influence interfacial phenomena and composite performance. Surface treatments are generally classified as chemical (e.g., alkali, silane, MAPP, enzymatic, acetylation) or physical (e.g., plasma, corona). Across these approaches, the key objective is to mitigate the intrinsic incompatibility between hydrophilic lignocellulosic fibers and typically hydrophobic

polymer matrices. More specifically, treatments may (i) remove weak boundary layers and impurities (waxes, pectin, hemicellulose, lignin), (ii) increase surface roughness and promote fibrillation to enhance mechanical interlocking, (iii) expose cellulose and create a more reactive surface, and/or (iv) introduce functional groups or compatibilizing bridges that strengthen the interphase and reduce moisture sensitivity [23, 24]. Because fiber composition and morphology vary significantly with species, extraction method, and batch, treatment efficiency is strongly dependent on fiber type, matrix chemistry, processing route, and the selected parameters (concentration, time, temperature, curing). Therefore, careful optimization is required to avoid fiber damage or incomplete modification and to maximize the property gains [23, 24].

- **Alkali (NaOH).** Alkali treatment remains one of the most common chemical modifications for natural fibers. Its main action is the partial removal of amorphous constituents (hemicellulose, lignin, pectin) and surface impurities, which exposes a cleaner surface rich in cellulose and often induces fibrillation (splitting of bundles into finer filaments) [1, 2, 12]. These effects typically increase roughness and effective surface area, improving stress transfer across the interface. As a result, improved tensile and flexural properties are frequently reported for bast fibers such as jute, flax, hemp, and kenaf in thermoplastic matrices, including PP [3, 4]. At the same time, alkali treatment is highly sensitive to processing conditions: excessive concentration or exposure can attack cellulose and reduce intrinsic fiber strength, leading to diminished composite performance [1]. For this reason, the literature commonly emphasizes using moderate NaOH levels with controlled time and temperature [1, 2].

- **Silane.** Silane coupling agents are designed to form a molecular bridge between the fiber surface and the polymer/resin. They can react with hydroxyl groups on cellulose while also interacting with the matrix, increasing chemical compatibility and interfacial load transfer [1, 12]. A key benefit frequently reported is reduced hydrophilicity, which contributes to lower water absorption and improved dimensional stability, especially relevant for long-term durability [2]. Silanes are widely applied to thermosetting matrices (epoxy, polyester) and some biodegradable polymers, where covalent linkage or strong interfacial interactions can be established [3]. In polyolefin systems such as PP, silanes may still be beneficial, but reviews often indicate that their effectiveness is matrix-dependent and that alternative compatibilization is typically preferred for maximizing adhesion in PP-based NFRCs [1, 2].

- **MAPP (MA-g-PP).** Maleic anhydride-grafted polypropylene (MAPP, MA-g-PP) is one of the most effective compatibilizers for natural fiber/PP composites. It enhances fiber wetting and dispersion during processing and promotes the forma-

tion of a stronger interphase, commonly attributed to interactions between maleic groups and fiber hydroxyls, while remaining fully compatible with the PP matrix [1, 2, 12]. As discussed in the literature, the quality of this interphase is critical for load transfer and for limiting interfacial defects [2, 12]. Reviews also highlight that combining fiber cleaning/roughening (e.g., NaOH) with MAPP can be particularly effective, as the former improves surface accessibility while the latter provides chemical/compatibilizing linkage [23]. Experimental evidence supports this synergistic approach: for example, strength improvements have been reported when fibers treated with alkali are subsequently compatibilized with MA-g-PP [18]. Additional studies further quantify the benefits, showing consistent increases in tensile strength and modulus for MA-g-PP compatibilized systems compared with untreated systems or systems treated only with alkali [25].

- **Enzymatic.** Enzymatic treatments are increasingly discussed as a selective and environmentally friendlier alternative to conventional chemical methods. Operating under mild conditions, enzymes can target non-cellulosic constituents (hemicellulose, pectin, and partly lignin) while preserving the cellulose backbone, thereby reducing the risk of fiber degradation [12]. The resulting surface cleaning and microstructural changes may increase porosity and surface area, improving fiber dispersion and mechanical interlocking, while also helping to reduce void formation [2, 4]. Beyond property enhancement, a recurrent theme in reviews is that enzymatic approaches may improve reproducibility and align with greener processing routes, which is valuable for upscaling NFRC manufacturing [2]. Specific enzymatic protocols have been reported to produce refined flax fibers with improved flexural performance, suggesting that enzymatic modification can be not only cleaner but also technically effective [25].

- **Acetylation.** Acetylation is primarily used to reduce moisture sensitivity by decreasing the concentration of free hydroxyl groups on the fiber surface. By introducing more hydrophobic acetyl groups, this treatment improves compatibility with nonpolar matrices (including PP) and generally leads to reduced water uptake and improved dimensional stability in humid environments [1, 12]. In addition to improved moisture resistance, acetylation is often discussed in relation to durability, since limiting accessible hydroxyl sites may also reduce susceptibility to hydrolytic or microbial attack, depending on the application conditions [2].

- **Plasma / corona.** Physical activation methods such as plasma and corona discharge modify only the outer fiber surface, increasing surface energy and introducing functional groups containing oxygen that promote improved wettability and adhe-

sion [2, 12]. Their main advantage is the absence of liquid chemical reagents, which reduces environmental burden and avoids bulk fiber alteration. Reviews note that these techniques can be particularly attractive when chemical treatments are undesirable and can also be combined with compatibilizers to further enhance interfacial strength [1, 2].

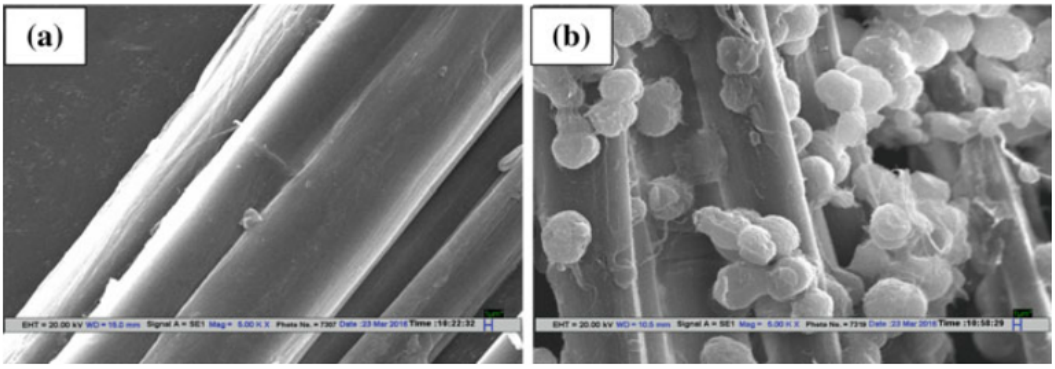


Figure 2.3: SEM images [23]: (a) untreated flax fibers; (b) MAgPP treated flax fibers.

SEM observations provide additional insight into the microstructural mechanisms behind the property changes discussed above and offer a key means to assess fiber–matrix adhesion quality. The SEM images reported in Figures 2.4 and 2.5 [23] clearly illustrate these effects. Figure 2.4 (untreated flax yarn composite) shows widespread fiber pull-out and poor matrix wetting, which are typical signatures of weak interfacial adhesion and are consistent with the lower mechanical performance generally observed in untreated systems. Conversely, Figure 2.5 (MAgPP-treated flax yarn composite) shows a markedly improved interface, with reduced/absent pull-out and cleaner fracture surfaces, indicating more efficient stress transfer through the interphase. Overall, these observations highlight the combined role of surface treatment and fiber architecture in controlling the effective interphase and the resulting composite performance.

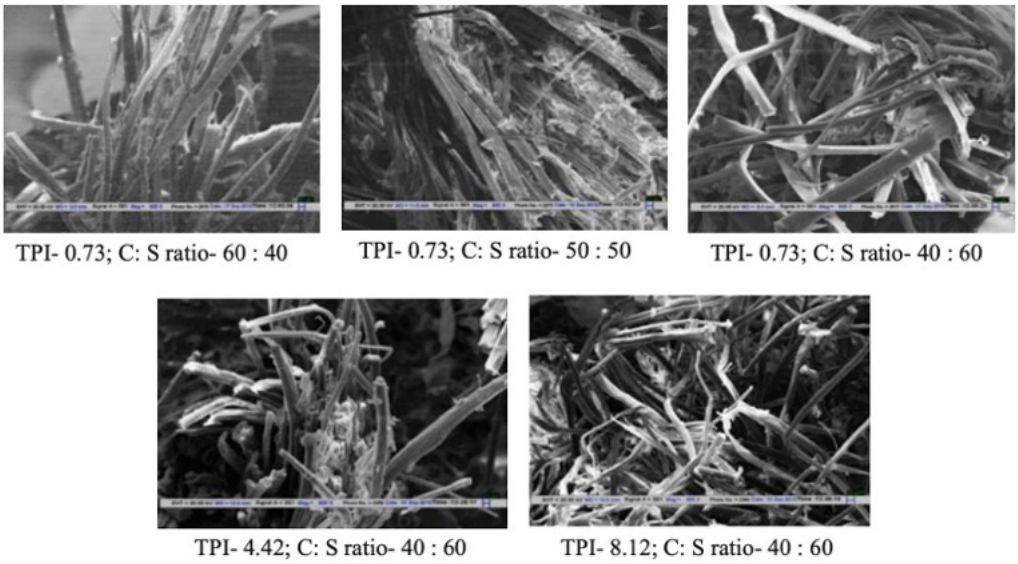


Figure 2.4: SEM images of untreated flax core-based hybrid yarn reinforced, tensile fracture composites ends [23].

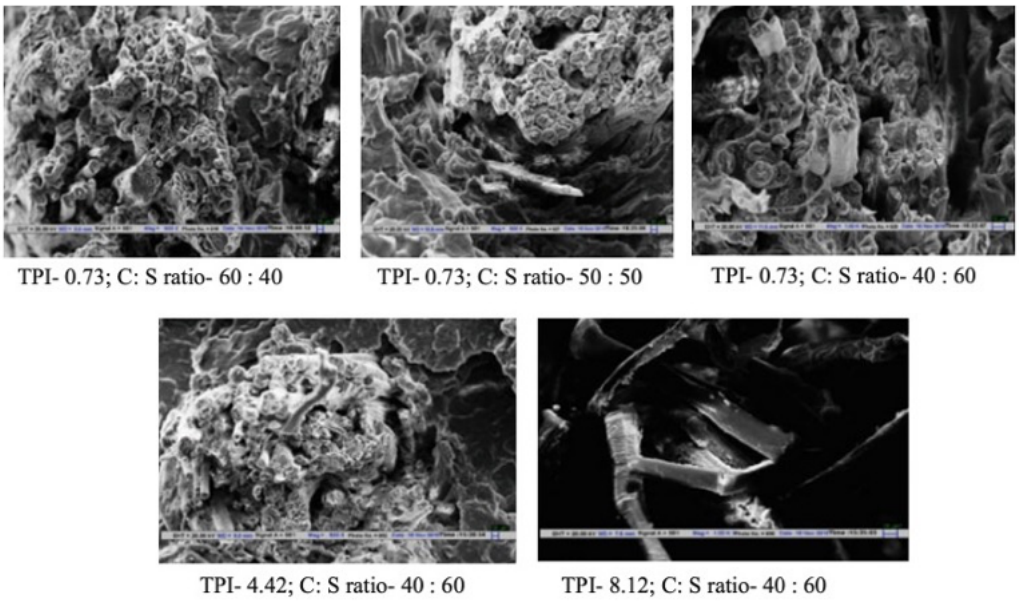


Figure 2.5: SEM images of MAgPP treated flax core-based hybrid yarn reinforced, tensile fracture composites ends [23].

## 2.4. Manufacturing processes

The manufacturing method chosen for NFRCs plays a crucial role in determining fiber dispersion, interfacial bonding, void content, and overall mechanical performance. Natural

fibers introduce specific challenges, such as variability, thermal sensitivity, and moisture absorption, that influence processing decisions and require careful control to avoid degradation or inconsistencies. In addition, for thermoplastic NFRCs, the ability to recycle and reprocess the material is a key practical aspect, since each additional processing cycle may alter fiber morphology and interface quality, thus affecting performance [1–4]. In this thesis, twin-screw extrusion (for compounding) and injection molding (for specimen production) are adopted. Manufacturing stability is particularly critical when scaling up production. Khanlou et al. (2018) [26] demonstrated that time-dependent temperature fluctuations during curing can significantly affect the mechanical consistency of natural fiber composites, especially in compression molding and resin transfer molding (RTM) processes. Their findings highlight the need for tight thermal control and process standardization to ensure uniform quality and repeatable performance in NFRC components.

The main manufacturing techniques adopted for NFRCs are briefly outlined below; each route imposes specific processing conditions that directly affect fiber dispersion, fiber attrition, void content, and interfacial quality.

- **Twin-screw extrusion - used in this thesis.** Twin-screw extrusion is a reference route for thermoplastic NFRC compounding because it enables controlled distributive/dispersive mixing and continuous production of compounded pellets for downstream shaping [1, 3, 4]. For natural fibers, process settings must balance dispersion against fiber length reduction (attrition under shear) and thermal degradation: screw configuration (kneading intensity), screw speed, residence time, and the temperature profile govern this balance [2–4]. Practical strategies frequently reported include careful temperature control (to limit fiber damage), drying/handling to mitigate defects realted to moisture, and the use of compatibilizers (e.g., MAPP in PP systems) to strengthen the interphase after compounding [1–3]. Mann et al. (2020) [3] describe multiple NF/thermoplastic systems processed via twin-screw extruders, highlighting the suitability of this route for scalable compounding and property improvements when mixing and interface are properly managed.
- **Injection molding - used in this thesis.** Injection molding is ideal for high-volume manufacturing and complex geometries, and it is widely used to produce standardized test specimens from compounded pellets [1, 4, 7]. Since the high shear fields in the screw and gate region can further shorten fibers, NFRC injection molding typically relies on short fibers and optimized processing parameters to preserve reinforcement efficiency while ensuring good filling and surface quality [1, 4]. In PP-based NFRCs, compatibilization is particularly important: Zampaloni et al. (2007) [7] emphasized the role of MAPP in improving dispersion/adhesion and, con-

sequently, mechanical consistency in injection-molded kenaf/PP systems. Overall, injection molding produces a characteristic orientation state, so mechanical response reflects not only material formulation but also the fiber alignment generated during mold filling [1, 2, 4].

- **Compression molding.** A common method for panels and mildly contoured parts: a fiber–polymer charge is pressed in a heated mold, generally enabling good wetting and limiting fiber damage associated with high shear. [2, 4]. Faruk et al. (2012) [4] reported successful flax/PP and kenaf/PP implementations, often in combination with fiber treatments/compatibilization to improve the interface.
- **Thermoforming.** Thermoforming shapes pre-consolidated thermoplastic sheets, making it attractive for lightweight automotive interior parts and packaging where short cycle times are needed [1, 3, 7].
- **Hand lay-up and RTM.** Hand lay-up is flexible for low-volume parts, while RTM improves impregnation and surface finish through closed-mold control [2]. Dev et al. (2023) [2] report improved properties in jute-epoxy RTM composites when interfacial treatments are adopted.
- **Other techniques.** VARTM, pultrusion, and filament winding are also used depending on geometry and production needs: VARTM can reduce voids in closed-mold parts; pultrusion is efficient for constant cross-section profiles; filament winding enables controlled orientation in tubular components [3, 4, 11].

While detailed performance metrics for each processing method may vary, consensus across the literature confirms that process choice, fiber conditioning, and compatibilizer selection are key to optimizing natural fiber composite properties and ensuring reproducibility across batches [2–4]. To visually summarize the main NFRC manufacturing techniques discussed, Figure 2.6 provides a schematic representation of the most widely used processes:

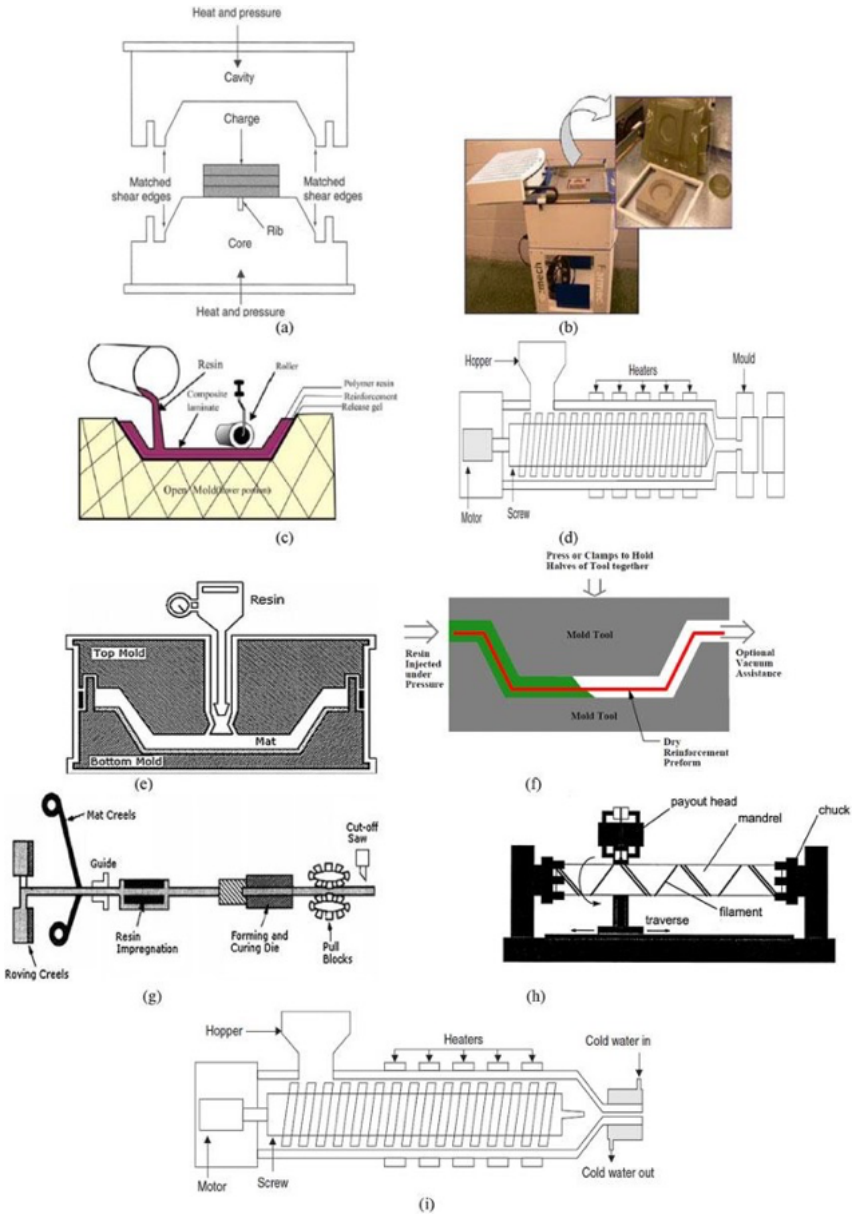


Figure 2.6: Manufacturing processes [3]: (a) compression molding; (b) thermoforming process; (c) hand layup process; (d) injection molding process; (e) resin transfer process; (f) vacuum-assisted resin transfer process; (g) pultrusion process; (h) filament winding; (i) extrusion process.

Building on the manufacturing routes outlined above, an additional key aspect for thermoplastic NFRCs is their recyclability: repeated reprocessing (e.g., re-extrusion and re-injection molding) can alter fiber morphology and interfacial quality, with direct consequences on mechanical performance, and is therefore specifically investigated in this thesis [1, 2]. A key advantage of thermoplastic matrices (such as PP) is their inherent reprocessability, enabling mainly mechanical recycling routes based on size reduction

(grinding/shredding), pelletizing (regranulation), and remelting followed by reshaping (e.g., re-extrusion and re-injection molding) [1–3, 27].

Several reprocessing strategies are reported for thermoplastic NFRCs, each with specific advantages and limitations:

- **Direct remelting and re-molding** (e.g., re-injection of reground parts). Industrially attractive due to simplicity and scalability [27]; however, high shear during plasticization and at the gate can accelerate fiber attrition (reduced effective aspect ratio), often lowering reinforcement efficiency, especially for stiffness and strength [1, 4].
- **Re-extrusion/compounding followed by molding**. A twin-screw step can improve homogenization and enables the addition of make-up material (virgin PP, fresh fibers, stabilizers, and/or compatibilizer) to restore processability and partially recover properties. The drawback is that the additional melt/shear history may amplify fiber damage and thermal oxidation if temperature control and residence time are not carefully managed [2, 3].
- **Blending / downcycling**. Mixing recycled NFRC pellets with virgin polymer (and, if needed, fresh fibers) can stabilize processing and properties, improving consistency and reducing variability, but it dilutes recycled content and may introduce compatibility constraints [28, 29].

More generally, additive packages (antioxidants/thermal stabilizers and coupling agents) are often suggested to mitigate degradation, while the literature also highlights that such mitigation strategies may have practical limitations related to degradation and incompatibility [1, 29].

Overall, multiple processing cycles can modify the reinforcement efficiency and the interphase: repeated shear and thermal histories may promote fiber shortening and damage, changes in fiber dispersion/orientation, and interfacial degradation (or, depending on formulation, partial re-wetting and consolidation effects) [1, 2, 4]. In PP-based NFRCs, compatibilizers such as MA-g-PP (MAPP) are frequently reported as beneficial not only for initial processing but also for maintaining more consistent interfacial stress transfer upon reprocessing, by improving wetting and limiting interfacial defects [1, 3]. Overall, the literature indicates that the recycling response should be assessed under well controlled processing conditions, linking property changes to microstructural evolution across reprocessing steps [2, 12].

## 2.5. Mechanical behavior of NFRCs

Natural fiber-reinforced composites have attracted considerable research interest due to their favorable mechanical properties, biodegradability, and low environmental impact. However, their performance varies widely depending on the type of fiber used, fiber treatment, matrix compatibility, and processing method. In particular, the structural characterization of cellulose nanofibrils (CNFs) has emerged as a key factor in optimizing reinforcement performance in nano-engineered green composites. Onyianta et al. (2018) [30] proposed a method based on sedimentation to estimate the aspect ratio of charged CNFs, providing a valuable tool for correlating morphological features with mechanical properties. This characterization enhances the ability to design tailored nanocomposites with improved interfacial interactions and load transfer efficiency. In addition, Poilâne et al. (2018) [31] highlighted the nonlinear tensile behavior of unidirectional plant fiber composites, showing that traditional linear elastic models may underestimate their actual mechanical response. This underscores the need for advanced simulation strategies and refined testing protocols that can account for rate effects and strain dependent responses, especially for structural or fatigue critical NFRC components. This section offers a deeper discussion of mechanical performance across different fiber types and NFRC systems.

- **Tensile strength and modulus.** Tensile properties of NFRCs strongly depend on interfacial quality, which is often improved via surface treatments (e.g., alkali/silane) or compatibilizers (e.g., MAPP in PP systems) [1, 2, 4]. For reference, Table 2.3 reports single-fiber tensile strength and Young's modulus values gathered from the literature. Flax typically exhibits high tensile strength (800-1500 MPa) and modulus (60-80 GPa), while hemp shows broader scatter (270-900 MPa; 23.5-90 GPa) due to variability in extraction and processing [6]. Jute remains attractive for cost-driven applications, with tensile strength around 393-800 MPa and modulus in the 10-30 GPa range [6]. Abaca reaches comparatively high strengths (about 500-764 MPa) with modulus commonly reported between 6.5 and 30 GPa [6]. Pineapple leaf fibers (PALF) also show wide literature ranges (150-1627 MPa; 11-82 GPa) [11]. In composites, these intrinsic fiber properties contribute to the overall mechanical response, which is also strongly influenced by interface quality and processing; for example, hemp pulp reinforced PLA composites showed the highest tensile strength among hemp fractions due to improved dispersion and stress transfer [14]. Placet et al. (2018) [15] further showed that retting/decortication quality strongly affects hemp fiber strength, and moderate twisting can slightly increase yarn strength. Finally, processing conditions remain critical: Vila et al. (2018) observed limited tensile

gains when dispersion was insufficient, whereas Dantas et al. (2018) highlighted property losses at excessive consolidation times due to fiber degradation, defining the need for optimized processing windows [18, 19].

| | Tensile Strength (MPa) | Young's Modulus (GPa) | Source |
|---|---|---|---|
| **Flax** | 800-1500 | 60-80 | [6] |
| **Hemp** | 270-900 | 23.5-90 | [6] |
| **Jute** | 393-800 | 10-30 | [6] |
| **Kenaf** | 223 | 14.5 | [6] |
| **Coir** | 95-220 | 2.8-6 | [6] |
| **Abaca** | 500-764 | 6.5-30 | [6] |
| **Pineapple** | 150-1627 | 11-82 | [11] |

Table 2.3: Mechanical properties of natural fibers single-fiber values.

- **Flexural strength.** Flexural strength is a key indicator of a composite's resistance to bending loads and depends strongly on fiber type, fiber content and architecture, dispersion, and especially the quality of the fiber-matrix interface. In PP-based NFRCs, compatibilizers such as MA-g-PP (MAPP) can enhance flexural performance by improving wetting and stress transfer at the interface, whereas alkaline and silane treatments may similarly increase bending strength by cleaning/activating the fiber surface and promoting adhesion [18, 19, 23]. Nanoscale and chemical interface engineering can further boost bending response: for instance, nanocellulose-coated jute/green epoxy composites showed a flexural strength increase from 32.94 MPa to 48.66 MPa (about +47%), attributed to improved interfacial adhesion and stiffness [32]. In jute fabric/PP laminates, the use of PP-g-MA led to a peak flexural strength around 52 MPa at 40% fiber content, while higher loadings caused a drop due to void formation and poorer consolidation [24]. Other natural fabric systems (e.g., manicaria saccifera with PLA) achieved moderate flexural strength (32.7 MPa) while maintaining good impact absorption, indicating a balance between stiffness and energy dissipation [33]. Conversely, raffia fiber reinforced geopolymers exhibited much lower flexural strength (about 3.05 MPa) but remain adequate for non-structural building applications [34]. Overall, these results emphasize that flexural performance in NFRCs is primarily controlled by processing quality (void content, impregnation, dispersion) and interfacial design, rather than being an intrinsic property of the fiber alone [2, 19].

- **Impact strength.** Impact resistance in natural fiber-reinforced composites is largely controlled by interfacial bonding, fiber morphology, and the energy dissipation mechanisms activated during crack growth. Coir-based composites often show high impact absorption despite modest fiber tensile strength, mainly due to coir's high lignin content and intrinsic compliance, which promote progressive failure and fiber pull-out [23]. Banana fibers can also improve toughness, especially in hybrid systems and when longer fibers are retained, increasing crack-bridging and pull-out work [4]. Interface engineering is therefore crucial: treatments and compatibilizers can enhance impact response by improving wetting and stress transfer while limiting premature debonding [23]. Matrix choice also matters; for instance, jute-fabric laminates with PLA were reported to outperform PP-based counterparts in impact, consistent with different matrix stiffness and failure behavior [24]. Hemp/PLA systems further highlight the role of fiber form: hemp pulp increased impact strength relative to neat PLA, whereas coarser untreated fibers reduced it, stressing the importance of dispersion and interface quality [14]. Hybridization strategies can be particularly effective under dynamic loads: combining natural and glass fiber plies improved resistance to impulsive loading [35], while manicaria saccifera fabric/PLA biocomposites showed strong energy absorption under ballistic impact [33]. Overall, impact performance should be treated as an overall composite property governed by fiber architecture, matrix selection, processing quality, and interfacial design [4, 23].
- **Fracture toughness and crack propagation.** Crack growth resistance in NFRCs is mainly governed by fiber-matrix adhesion, fiber architecture, and the activation of energy-dissipation mechanisms such as debonding, pull-out, and crack deflection. Surface treatments (e.g., alkali, silane) and improved compatibilization can strengthen the interphase, reducing premature interfacial debonding and delaying crack initiation [1, 19]. Hybrid reinforcements (e.g., jute-bamboo systems) may further slow crack propagation through synergistic mechanisms compared with single-fiber composites [12]. Microstructural observations consistently link higher toughness to better interface quality and more uniform fiber distribution: SEM studies report that interfacial voids and poor wetting act as crack starters, whereas improved matrix penetration and adhesion reduce failure zones and limit matrix cracking [18, 23]. In nanocellulose-coated jute/green epoxy composites, the fracture toughness $K_{IC}$ increased from 2.64 to 3.49 MPa·m$^{1/2}$, with a shift toward more ductile fracture and clear evidence of crack deflection and fiber pull-out [32]. For natural-fabric PLA laminates (manicaria saccifera), postmortem analyses identified interlaminar delamination and fiber rupture as dominant damage modes under

high-energy fracture [33]. Overall, improving interfacial bonding while maintaining controlled pull-out and avoiding voids is key to enhancing toughness and mitigating brittle crack propagation in NFRCs [1, 23].

## 2.6. Hybrid composites

Hybrid composites combine two or more types of fibers within a single matrix system to optimize the balance of mechanical, thermal, and environmental performance. In natural fiber-reinforced composites (NFRCs), hybridization is used both to integrate different natural fibers (e.g., jute-banana, flax-hemp) and to blend natural with synthetic fibers (e.g., jute-glass, flax-basalt). This strategy allows the limitations of one fiber (e.g., low stiffness, moisture sensitivity, or limited fatigue resistance) to be mitigated by the complementary response of a second reinforcement. In this thesis, the hybridization of two natural fibers, pineapple leaf fiber (PF) and jute fiber (JF), is specifically investigated in the experimental chapters, with the aim of assessing their combined effect on processing behavior and composite performance. Although PF-JF hybrid systems are less frequently reported in the open literature compared to more established pairings, both reinforcements have been extensively studied in polypropylene-based NFRCs, either individually or in comparative studies, providing a solid reference background for the present investigation [4, 5, 17, 36].

For instance, Faruk et al. (2012) [4] reported that hybrid NFRCs such as jute-banana can outperform monofiber systems because the two reinforcements play complementary roles: banana fibers contribute higher impact absorption and toughness, whereas jute provides higher tensile strength and stiffness. The combined effect is a more balanced composite response and potentially improved damage tolerance. Zampaloni et al. (2007) [7] likewise discussed the use of natural-fiber hybrids in polypropylene for lightweight applications, noting improvements in overall processability and structural performance.

Mechanistically, hybridization benefits are generally attributed to improved stress redistribution between the reinforcements, enhanced crack bridging, and a reduction of unstable fiber pull-out, which together delay failure initiation and slow crack propagation. These effects become more pronounced when the interface is engineered to improve wetting and load transfer, for instance through coupling agents such as MA-g-PP (MAPP) or silane treatments [1]. Extending this concept, Rana et al. (2018) [37] proposed a multi-scale approach by adding microcrystalline cellulose (MCC) alongside natural fibers to increase stiffness and improve dispersion, reducing agglomeration and improving load transfer.

Natural-synthetic hybrids (e.g., flax-glass, jute-glass, flax-basalt) are often adopted when higher structural performance is required than what fully natural systems can deliver.

In layered laminates, the synthetic plies are commonly placed on the outer skins, where bending stresses are highest, so they carry most of the load and provide high stiffness and strength; the natural-fiber plies can be placed closer to the mid-plane to reduce weight and cost while contributing damping and energy absorption [35]. This stacking strategy can delay failure initiation, improve impact tolerance and resistance to impulsive loads, and promote a more gradual damage progression compared with purely natural laminates [35]. Beyond impact, natural-synthetic hybrids can also improve long-term stability in demanding environments: synthetic reinforcements reduce sensitivity to moisture-driven property losses and creep, while natural fibers help keep density and environmental footprint lower [2, 12]. In practice, the benefits depend strongly on interface quality and design choices (fiber sizing/coupling agents, ply sequence, fiber volume fraction, and processing), since poor adhesion or high void content can suppress the expected hybrid effect [2, 12].

## 2.7. Applications in engineering sectors

Natural fiber composites are increasingly being adopted across various engineering sectors, driven by sustainability imperatives and the improved mechanical performance made possible through fiber hybridization, surface treatments, and matrix optimization.

- **Automotive sector.** NFRCs are widely used in vehicle components such as door panels (Figure 2.7), trunk liners, dashboards, and roof modules. Materials such as jute-polypropylene (PP), kenaf-polylactic acid (PLA), and flax-epoxy have been adopted for their low weight, good impact resistance, and renewable origin [4]. Jute is among the most established reinforcements for interior trim parts; for example, Mercedes introduced jute-based door panels already in the 1990s [3]. Prestigious manufacturers including Audi, BMW, and Mercedes-Benz have implemented natural fiber-reinforced parts. Notably, the Mercedes E-Class (1996) used jute-epoxy panels, the BMW i3 employs hemp fibers in door panels, and the Mercedes S-Class increased renewable content by 73% by adopting natural fiber-reinforced plastics, resulting in a weight reduction of up to 43 kg per vehicle [1]. This is supported by Mann et al. (2020) [3], who report widespread use of flax-, hemp-, and jute-based composites in interior automotive components across manufacturers such as BMW, Renault, Ford, and Volkswagen. Furthermore, Chandgude et al. (2021) [11] highlight structural applications of hybrid jute/PP composites in bumpers and dashboard panels, with mechanical gains up to 14% in tensile strength and 11% in flexural strength compared to untreated systems. In addition to bast fibers, leaf

fibers such as pineapple leaf fiber (PALF) have been investigated as lightweight reinforcements for polymer composites; due to its high cellulose content and high specific properties, PALF is often discussed as a candidate for automotive components and lightweight panels [16].

Figure 2.7: Automotive sector [23]: composite door panel of S-Class Mercedes-Benz.

- **Construction applications.** In the construction sector, NFRCs are used in wall panels, insulation materials, and geopolymer-based formworks. Flax, cotton, coir, and raffia fibers embedded in fly ash-based geopolymers exhibit thermal stability up to 400 °C and durability in alkaline conditions. These composites contribute to fire resistance, structural stability, and environmental performance, making them attractive for semi-structural and thermal insulation applications [34]. In addition to geopolymer applications, hemp-clay and hemp-lime composites have been explored as alternative building materials in both temperate and humid climates [38]. Beyond these systems, PALF is also commonly cited among candidate plant fibers for building and construction materials thanks to its high specific stiffness and strength [16]. Montacchini et al. (2018) [39] explored industrial hemp for modular rural housing in Colombia, emphasizing its environmental and socio-economic potential. As illustrated in Figure 2.8, their system highlighted hemp's carbon sequestration, affordability, and suitability for decentralized local production, reducing dependence on conventional building materials with a high environmental footprint [39].

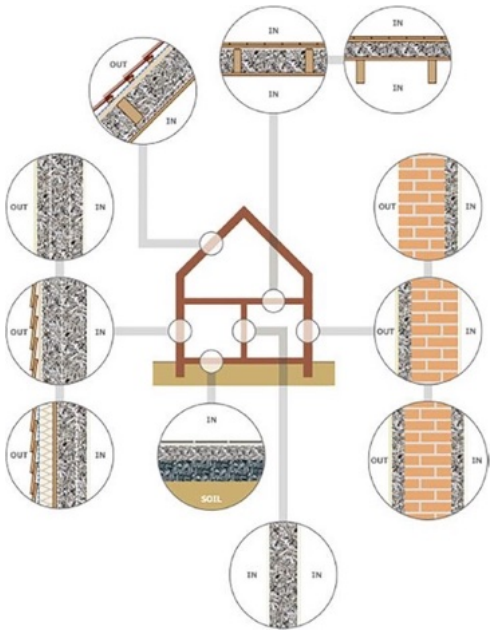


Figure 2.8: Construction sector [39]: use of hemp and lime bio-composites in buildings.

- **Marine and aerospace.** Natural fibers are also finding emerging applications in marine and aerospace sectors where lightweight design and damping are key. For instance, flax/epoxy composites have been used to construct canoes and kayaks with performance approaching that of fiberglass [1]. Similarly, in the aerospace sector, Figure 2.9 illustrates examples of components where natural fibers, such as flax, have been successfully integrated showcasing their potential in reducing weight while providing adequate mechanical and dielectric properties [2].

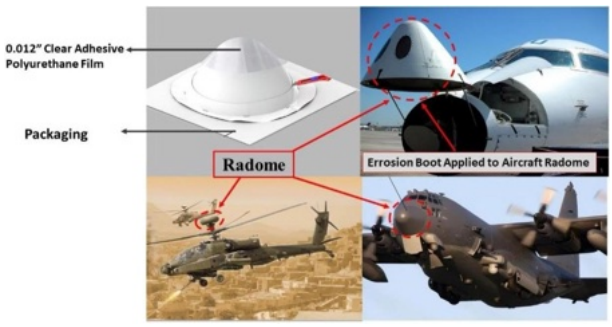


Figure 2.9: Aerospace sector [2]: applications of natural fibers in an aircraft (Radome).

- **Consumer goods and packaging.** In the packaging sector (Figure 2.10) and in consumer goods, natural fibers such as coir, sisal, and banana are incorporated into compostable bioplastics like PLA to produce items such as trays, cartons, rigid food containers, as well as everyday products (e.g., phone cases, small housings,

disposable utensils, and household accessories) [2]. More generally, adding natural fibers to PLA can enable food grade biodegradable packaging with improved mechanical strength and thermal behavior [3]. Jute is also widely used in high-volume, short-life products beyond composites (e.g., wrapping and packaging textiles), which supports its strong industrial availability and supply chain maturity for composite applications [2]. PALF has been widely discussed as a promising reinforcement for lightweight consumer panels and semi-structural products due to its high specific properties [16].


Figure 2.10: Packaging sector [2]: Packaging made with coconut fiber by Enkev manufacturer.

- **Biomedical applications.** Natural fiber composites are also being investigated for biomedical applications such as scaffolds (Figure 2.11), prosthetic components, and drug delivery systems, owing to their biocompatibility, biodegradability, and structural tunability [3].

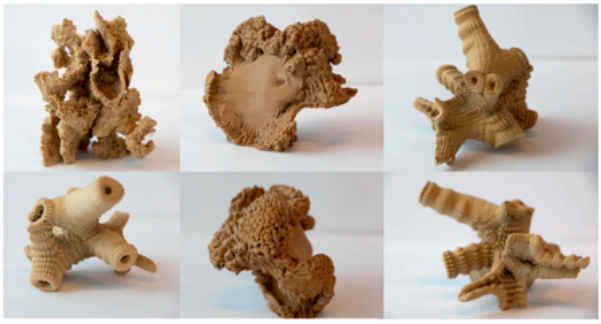

Figure 2.11: Biomedical applications [40]: scaffold for tissue engineering.

- **Functional applications and electrical sector.** Recent research has expanded the scope of NFRCs beyond structural and mechanical functions, exploring their potential for functional applications such as electrical conductivity and electromagnetic interference (EMI) shielding [41].

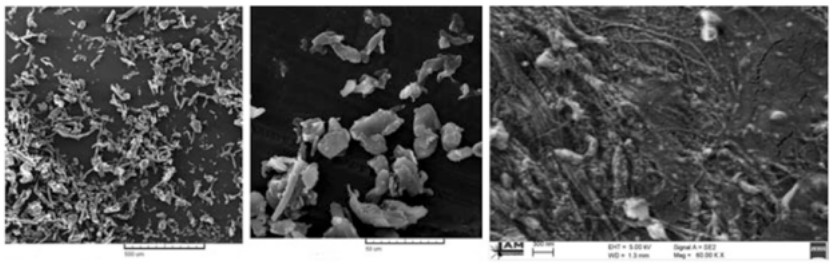


Figure 2.12: Electrical conductivity [41]: microstructure of activated carbon nanoparticles after milling (a) one hour, (b) two hours, (c) three hours.

# 3 | Materials and manufacturing

## 3.1. Materials

This chapter describes the materials selected and the manufacturing routes adopted to produce the composite specimens investigated in this work. First, the constituent raw materials are introduced, including the natural fiber reinforcements (pineapple and jute fibers) and the polypropylene matrix, together with their main characteristics relevant to processing. The second part outlines the complete manufacturing workflow used to obtain injection-moldable feedstock and as-molded parts, covering the virgin production route (drying, melt compounding by extrusion, and injection molding) as well as the recycling route based on mechanical size reduction and re-injection molding. The aim is to provide a clear and reproducible description of the material system and processing history prior to the experimental testing campaign.

### 3.1.1. Pineapple fibers and jute fibers

Two lignocellulosic fibers were selected as reinforcements: pineapple fibers (PF) and jute fibers (JF). These fibers were chosen to investigate the mechanical and physical response of polypropylene-based composites reinforced with natural fibers, comparing single-fiber systems against hybrid PF–JF configurations at two different total fiber contents.

PF and JF were supplied in chopped fibers, partially in small bundles, as typically observed for lignocellulosic fibers, with a nominal length of 2 mm and were used as received.

(a) (b)

Figure 3.1: (a) Pineapple fibers; (b) jute fibers.

The fibers were characterized by a relatively low density and hygroscopic behavior typical of natural reinforcements; therefore, careful handling and pre-conditioning were adopted to limit moisture-related variability during processing. The fibers were used without chemical surface treatments and without coupling/compatibilizing agents, in order to focus on the isolated effects of fiber type (PF vs. JF), fiber content, and hybridization.

Key technical information for PF and JF is summarized in Table 3.1. Values refer to supplier datasheet and literature sources.

| | **Pineapple fibers** | **Jute fibers** | **Unit** |
|---|---|---|---|
| **Producer** | Food Reborn | Sanyo Kasei Co., Ltd. | – |
| **Density** | ≈ 1.53 | ≈ 1.46 | $\frac{g}{cm^3}$ |
| **Length** | 2 | 2 | $mm$ |
| **Bundles diameter** | ≈ 5-100 | ≈ 25-250 [12] | $\mu m$ |
| **Single fiber diameter** | ≈ 20 | ≈ 20-25 [42] | $\mu m$ |
| **Tensile modulus** | 34.5-82.51 [16] | 10-30 [16] | $GPa$ |

Table 3.1: Key properties of natural fibers, obtained from the supplier datasheet and bibliography.

### 3.1.2. Polypropylene

Polypropylene (PP) was selected as the thermoplastic matrix due to its industrial relevance, low density, and suitability for recycling and reprocessing. In this work, PP was used in pellet form and was classified as a homopolymer. It was chosen to ensure process compatibility with natural fibers within typical extrusion and injection molding temperature windows.


(a) (b)

Figure 3.2: (a) PP pellet; (b) polypropylene packaging sack.

The main technical specifications of the polymer are reported in Table 3.2.

| | Polypropylene | Unit |
|---|---|---|
| **Producer** | Prime Polymer Co., Ltd. | – |
| **Product name** | prime polypro | – |
| **Density ISO1183** | 0.9 | $\frac{g}{cm^3}$ |
| **Deflection temperature under load (0.45 MPa) ISO75** | 120 | $°C$ |
| **Tensile yield stress ISO527** | 41 | $MPa$ |
| **Tensile fracture strain, nominal tensile strain at break ISO527** | 30 | % |
| **Tensile modulus ISO527** | 2050 | $MPa$ |
| **Charpy impact strength ISO179** | 2.5 | $\frac{kJ}{m^2}$ |
| **Surface hardness Rockwell hardness ISO2039-2** | 110 | $R\,scale$ |
| **Melt mass flow rate (230°C) ISO1133** | 15 | $\frac{g}{10min}$ |

Table 3.2: Key properties of polyproprylene, obtained from the supplier datasheet.

### 3.1.3. Composite formulations, material handling and storage

Seven composite formulations were investigated, including five single-fiber composites (PF/PP and JF/PP) and two hybrid PF–JF/PP composites, each produced at a total fiber content of 15 wt% and 30 wt%. These two reinforcement levels were selected to enable a direct comparison between a moderate and a high fiber loading while remaining compatible with the processing capabilities of the available laboratory equipment. In particular, 30 wt% was considered close to the practical upper limit for the adopted extrusion setup, beyond which stable feeding and the maintenance of a constant fiber weight fraction along the run become increasingly difficult. Accordingly, 15 wt% was chosen as a lower, processable reference level, consistent with being exactly half of the high-loading condition. In addition, neat polypropylene (neat PP) was considered as a reference material to provide a baseline for assessing the effect of natural-fiber reinforcement. The complete set of formulations is reported in Table 3.3. A consistent naming convention was adopted: the material code indicates reinforcement family (PF, JF, or HYB) and total fiber content (15 or 30). This labeling is used throughout the thesis to identify the materials in figures, tables, and discussions. Neat PP is referred to as PP throughout the manuscript.

| Material code | PF (wt%) | JF (wt%) | PP (wt%) | Composite type |
|---|---|---|---|---|
| **PP** | 0 | 0 | 100 | neat matrix only |
| **PF15(1)** | 15 | 0 | 85 | single-fiber |
| **PF15(2)** | 15 | 0 | 85 | single-fiber |
| **PF30** | 30 | 0 | 70 | single-fiber |
| **JF15** | 0 | 15 | 85 | single-fiber |
| **JF30** | 0 | 30 | 70 | single-fiber |
| **HYB15** | 7.5 | 7.5 | 85 | hybrid |
| **HYB30** | 15 | 15 | 70 | hybrid |

Table 3.3: Composite formulations and neat PP investigated in this study (virgin materials): material codes, fiber contents, and PP fraction.

The chosen formulation matrix was designed to independently assess: the effect of fiber type (PF vs. JF), the effect of fiber content (15 vs. 30 wt%), and the effect of hybridization (PF/JF combination vs. single-fiber systems), while keeping the thermoplastic matrix and processing route constant.

Natural fibers are hygroscopic; therefore, PF and JF were stored in moisture-barrier bags under controlled temperature/humidity to minimize moisture uptake prior to processing. Polypropylene pellets were stored in original packaging. The drying procedure applied before extrusion and injection molding is described in Section 3.2.

After completion of the experimental characterization of the eight as-produced materials, the same batches were subsequently reprocessed to evaluate the effect of recycling on composite performance. Recycled materials are identified using the same nomenclature described above, with the suffix “R” appended to the original code, indicating that the specimens were produced from recycled (reprocessed) material, as reported in Table 3.4.

| Material code | PF (wt%) | JF (wt%) | PP (wt%) | Composite type |
|---|---|---|---|---|
| **PPR** | 0 | 0 | 100 | neat matrix only |
| **PF15(1)R** | 15 | 0 | 85 | single-fiber |
| **PF15(2)R** | 15 | 0 | 85 | single-fiber |
| **PF30R** | 30 | 0 | 70 | single-fiber |
| **JF15R** | 0 | 15 | 85 | single-fiber |
| **JF30R** | 0 | 30 | 70 | single-fiber |
| **HYB15R** | 7.5 | 7.5 | 85 | hybrid |
| **HYB30R** | 15 | 15 | 70 | hybrid |

Table 3.4: Composite formulations and neat PP investigated in this study (recycled materials): material codes, fiber contents, and PP fraction.

## 3.2. Manufacturing

### 3.2.1. Manufacturing route

The composites investigated in this work were manufactured through a thermoplastic compounding route designed to obtain injection-moldable pellets and, subsequently, as-molded parts suitable for mechanical and physical testing. The overall manufacturing chain consisted of: (i) drying of raw materials, (ii) melt compounding by extrusion, (iii) pelletizing of the extrudate, and (iv) injection molding of as-molded parts later converted into standardized test specimens.

In total, seven material batches were produced. Besides the six target formulations (PF/PP, JF/PP, and hybrid PF–JF/PP at 15 wt% and 30 wt% total fiber content), the 15 wt% PF + 85 wt% PP formulation was manufactured twice, hereafter referred to as PF15(1) and PF15(2), in order to compare two different hopper-feeding strategies during extrusion compounding. For all seven batches, the total mass of material prepared for each extrusion run was kept constant at 1 kg. In addition, neat polypropylene (PP) was processed as a reference material. For neat PP, the extrusion and pelletizing steps were not required, since the matrix was available as commercial pellets; therefore, neat PP specimens were produced by drying and direct injection molding, following the same molding procedure adopted for the compounded materials.

Figure 3.3 schematically summarizes the manufacturing route adopted in this study.

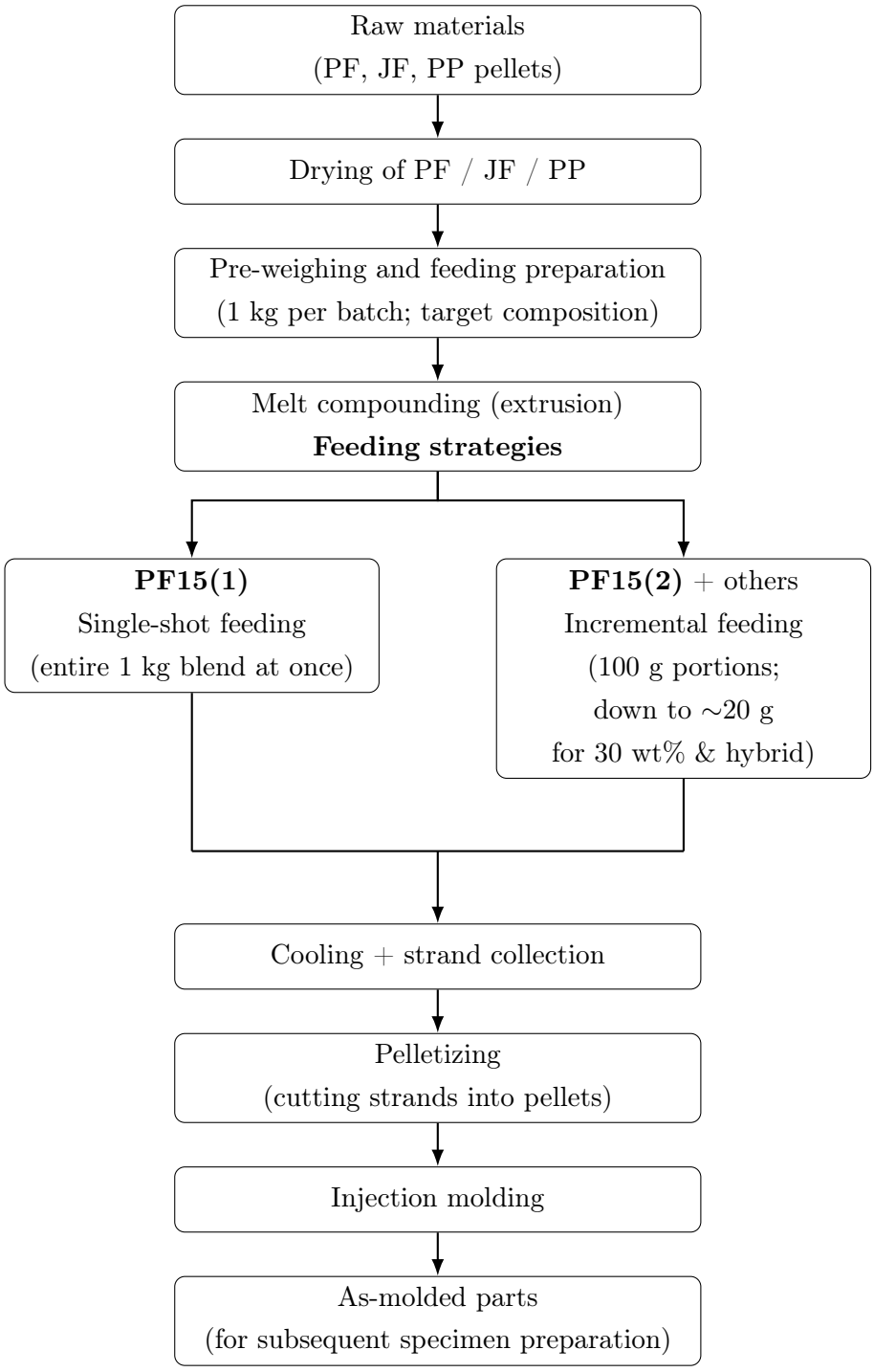


Figure 3.3: Manufacturing route adopted for the investigated virgin composites. For neat PP, extrusion and pelletizing steps are omitted (pellets are used as received).

After the primary manufacturing and testing campaign, the investigated composites were additionally processed to assess the effect of mechanical recycling (reprocessing) on material performance. Specifically, the remaining material from each formulation, consist-

ing of production scraps and/or tested specimens, was collected and ground to obtain reprocessed pellets. The resulting recycled feedstock was then directly used in the injection molding machine to manufacture a new set of specimens, which were employed to repeat the mechanical testing under the same experimental conditions adopted for the as-produced materials. Figure 3.4 schematically summarizes the manufacturing route adopted for the recycled composites and for neat PP.

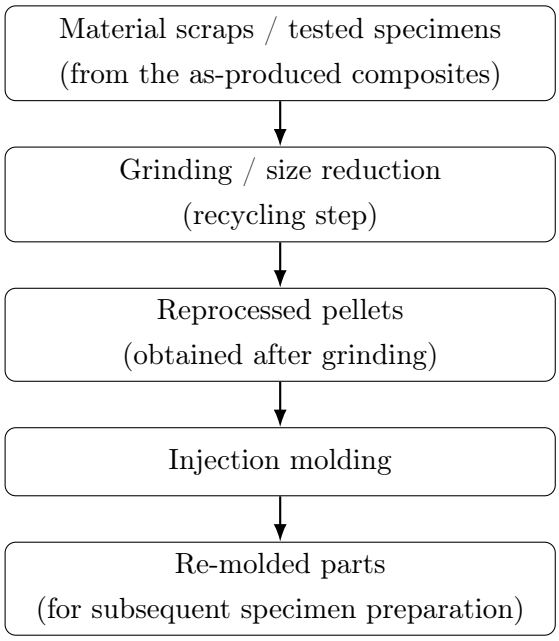


Figure 3.4: Manufacturing route adopted for recycled (reprocessed) composites.

### 3.2.2. Pre-processing: drying

Moisture control is a critical pre-processing step in the manufacturing of natural fiber-reinforced thermoplastics, due to the hygroscopic nature of lignocellulosic fibers. Excess moisture can promote void formation during melt processing, reduce the quality of the fiber–matrix interface, and lead to unstable feeding and flow behavior during extrusion and injection molding. For these reasons, pineapple fibers (PF) and jute fibers (JF) were dried prior to compounding. Polypropylene (PP) pellets were also dried to minimize moisture-related variability and ensure consistent processing conditions across all batches. This drying protocol is reported here in the context of the virgin manufacturing route, for instance, the preparation of raw materials for producing the as-produced (virgin) pellets; any additional drying steps applied to pellets prior to injection molding (including reprocessed material) are described in the corresponding downstream sections.

Drying was performed in a cabinet-type forced-convection (hot-air) drying oven (manu-

facturer Isuzu Seisakusho Co., Ltd., model ISUZU CAP VTEC-216), shown in Figure 3.5. The oven temperature was controlled via an integrated digital controller (setpoint: 80 °C).


(a) (b)

Figure 3.5: Drying equipment used for conditioning: (a) dryer unit; (b) temperature control panel.

The general drying setup, including the placement of fibers and pellets on trays, and the tray layout inside the dryer, is illustrated in Figure 3.6.

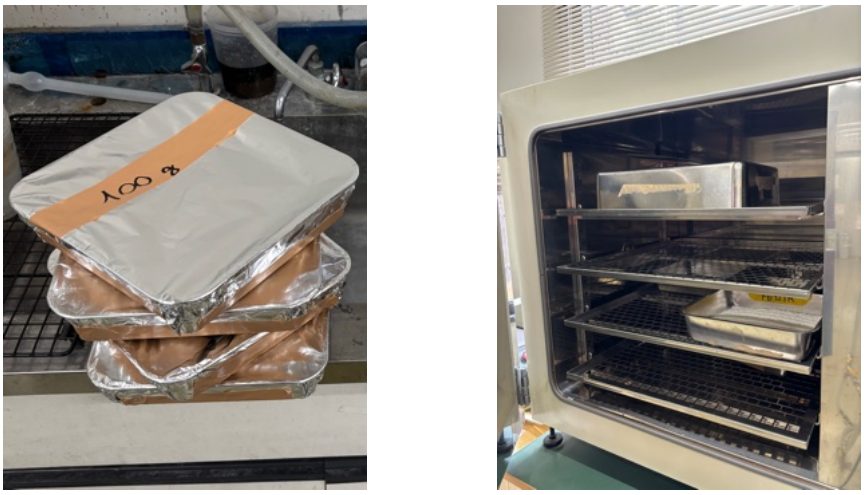

(a) (b)

Figure 3.6: Drying setup adopted for raw materials: (a) metal trays; (b) trays arranged inside the dryer during conditioning.

PF, JF, and PP pellets were dried at 80 °C for 24 h. During drying, the fibers were spread in metal trays and loosely covered with aluminum foil to prevent fiber movement and dispersion inside the dryer while still allowing moisture removal; the fiber load was approximately 100 g per tray. In contrast, PP pellets were placed in metal trays without any cover, as pellet entrainment was not an issue under the adopted drying conditions; the PP batch size was 1 kg.

After drying, the required amounts of PF, JF and PP were weighed and mixed to obtain the target composition for each batch. The blends were then prepared for extrusion feeding using the two investigated hopper-feeding approaches (single-shot feeding for PF15(1) and incremental feeding for PF15(2) and the remaining formulations). The time between the end of drying and extrusion was kept as short as reasonably possible to limit moisture re-absorption, particularly for PF and JF. The same drying procedure was applied before each extrusion run to maximize repeatability among formulations.

### 3.2.3. Extrusion

Melt compounding was carried out to incorporate PF and JF into the polypropylene matrix and to obtain composite pellets suitable for subsequent injection molding. This extrusion step refers exclusively to the production of the as-produced (virgin) pellets used to manufacture the virgin materials investigated in this work. The extrusion stage was performed using a consistent compounding route across all formulations in order to maximize repeatability and enable a fair comparison among materials with different fiber types and fiber contents.

#### 3.2.3.1. Extrusion equipment

Compounding was performed using a twin-screw extruder (manufacturer Thermo Fisher Scientific, model TSE 24 MC), configured for strand extrusion and pellet production. The extrusion line comprised the main processing unit (barrel and screws), a feeding system, a heated strand die, and downstream units for strand cooling, collection, and pelletizing. An overall view of the extrusion setup is shown in Figure 3.7.


(a)

(b)

Figure 3.7: Extruder: (a) extruder overview; (b) extruder monitor.

The extruder was a 24 mm co-rotating twin-screw unit with an L/D ratio of 40, providing adequate residence time for progressive PP melting and subsequent dispersive/distributive mixing of the fiber-filled melt. As shown in Figure 3.8, the screw setup was based on a modular configuration combining conveying sections and multiple kneading-disc blocks arranged in distinct mixing segments (Mixing Zones 1–3) along the barrel. In particular, the mixing functionality was provided exclusively by kneading disks (i.e., kneading blocks at different staggering angles, such as 0° and 90°), while XBD (Fixed Blister Disk) elements were not used. This layout was selected to promote melt homogenization and fiber dispersion within the PP matrix while maintaining a consistent compounding route across all formulations. Representative images of the screws and their modular element layout are reported in Figure 3.9.

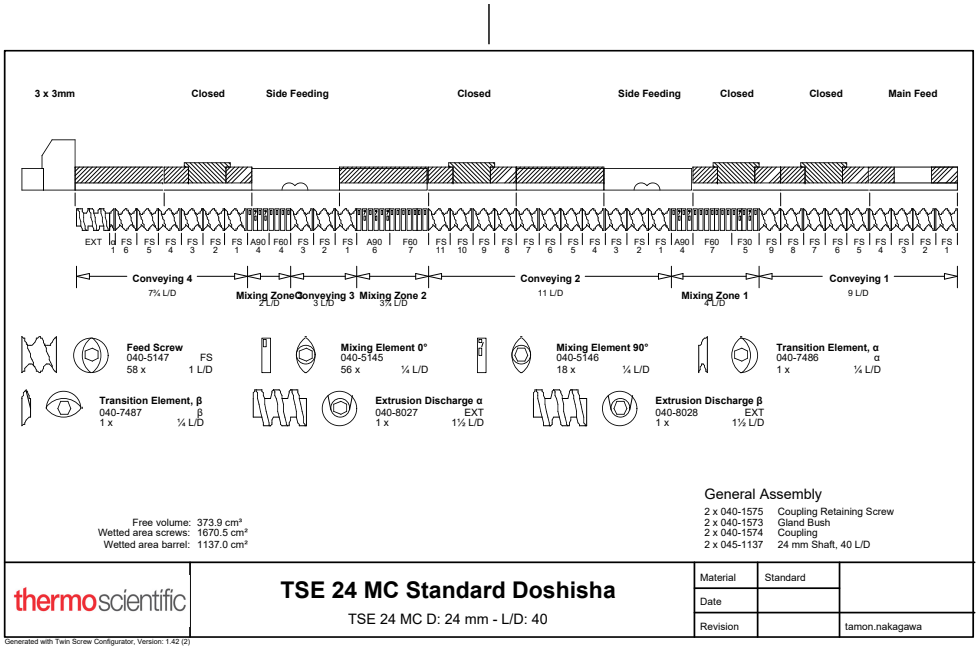


Figure 3.8: Screws configuration.

Figure 3.9: Screws.

The feeding unit consisted of a gravimetric feeder, providing a mass-controlled feed rate displayed in kg/h. The hopper was equipped with an internal agitator and twin metering screws that conveyed the material to the main screw inlet. Photographs of the feeder, including external and internal views, are reported in Figure 3.10.

(a) (b)

Figure 3.10: Feeder: (a) outside of the feeder; (b) inside of the feeder.

In the present work, the feeding strategy was adapted to the different formulations and fiber loadings, while maintaining the same extrusion hardware and process architecture. When natural fibers are processed, stable feeding can be influenced by bulk density differences and segregation tendencies between fibers and pellets; for this reason, both the hopper design and the feeding practice were considered important aspects of the overall compounding setup.

Temperature control was provided by ten independent heating zones along the barrel, with an additional control at the die (die temperature and pressure controller). The machine was operated via an integrated control interface (control panel shown in Figure 3.7b), which allowed the operator to set and monitor key process variables such as barrel temperature setpoints and screw speed. These monitored variables were used to check the stability of the process during each run and to ensure repeatability among batches.

At the end of the barrel, the compounded melt was discharged through a strand die (manufacturer Thermo Fisher Scientific, model 037-5354) to form multiple continuous filaments (strands). A close-up view of the die and the strand exit region is provided in Figure 3.11.

Figure 3.11: Die.

The strand extrusion configuration was selected because it provides a straightforward and reproducible route for producing pellets from compounded material. After leaving the die, the strand was water-cooled using a downstream cooling section (see Section 3.2.4), then collected and subsequently cut into pellets by the pelletizing unit. The adoption of this strand-based route ensured that all formulations were processed with a consistent pellet geometry prior to injection molding. A summary of the extrusion setpoints and operating parameters adopted in this work is reported in Table 3.5.

| | |
|---|---|
| **Extruder type** | Twin-screw |
| **Manufacturer / model** | Thermo Fisher Scientific / TSE 24 MC |
| **Screw diameter,** $D$ **[**$mm$**]** | 24 |
| **L/D ratio [-]** | 40 |
| **Screw configuration** | co-rotating |
| **Heating zones** | Ten zones along the barrel + one zone at the die |

Table 3.5: Extruder specifications.

### 3.2.3.2. Compounding strategy

For each extrusion run, a total batch mass of 1 kg was prepared by weighing PP pellets and fibers according to the target formulation (Section 3.1.3). After drying (Section 3.2.2),

the constituents were combined to obtain a premixed blend prior to feeding.

The mixing and pre-feeding preparation step was conducted using two different approaches, depending on the hopper-feeding strategy adopted during extrusion. For the single-shot feeding approach (PF15(1)), the entire 1 kg batch (PP pellets and fibers at the target composition) was combined in a single sealed bag and manually mixed by shaking and tumbling. This procedure aimed to obtain an apparently homogeneous blend prior to pouring the full batch into the extruder hopper in one step. A representative image of the sealed-bag premixing procedure is reported in Figure 3.12.

Figure 3.12: Sealed bag.

In contrast, for the incremental feeding approach (PF15(2) and all other formulations), the batch was not handled as a single 1 kg blend. Instead, PP pellets and fibers were portion-wise distributed into individual cups, each prepared to maintain the target composition. For the 15 wt% fiber formulations, the 1 kg batch was divided into ten cups of 100 g each; for the 30 wt% fiber and hybrid formulations, it was divided into fifty cups of 20 g each. The portioned preparation workflow and the pre-weighed cups are shown in Figure 3.13.

(a)

(b)

Figure 3.13: Incremental feeding: (a) 20 g each; (b) 100 g each.

During extrusion, these cups were subsequently fed into the hopper one at a time. This practice was adopted to avoid overloading the hopper with a large amount of material, which may promote segregation inside the hopper: PP pellets tend to flow and descend towards the screws more readily than chopped fibers, potentially leading to fiber accumulation (bridging) and local fluctuations in fiber content as the run progresses. The feeding operation is illustrated in Figure 3.14: an example of single-shot hopper loading and a close-up of the hopper outlet (feed throat), where the blend enters the screw intake region.

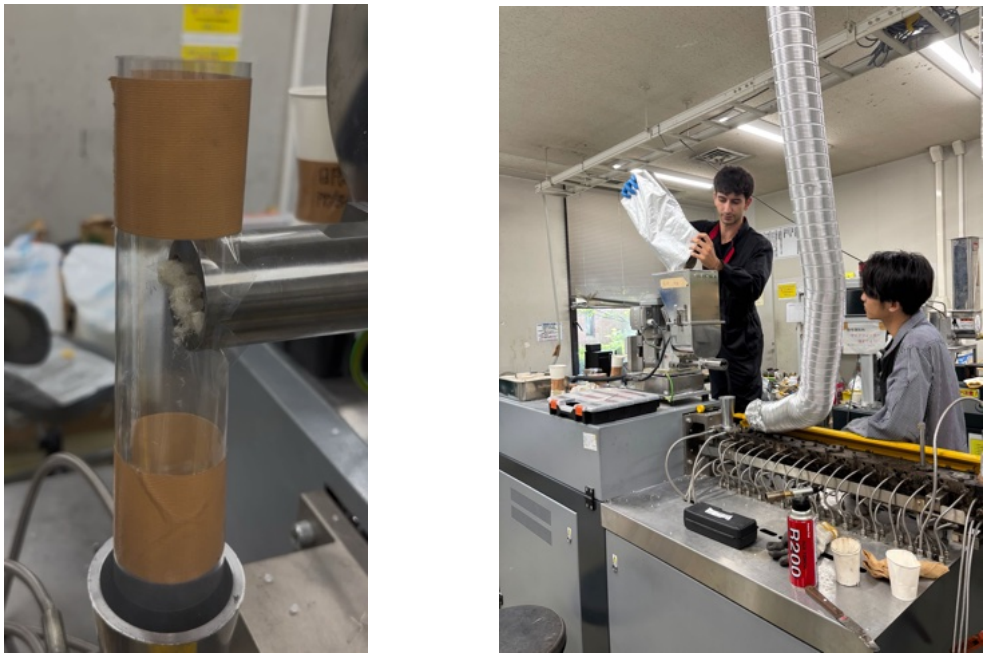

(a) (b)

Figure 3.14: Feeding operation during extrusion compounding: (a) close-up of the hopper outlet leading to the screw intake region; (b) single-shot loading of the premixed blend into the hopper.

The overall compounding approach was designed to promote adequate fiber dispersion within the PP melt while maintaining repeatable operating conditions. In practice, this was pursued by keeping the extrusion hardware and nominal processing settings constant across formulations, and by controlling the feeding operation to minimize composition fluctuations during the run.

#### 3.2.3.3. Processing conditions

All formulations were compounded using the same nominal extrusion conditions in order to ensure comparability among fiber types (PF vs JF), fiber contents (15 vs 30 wt%), and hybrid systems. The barrel temperature profile was controlled across ten heating zones along the barrel, with an additional independently controlled zone at the die, in order to promote progressive melting of the PP pellets and subsequent incorporation of the fibers. The corresponding zone setpoints and real-time temperature readings were displayed on the extruder control monitor (Figure 3.7b). The setpoints were all set at 180 °C, with the die temperature set to 180 °C. The screw speed was kept at 200 rpm for all runs. The average throughput (mass flow rate) was approximately 2.5 kg/h. Although the feeding

operation differed depending on the investigated approach (single-shot vs incremental), the same nominal machine settings were maintained to isolate the effect of formulation and feeding strategy from changes in processing conditions. A summary of the operating parameters adopted in this work is reported in Table 3.6.

| Parameter | Value | Unit |
|---|---|---|
| **Barrel temperature profile** | Z1 - Z10 : 180 | $(°C)$ |
| **Die temperature** | 180 | $(°C)$ |
| **Screw speed** | 200 | $(rpm)$ |
| **Throughput** | 2.5 | $(kg/h)$ |

Table 3.6: Extrusion setpoints and operating parameters.

At the beginning of each run, the extruder was brought to the set temperature profile and allowed to stabilize prior to feeding. The first portion of extrudate was considered transient, as it may reflect incomplete thermal stabilization and non-uniform initial feeding. Material was collected only after the strand appearance became continuous and uniform and after process signals reached a stable regime. During compounding, process stability was assessed by monitoring the feeder and the main process parameters shown on the machine interface, together with visual inspection of the strand at the die exit. In particular, the feeding system was monitored to ensure continuous material supply; when the hopper level dropped below the minimum threshold, an alarm was triggered to prevent unstable feeding conditions. These parameters were used as indicators of steady operation, and abrupt changes were interpreted as potential signs of transient feeding conditions or variations in melt viscosity and flow.

At the end of each run, the remaining material in the hopper and barrel was extruded until empty to minimize cross-contamination between formulations. The screws and barrel were flushed with neat PP, and the line was returned to a baseline condition before processing the subsequent formulation. The processing order of materials was from low to high fiber content to reduce carryover effects between batches.

Finally, the extrudate exiting the strand die was guided directly into a cooling bath to solidify the strands prior to pelletizing. The cooling bath setup and the downstream pelletizing procedure are described in the following section (Section 3.2.4).

### 3.2.4. Feedstock preparation for injection molding

Feedstock preparation was used to obtain injection-moldable material for both sets investigated in this work, namely the as-produced (virgin) composites and the reprocessed (recycled) composites.

In the primary virgin route, the extruded composite was converted into pellets through strand pelletizing: after exiting the strand die, the filaments were guided into a cooling bath to solidify the extrudate and stabilize strand geometry prior to cutting, and the cooled strands were then conveyed to the strand pelletizer, where they were cut into pellets suitable for subsequent injection molding.

In the recycling route, injection-moldable feedstock was prepared by mechanical grinding of the available composite material (production scraps and/or tested specimens), yielding reprocessed granules that were subsequently re-injection molded.

#### 3.2.4.1. Strand pelletizing (virgin material)

The pelletizing line comprised: (i) a water cooling bath for solidifying the extruded strands exiting the strand die and (ii) a strand pelletizer for cutting the solidified strands into injection-moldable pellets.

The cooling stage was performed using a water cooling bath (manufacturer PELL-TEC Pelletizing Technology GmbH, model CT 120-100-2000), shown in Figure 3.15. The bath consisted of a stainless-steel tank with an effective length of 2 meters. The extruded strands were guided through the bath using guide rollers in order to maintain strand alignment and a stable transport path toward the pelletizer.

Figure 3.15: Cooling bath.

The cooling bath was operated using tap water at approximately ambient supply temperature. A continuous refresh of the bath was ensured by keeping the inlet and outlet lines slightly open throughout the run, so as to avoid excessive warming of the bath during extrusion. The strand residence time in the bath was set to be sufficient to cool and fully solidify the filaments prior to cutting, while remaining short enough to prevent strand accumulation at the die exit and to maintain a smooth, continuous take-up into the downstream pelletizing unit.

After cooling, the strands were conveyed to the pelletizer. Pelletizing was carried out using a strand pelletizer (manufacturer Isuzu Kako Kikai Co., Ltd., model SCF-50), shown in Figure 3.16a. The unit consisted of a strand intake section and a cutting head equipped with rotating blades against a counter-knife, designed to continuously cut the incoming strands at a controlled rate. A close-up of the cutting area is shown in Figure 3.16b.


(a) (b) (c)

Figure 3.16: Pelletizer: (a) pelletizer overview; (b) pelletizer cutter; (c) pelletizer controller.

Pelletizing conditions were selected to obtain pellets with a geometry suitable for injection molding and to ensure repeatability. The strands were conveyed to the pelletizer under steady, motor-driven transport provided by the pelletizer feed rollers, which ensured continuous strand intake into the cutting chamber and a stable cutting operation. The pellet length was governed by the cutting settings, defined by the pelletizer line speed (strand feed speed) set to ∼25 m/min on the controller (Figure 3.16c). The target pellet length was approximately 5 mm and was verified by visual inspection. Representative images of the as-produced pellets are provided in the Appendix A.1.

To minimize moisture-related variability after cooling and cutting, the freshly pelletized material was collected and subsequently dried in the dryer for approximately 2 hours at a temperature of 80 °C. After this post-pelletizing drying step, the pellets were sealed in moisture-barrier bags and stored until injection molding.

#### 3.2.4.2. Grinding (recycled material)

Mechanical grinding was adopted to obtain a reprocessed feedstock suitable for re-injection molding of the recycled material set. In this route, available composite material, consisting of production scraps and/or previously molded and tested parts, was reduced in size to produce granules compatible with the injection molding hopper and plasticizing unit. Because the composites contain natural fibers, particular care was taken to avoid excessive compaction and plastic deformation during size reduction, which can increase the risk of

clogging and material build-up inside the grinder.

Prior to grinding, the parts intended for recycling were pre-cut to reduce their characteristic dimensions and facilitate stable size reduction. Pre-cutting was carried out using an electric table saw (manufacturer Proxxon, model Mini Band Saw), shown in Figure 3.17a. Molded dog-bone blanks, runner systems, and other scraps were sectioned into smaller pieces of approximately 5 cm, as illustrated in Figure 3.17b. This step was introduced to improve feeding into the grinder and to reduce the risk of the grinding chamber becoming clogged when processing fiber-containing thermoplastics.


(a) (b)

Figure 3.17: Pre-cutting: (a) table saw; (b) precut pieces.

Grinding was then performed using a granulator (manufacturer Sansho Industry Co., Ltd.), shown in Figure 3.18a. A close-up view of the cutting chamber and rotor region is reported in Figure 3.18b. The unit comprised a rotating cutting rotor and stationary cutting elements housed within a closed grinding chamber. Processed material was collected in a sealed bag at the outlet (Figure 3.12), yielding a mixture of reprocessed granules and fine powder. The grinder was equipped with an internal screen, its nominal mesh size was 6 mm (Figure 3.18c).

(a) (b) (c)

Figure 3.18: Grinder: (a) grinder overview; (b) grinder rotor; (c) grinder screen.

Grinding was carried out in batches to maintain stable operation and limit excessive heat generation. Feeding into the grinding chamber was performed manually in small portions to avoid overloading the cutting region and to maintain continuous cutting.

The reprocessed output pellets exhibited a broader size distribution compared to the virgin pellets produced by strand pelletizing. In particular, the ground material included coarser granules together with a fraction of powder, as shown in Figure 3.19. The total mass recovered after grinding was approximately 200–400 g per material, consistent with the limited amount of recyclable material available after the primary manufacturing and testing stages.

Figure 3.19: Ground material.

After grinding, the reprocessed feedstock was promptly transferred to sealed moisture-barrier bags (Figure 3.12) and stored until injection molding to limit moisture uptake.

For completeness, the same grinding procedure and operating conditions described above were also applied to neat PP, providing a recycled PP reference processed under the same mechanical reprocessing route.

Representative images of the as-produced pellets are provided in the Appendix A.2.

### 3.2.5. Injection molding

Injection molding was used to convert the compounded pellets into as-molded parts suitable for subsequent cutting into standardized test specimens. All formulations were injection molded following a consistent procedure in order to minimize processing variability and to enable a direct comparison among fiber types, fiber contents, and hybrid configurations. In addition to the virgin pellets, reprocessed pellets obtained after mechanical recycling were also injection molded to manufacture a second set of specimens for repeated mechanical testing (Section 3.2.1).

#### 3.2.5.1. Injection molding equipment

Injection molding was carried out using a fully electric injection molding machine (manufacturer Toyo Machinery & Metal Co., Ltd., model ET-40V). The machine comprised a hopper for pellet feeding, a plasticizing unit based on a reciprocating screw, and a clamp-

ing unit designed to hold the mold closed during filling, packing, and cooling. An overview of the injection molding setup is shown in Figure 3.20a. The plasticizing unit consisted of a reciprocating screw and the barrel temperature was controlled through four heating zones (HT1–HT4), allowing the polymer to melt and homogenize before injection into the mold. An additional setpoint was displayed for the hopper unit (Hopper 1). The machine control interface used to set and monitor molding parameters (e.g., temperature setpoints, injection speed, injection/holding pressure, cooling time) is shown in Figure 3.20b.


(a) (b)

Figure 3.20: Injection molding machine: (a) injection molding overview; (b) injection molding panel.

In addition to the injection molding machine, the mold tool plays a central role in defining the geometry and quality of the molded parts. In this work, a dedicated mold was selected to produce parts compatible with the subsequent preparation of standardized specimens for mechanical and physical testing. The mold used in this study is shown in Figure 3.21a. The mold configuration included two cavities producing ISO 527 tensile dog-bone specimens (Figure 3.21b). The gating and runner system consisted of a cold-runner layout with a central sprue and runner feeding the two cavities, with the gate located at the specimen end region.

Cooling of the mold was achieved through water channels, with the mold temperature controlled at 50 °C using water circulation. Part release was assisted by the mold ejection

mechanism, and the as-molded parts were subsequently removed manually. Selecting a mold geometry consistent with the intended test standards was essential to ensure that specimen preparation could be carried out reproducibly and with minimal machining-induced variability.


(a) (b)

Figure 3.21: Injection molding mold: (a) mold overview; (b) as-molded dogbones.

### 3.2.5.2. Feeding procedure

Two feedstock conditions were injection molded:

- Virgin pellets (as-produced): pellets obtained from the primary extrusion route (Section 3.2.4.1) were dried prior to molding and then fed into the injection molding hopper. Owing to the uniform pellet geometry, hopper feeding could be performed in incremental additions of approximately 100–200 g without a significant risk of bridging or blockage at the hopper–barrel transition.
- Recycled pellets (reprocessed): after the primary testing campaign, remaining material and tested specimens were mechanically ground to obtain reprocessed granules. In contrast to the as-produced pellets, the recycled feedstock exhibited a broader particle-size distribution, including coarser fragments and fine powder (Section 3.2.4.2). For this reason, hopper feeding was carried out more cautiously, typically in smaller portions ($<$100 g, down to 50 g), to reduce the likelihood of obstructing the feed throat and to maintain stable plasticization.

In addition, neat PP was injection molded as a reference material in both feedstock conditions, namely from commercial virgin pellets and from recycled pellets obtained by grinding. In this case, extrusion and strand pelletizing were not required, since the polymer was available as commercial pellets directly suitable for molding; therefore, virgin neat PP pellets were simply dried prior to processing and fed into the injection molding

hopper following the same procedure adopted for the as-produced materials. Likewise, the ground PPR feedstock was dried and then injection molded using the same mold and processing route adopted for the recycled composite batches.

Before each molding session, pellets were dried to reduce moisture-driven variability associated with the hygroscopic nature of the fibers. The total mass of pellets processed per batch depended on material availability. For virgin materials, the injected mass ranged from 650 g to 850 g, reflecting differences in pellet yield from extrusion and pelletizing. For recycled materials, the injected mass was typically lower ( 200–400 g), as the amount of reprocessed feedstock available after grinding was limited, consistent with the material recovery described in the recycling stage. Molding was initiated once stable operating conditions were reached, and feeding was continued portion-wise throughout the run to maintain consistent hopper level and process stability.

To reduce cross-contamination between materials, the barrel and screw were purged with the next material, and the first molded parts were discarded until the melt appeared visually consistent.

#### 3.2.5.3. Processing conditions

All materials were molded using a consistent parameter set. The barrel temperature was set to 180 °C and the additional setpoint was set to 50°C. Injection speed was 100 mm/s, with an injection pressure limit of 100 MPa. The holding stage was applied at 50 MPa for 5 s, followed by a cooling time of 25 s before part ejection. A summary of the injection molding parameters is reported in Table 3.7.

The same molding conditions were applied to virgin and recycled feedstocks to isolate the effect of reprocessing from changes in injection settings.

| Parameter | Value | Unit |
|---|---|---|
| **Barrel temperature profile** | Z1 - Z4 : 180 | $°C$ |
| **Mold temperature** | 50 | $°C$ |
| **Screw rotation speed** | 80 | $min^{-1}$ |
| **Plasticizing, screw travel** | 88 | $mm$ |
| **Resin pressure during plasticizing** | 2.5 | $MPa$ |
| **Suck back/decompression** | 2 | $mm$ |
| **Injection speed** | 100 | $mm/s$ |
| **Primary injection pressure limit** | 100 | $MPa$ |
| **Holding pressure** | 50 | $MPa$ |
| **Holding time** | 5 | $s$ |
| **Cooling time** | 25 | $s$ |

Table 3.7: Injection molding parameters.

The mold was designed to produce ISO 527 tensile dog-bone blanks (Figure 3.21b). A portion of the as-molded dog-bones was used directly for tensile testing, whereas additional parts were used as stock material and subsequently cut to obtain specimens for flexural (bending) and impact tests, following the procedures and standards described in Chapter 4. The exact specimen dimensions and final geometries are reported in the subsequent chapter.

# 4 | Experimental devices and procedures

This chapter describes the experimental devices and procedures adopted to prepare the test specimens and to conduct the mechanical and physical characterization of the investigated materials. The same methodology was applied to both virgin and recycled materials, without procedural distinctions between the two. The chapter is presented without discussion of the results, focusing instead on equipment, specimen preparation steps, testing conditions, and data acquisition protocols.

## 4.1. Specimen preparation

All specimens used for mechanical and physical testing were obtained from injection-molded parts produced as described in Chapter 3. The starting geometry after injection molding consisted of a molded component featuring ISO 527 tensile specimen geometries; however, a post-processing step was required to separate and finish the individual ISO 527 tensile specimens. Flexural and impact specimens were subsequently derived from these ISO 527 tensile specimens by additional cutting operations, in order to ensure a consistent processing history across all test types and reduce inter-specimen variability. To minimize the risk of contamination from residual material remaining in the injection molding unit after material changeover, the first three injection-molded parts produced at the beginning of each run (each containing two ISO 527 tensile specimens) were discarded and not considered for testing for the virgin material set. For the recycled material set, due to the limited amount of available moulded material, the second and third injection-molded parts were also used for some formulations (PF15(2)R and JF15R only) in order to obtain a sufficient number of specimens to perform at least the tensile and impact tests.

ISO 527 tensile specimens were obtained from the injection-molded part using a table saw (manufacturer Y.S. Industry Co., Ltd, model YS-410). The operation consisted of separating the molded part and performing the necessary trimming to obtain individual specimens with clean edges while preserving the ISO 527 geometry. Each specimen was

visually inspected to exclude pieces presenting macroscopic defects. When present, minor flash was removed without affecting the gauge section. The table saw employed for (i) tensile specimen separation and (ii) extraction of rectangular bars for flexural and impact tests is shown in Figure 4.1.


Figure 4.1: Table saw.

Flexural test specimens (rectangular cross-section bars) were obtained by cutting the prepared ISO 527 tensile specimens using the same table saw showed in Figure 4.1, following a controlled and repeatable cutting layout. The flexural specimens were obtained by cutting the central rectangular (parallel/gauge) section of the ISO 527 dog-bone tensile specimen, so as to meet the required ISO 180 / Type 3A specimen geometry. The longitudinal axis of the extracted bar coincided with the main axis of the original tensile specimen.

Impact test specimens were prepared in two steps: (i) cutting rectangular bars identical to those used for the bending tests from the central rectangular (parallel/gauge) section of the ISO 527 tensile specimens using the table saw shown in Figure 4.1, followed by (ii) machining a V-shape notch on each specimen using a dedicated notching device (manufacturer ENSHU, model ESK). The notch was introduced at mid-length of the bar, as required by the selected impact standard (ISO 187 Izod). The notching machine is documented in Figure 4.2.

Figure 4.2: Notcher.

Water uptake specimens were prepared from the same injection-molded ISO 527 tensile specimens described above, in order to preserve a consistent processing history. For each formulation investigated in the water uptake study, the central rectangular (parallel/gauge) section of an ISO 527 dog-bone specimen was used as the parent material, from which multiple small sections were sectioned using the table saw shown in Figure 3.17a. The cutting layout was kept controlled and repeatable to obtain comparable specimens. This specimen preparation route was adopted to provide water uptake test coupons suitable for evaluation based on ISO 62.

## 4.2. Density measurement

Material density was measured to support the comparison between virgin and recycled formulations and to provide complementary information for the interpretation of the experimental results. Density measurements were performed for both virgin and recycled materials following the same procedure, without distinctions. For each formulation, three fragments were analyzed in order to obtain a representative mean value and quantify data scatter, and results are presented in Chapter 5.

Density was measured on small solid fragments obtained from the investigated materials; fragments had variable size and geometry, as they were collected either from mechanically tested specimens (e.g., broken pieces after impact tests) or from additional sections prepared for SEM observations. Density measurements were carried out using an electronic densimeter (manufacturer Alfa Mirage, model SD-200L) operating according to

the Archimedes principle and equipped with the dedicated immersion kit for density determination. An overview of the balance is provided in Figure 4.3a, while a close-up of the immersion setup (sample holder, beaker, and submerged weighing region) is shown in Figure 4.3b. The immersion fluid was water at room temperature. To minimize errors associated with air bubbles adhering to the specimen surface during immersion, a small amount of dishwashing detergent acting as a surfactant was added to the water.

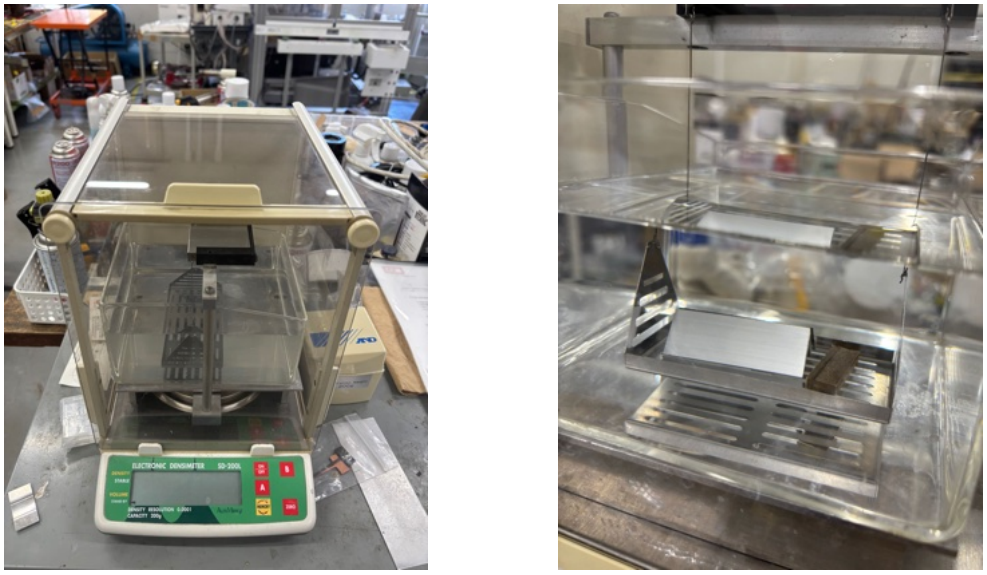

(a) (b)

Figure 4.3: Electronic densimeter: (a) balance overview; (b) balance set-up.

Before measurements, the balance was levelled and calibrated according to the manufacturer's procedure. For each fragment, the instrument acquired the mass in air and the apparent mass when submerged in the immersion fluid, and the balance software computed the density. In some cases, due to the low density and small size of the fragments, specimens tended to float rather than remain on the submerged support; therefore, an additional retaining piece was placed on the submerged platform to keep the fragment fully immersed during the measurement. This auxiliary support is also visible in the setup photograph previously reported (Figure 4.3b). The density value was directly provided as an output for each replicate. After each measurement, the specimen was removed and gently dried, and the setup was checked to ensure consistent immersion conditions.

For each formulation, the reported density corresponds to the mean of three measurements, while data scatter was quantified using the standard deviation. To quantify the effect of recycling, the density variation between the virgin and recycled counterparts was evaluated as a relative change with respect to the virgin material:

$$\Delta\rho\,[\%] = \frac{\rho_{\text{recycled}} - \rho_{\text{virgin}}}{\rho_{\text{virgin}}} \cdot 100 \tag{4.1}$$

where $\rho_{\text{virgin}}$ and $\rho_{\text{recycled}}$ are the mean density values measured for the corresponding virgin and recycled formulations.

## 4.3. Tensile test

Tensile tests were performed on ISO 527-2/1A (JIS K 7139/A1) dog-bone specimens prepared as described in Section 4.1. The nominal specimen geometry and the corresponding dimensions adopted for the present work are reported in Table 4.1, and a representative specimen is shown in Figure 4.4.

| Parameter | Value | Unit |
|---|---|---|
| **Overall length** | 165 | *mm* |
| **Gauge length** | 80 | *mm* |
| **Gauge width** | 10 | *mm* |
| **End width** | 20 | *mm* |
| **Thickness** | 4 | *mm* |
| **Gauge length used for strain measurement $L_0$** | 50 | *mm* |

Table 4.1: Tensile test specimen dimensions.

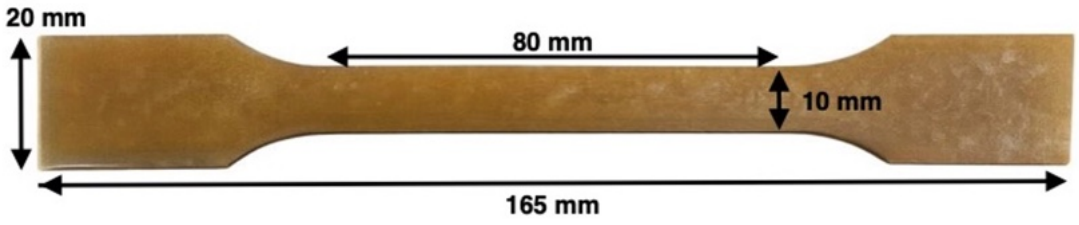


Figure 4.4: Tensile test specimen.

In the data reduction, nominal dimensions from the ISO standard were used to define the initial cross-sectional area. Individual specimen dimensions were not measured prior to testing.

Tensile tests were performed using a universal testing machine (UTM) (manufacturer Shimadzu, model Autograph AGS-X) equipped with a load cell of 10000 N. Specimens

were clamped using mechanical wedge grips with serrated grip faces to avoid slippage. An overview of the testing setup is shown in Figure 4.5a. Strain was measured using a video extensometer system (manufacturer Shimadzu, model TRViewX) with a nominal gauge length $L_0 = 50$ mm. The camera arrangement and optical tracking configuration adopted during testing are documented in Figure 4.5b. Force, crosshead displacement, and strain were recorded using software Trapezium, which was also used for real-time monitoring and data export; an example interface screenshot is provided in Figure 4.5c.


(a) (b) (c)

Figure 4.5: Tensile test: (a) tensile test machine; (b) video extensometer camera; (c) tensile test software.

Tests were carried out under the conditions summarized in Table 4.2.

| Parameter | Value | Unit |
|---|---|---|
| **Crosshead speed** | 1 | $mm/min$ |
| **Number of specimens (virgin materials)** | 7 | – |
| **Number of specimens (recycled materials)** | 5 | – |

Table 4.2: Tensile test conditions.

Engineering stress $\sigma$ and engineering strain $\varepsilon$ were calculated as:

$$\sigma = \frac{F}{A_0} \qquad \varepsilon = \frac{\Delta L}{L_0}$$

where F is the measured tensile force, $A_0$ is the nominal initial cross-sectional area defined from ISO 527 specimen dimensions, $\Delta L$ is the elongation measured by the video extensometer, and $L_0$ is the nominal gauge length reported in Table 4.1.

The following tensile properties were determined (the results are shown and discussed in the subsequent Chapter 5):

- Tensile modulus E: calculated as the slope of the initial linear portion of the stress-strain curve within the strain interval 0.1%–0.3% (defined according to ISO 527 recommendations).
- Tensile strength $\sigma_M$: defined as the maximum engineering stress recorded during the test, as defined in ISO 527-1 (maximum of the engineering stress–strain curve).
- Strain at break $\varepsilon_B$: recorded at specimen fracture, consistently with ISO 527 terminology.

For each formulation, the reported values correspond to the mean of seven specimens for virgin materials and five specimens for recycled materials. Data scatter was quantified using standard deviation, as reported in Chapter 5.

## 4.4. Bending test

Flexural properties were evaluated by three-point bending on rectangular specimens prepared as described in Section 4.1. This test was performed only on virgin materials. For recycled materials, the number of available specimens was not sufficient to cover all mechanical characterizations; therefore, the remaining recycled specimens were preferentially allocated to tensile and impact testing, and bending tests were not conducted for the recycled set. The test procedure followed the adopted standard ISO 178 (JIS K 7171).

Flexural specimens consisted of rectangular bars obtained from the central rectangular section of the ISO 527 dog-bone tensile specimen. The nominal specimen geometry and dimensions used in this work are reported in Table 4.3, and a representative specimen is shown in Figure 4.6.

| Parameter | Value | Unit |
|---|---|---|
| **Length** | 80 | $mm$ |
| **Width** | 10 | $mm$ |
| **Thickness** | 4 | $mm$ |

Table 4.3: Bending test specimen dimensions.

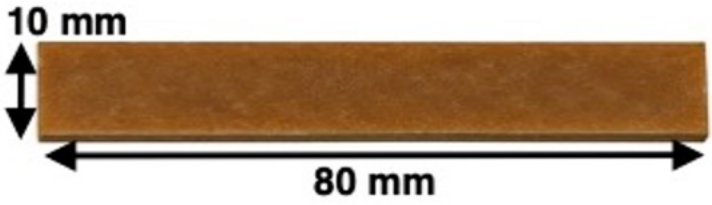


Figure 4.6: Bending test specimen.

In the data reduction, nominal dimensions from the selected standard were used. Individual specimen dimensions were not measured prior to testing.

Bending tests were performed using a universal testing machine (manufacturer Shimadzu, model Autograph AGS-X) equipped with a load cell of 1000 N, using a three-point bending fixture. An overview of the bending test machine and the three-point bending setup are shown in Figure 4.7a and Figure 4.7b. The fixture consisted of two supports and a central loading nose. The support span L was set to 64 mm, corresponding to a span to thickness ratio L/h = 16. Force and crosshead displacement were recorded using the software Trapezium, the same data acquisition and control software adopted for the tensile tests.

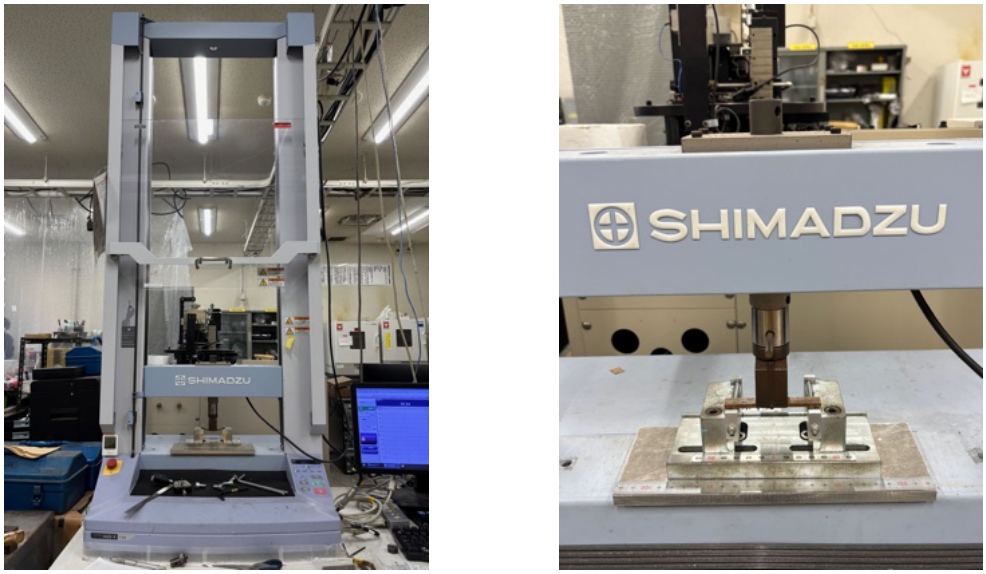


(a) (b)

Figure 4.7: Bending test: (a) bending test machine; (b) bending test set-up.

Test conditions are summarized in Table 4.4.

| Parameter | Value | Unit |
|---|---|---|
| **Crosshead speed** | 10 | $mm/min$ |
| **Span length** | 64 | $mm$ |
| **Number of specimens (virgin materials)** | 7 | – |
| **Number of specimens (recycled materials)** | 0 (not tested) | – |

Table 4.4: Bending test conditions.

Flexural stress $\sigma_f$ and flexural strain $\varepsilon_f$ were calculated from the recorded load–deflection response according to the adopted standard for a rectangular specimen tested in three-point bending. Using the applied load F, the support span L, specimen width b, specimen thickness h, and mid-span deflection s, the flexural stress and strain were computed as:

$$\sigma_f = \frac{3FL}{2bh^2} \qquad \varepsilon_f = \frac{6hs}{L^2}$$

The following flexural properties were determined (the results are shown and discussed in the subsequent Chapter 5):

- Flexural modulus $E_f$: obtained from the slope (linear fit) of the initial quasi-linear portion of the flexural stress–strain curve, evaluated in the 0.30%–0.50% strain range

to avoid the initial measurement artefact (ISO 178 modulus is commonly defined at lower strains).

- Maximum flexural stress $\sigma_{f,M}$ (flexural strength): defined as the maximum flexural stress recorded during the test, in accordance with ISO 178.
- Flexural strain at break $\varepsilon_{f,B}$: recorded at specimen fracture (or at complete separation).

For each formulation, the reported values correspond to the mean of seven specimens for the virgin materials. Data scatter was quantified using standard deviation, as reported in Chapter 5.

## 4.5. Impact test

Impact resistance was evaluated on notched specimens prepared as described in Section 4.1. The same testing procedure was applied to both virgin and recycled materials, without procedural distinctions. Impact tests were conducted according to the standard ISO 180 Izod V-notch (JIS K 7110/3A).

Impact specimens consisted of rectangular bars obtained from the ISO 527 dog-bone tensile specimens. The initial rectangular bar geometry was identical to that used for the bending tests; subsequently, a notch was introduced at mid-length of each bar using a dedicated notching device.

The nominal specimen geometry and dimensions adopted in this work (including notch type and notch dimensions) are reported in Table 4.5, and a representative specimen is shown in Figure 4.8.

| Parameter | Value | unit |
|---|---|---|
| **Length** | 80 | $mm$ |
| **Width** | 10 | $mm$ |
| **Thickness** | 4 | $mm$ |
| **Notch depth** | 2 | $mm$ |
| **Notch type** | V-notch | – |

Table 4.5: Impact test specimen dimensions.

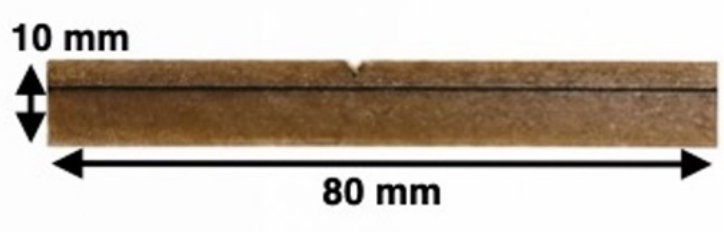


Figure 4.8: Impact test specimen.

In the data reduction, nominal dimensions from the selected standard were used. Individual specimen dimensions were not measured prior to testing.

Impact tests were performed using a pendulum impact tester (manufacturer Toyo Seiki Seisaku-sho, Ltd., model Impact Tester IT) configured for Izod testing (JIS K 7110/3A) and equipped with a pendulum of nominal energy 5.50 J (Hammer 2: J1055J). An overview of the impact tester is provided in Figure 4.9a. During testing, specimens were positioned and aligned according to the standard requirements, ensuring that impact occurred on the notched side in the prescribed configuration; a close-up view of the specimen positioning at the clamping region is shown in Figure 4.9b. The absorbed impact energy was directly recorded by the instrument and exported through the integrated control and data acquisition system of the impact tester. An example of the control interface, displayed on a Mitsubishi Electric GOT1000 monitor, is reported in Figure 4.9c.

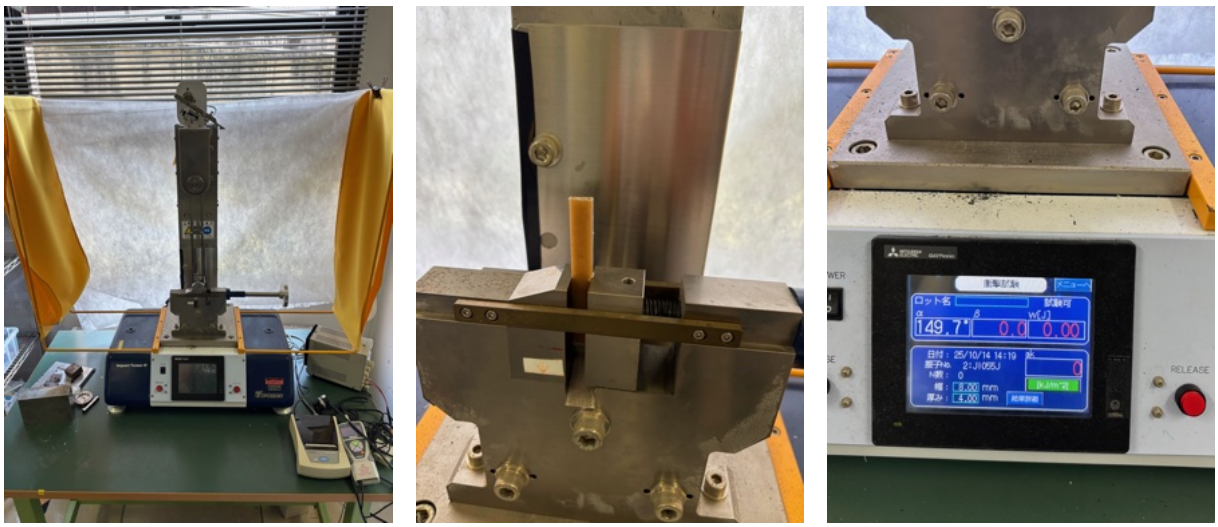

(a) (b) (c)

Figure 4.9: Impact test: (a) impact test machine overview; (b) impact test set-up; (c) impact test machine monitor.

Test conditions are summarized in Table 4.6.

| Parameter | Value | Unit |
|---|---|---|
| **Pendulum nominal energy (hammer energy)** | 5.5 | $J$ |
| **$\alpha$ release angle** | 149.7 | ° |
| **$\alpha$' corrected release angle** | 148.4 | ° |
| **Instrument calibration constant** | 2.943 | – |
| **Number of specimens (virgin materials)** | 7 | – |
| **Number of specimens (recycled materials)** | 3 or 5 | – |

Table 4.6: Impact test conditions.

No additional post-processing calculations were required for the impact results. For each test, the pendulum impact tester directly provided the absorbed energy W and the corresponding impact toughness $a_k$ once the specimen geometry (including the nominal cross-sectional dimensions at the notch and notch specification) had been entered in the instrument software. In particular, the absorbed energy W is computed by the instrument from the pendulum angles using the pendulum calibration constant WR reported in the Table 4.6. In the adopted configuration, the tester evaluates the energy loss between the post-fracture rise angle $\beta$ and a corrected reference angle $\alpha'$ (used to account for friction losses), according to:

$$W = WR\,(\cos\beta - \cos\alpha')$$

The impact toughness $a_k$ is then computed by normalizing the absorbed energy by the ligament cross-sectional area at the notch:

$a_k = \frac{W}{A}$ and reported in kJ/m$^2$.

The following outputs were therefore reported (the results are shown and discussed in the subsequent Chapter 5):

- Absorbed energy W: the energy dissipated during the impact event to initiate and propagate fracture in the notched specimen, as directly measured by the pendulum impact tester from the loss of pendulum potential energy.
- Impact toughness $a_k$ (notched impact strength): the absorbed energy normalized by the ligament cross-sectional area at the notch, in accordance with ISO 180. This parameter represents the material's specific impact energy absorption capability (energy per unit area) under a notched, dynamic loading condition, thus enabling a

more meaningful comparison between specimens by accounting for their geometry and effective fracture section.

For each formulation, the reported values correspond to the mean of seven specimens for virgin materials and three or five specimens for recycled materials. Data scatter was quantified using standard deviation, as reported in Chapter 5.

## 4.6. Water uptake test

Water uptake was measured to quantify the moisture absorption behavior of selected virgin composites as a function of immersion time and temperature. This test was performed only on virgin materials, specifically PF15(1), PF30, JF15, and JF30. Water uptake tests were not carried out on recycled materials. The procedure was based on ISO 62, with minor adaptations in specimen geometry, immersion temperatures, and measurement schedule to match the scope of this study.

Water uptake specimens were obtained from the central rectangular section of an ISO 527 tensile specimen for each material. For each formulation, five small coupons were prepared from the same parent tensile specimen in order to ensure comparable processing history within the material set. The coupons were approximately 10 mm × 10 mm with a thickness of approximately 4 mm. Since the water uptake calculations were based on mass variation, individual specimen dimensions were not measured; nominal dimensions are reported for completeness in Table 4.7.

| Parameter | Value | Unit |
|---|---|---|
| **Length** | $\approx 10$ | $mm$ |
| **Width** | $\approx 10$ | $mm$ |
| **Thickness** | $\approx 4$ | $mm$ |

Table 4.7: Water uptake test specimen dimensions.

Before immersion, all coupons were dried for 24 h using the dryer described in Chapter 3. After drying, the initial dry mass $m_0$ was recorded for each coupon. Figure 4.10 shows representative specimens before immersion. Mass measurements were carried out using an analytical balance (manufacturer Alfa Mirage, model SD-200L) with a readability of 0.1 mg. Since the same balance was used for both density measurements and water uptake mass measurements, the balance is not shown again here; reference is made to

Figure 4.3a. The immersion medium was deionized water, and specimens were stored in covered containers to minimize evaporation and maintain consistent conditions.

Figure 4.10: Water uptake test specimens.

Two immersion temperatures were investigated for a total duration of six weeks:

- 20 °C immersion: specimens were immersed in water and stored in a room maintained at 20 °C, as shown in Figure 4.11a
- 60 °C immersion: specimens were immersed in water maintained at 60 °C using thermostatic water bath (manufacturer Grant Instruments Ltd., England, model JB2), as shown in Figure 4.11b.

(a)

(b)

Figure 4.11: Water uptake test set-up: (a) water uptake test set-up at 20 °C; (b) water uptake test set-up at 60 °C.

For each material, five coupons were immersed under each condition; however, due to

time constraints and to limit repeated handling, only three specimens per material were periodically removed and weighed during the six-week exposure. The remaining specimens were kept immersed for the full duration. The specific number of measurements and the exact time points used in this study are reported in Chapter 5. At each measurement time $t_i$, the selected specimens were removed from water, gently blotted with lint-free paper to remove surface water, and weighed immediately to determine the wet mass $m(t_i)$. After weighing, specimens were returned to the corresponding bath.

Test conditions are summarized in Table 4.8.

| Parameter | Value | Unit |
|---|---|---|
| **Temperature** | 20 or 60 | $°C$ |
| **Immersion duration** | 6 | *weeks* |
| **Immersion medium** | distilled water | – |
| **Number of specimens prepared (virgin materials)** | 5 | – |
| **Number of specimens monitored (virgin materials)** | 3 | – |
| **Number of specimens prepared (recycled materials)** | 0 | – |

Table 4.8: Water uptake test conditions.

Water uptake was expressed as percentage mass gain relative to the initial dry mass:

$WA(t) = \frac{m(t)-m_0}{m_0} \cdot 100$

where $m_0$ is the dry mass recorded after 24 h drying and m(t) is the specimen mass after immersion time t. For each formulation and temperature condition, reported values correspond to the mean of the three monitored coupons, while data scatter was quantified using standard deviation, as reported in Chapter 5.

## 4.7. SEM observations

Scanning Electron Microscopy (SEM) observations were carried out to investigate the fracture surfaces and microstructural features of the composites after mechanical testing. SEM analysis was performed for all investigated materials and for each mechanical test type, namely tensile, bending, and impact tests; water uptake specimens were not analyzed by SEM.

SEM samples were obtained from fractured specimens after mechanical testing to ensure that the observed surfaces were representative of the failure mechanisms under the applied

loading conditions. For each formulation, fragments were collected from:

- tensile-tested ISO 527 specimens (fracture surface in the gauge region),
- flexural specimens after three-point bending failure (fracture region),
- notched Izod specimens after impact fracture (fracture region).

Prior to observation, specimens were handled to avoid contamination of the fracture surfaces (no polishing or mechanical alteration of the fracture plane was performed). When needed, small fragments were sectioned from the fractured parts to fit the SEM sample holder. Each fragment was mounted on an SEM stub using conductive carbon tape (Nisshin EM Co., Ltd., SV-8020), with the fracture surface oriented towards the electron beam. The mounting procedure and the stub used are shown in Figure 4.12b.

SEM observations were performed using a scanning electron microscope (manufacturer Hitachi, model Miniscope TM3030Plus), shown in Figure 4.12a. Images were acquired in secondary electron (SE) mode to emphasize surface topography and in backscattered electron (BSE) mode to enhance compositional contrast, depending on the features of interest. Magnification ranged from ×40 to ×2.0k; the SEM control software interface used to set and monitor the imaging parameters is shown in Figure 4.12c.


(a) (b) (c)

Figure 4.12: SEM: (a) SEM machine overview; (b) SEM set-up; (c) SEM software.

For each material and test type, SEM imaging was performed following a consistent acquisition protocol to enable qualitative comparison among formulations. After reaching stable vacuum and imaging conditions, the fracture surface was initially inspected at low magnification to identify representative regions (e.g., fiber-rich zones, matrix-dominated

zones, and interfaces). Higher-magnification images were then acquired to document microstructural features relevant to fracture and damage development, such as fiber pull-out and debonding evidence, interfacial adhesion characteristics, matrix plastic deformation and crack propagation patterns, voids/porosity and local defects, and fiber distribution and breakage morphology.

# 5 | Results and discussion

## 5.1. Chapter overview

This chapter presents and discusses the physical and mechanical results obtained for polypropylene (PP) composites reinforced with pineapple fibers (PF), jute fibers (JF), and their hybrid combinations (HYB), produced both as virgin and recycled materials. Neat PP (unreinforced polypropylene) was also manufactured and tested as a baseline reference, enabling direct quantification of the net effect of fiber reinforcement and of recycling relative to the same matrix processed under comparable conditions. The aim is to assess how the main variables (fiber type, fiber content, hybridization, recycling, and (for PF15) feeding strategy) affect density, quasi-static response, dynamic fracture resistance, and moisture sensitivity, supported where available by SEM evidence.

Seven virgin compounds were manufactured (PF15(1), PF15(2), PF30, JF15, JF30, HYB15, HYB30) plus neat PP as baseline; recycled counterparts were obtained by reprocessing the corresponding materials (excluding PF15(1)). The experimental campaign includes density, tensile, and impact tests for all virgin and recycled formulations (with neat PP reported when relevant), flexural tests for virgin only, water uptake tests for PF and JF at 15 and 30 wt%, and SEM observations to support microstructural and fracture-mechanism interpretation.

For clarity, a summary table is provided (Table 5.1) listing each formulation and indicating which datasets are available. This table is intended as a roadmap to guide the reader through the comparisons, especially since not all tests were performed for all material families.

| Material | Family | Density | Tensile | Flexural | Impact | Water uptake |
|---|---|---|---|---|---|---|
| **PP** | virgin | ✓ | ✓ | – | ✓ | – |
| **PF15(1)** | virgin | ✓ | ✓ | ✓ | ✓ | ✓ |
| **PF15(2)** | virgin | ✓ | ✓ | ✓ | ✓ | – |
| **PF30** | virgin | ✓ | ✓ | ✓ | ✓ | ✓ |
| **JF15** | virgin | ✓ | ✓ | ✓ | ✓ | ✓ |
| **JF30** | virgin | ✓ | ✓ | ✓ | ✓ | ✓ |
| **HYB15** | virgin | ✓ | ✓ | ✓ | ✓ | – |
| **HYB30** | virgin | ✓ | ✓ | ✓ | ✓ | – |
| **PPR** | recycled | ✓ | ✓ | – | ✓ | – |
| **PF15(1)R** | recycled | ✓ | – | – | – | – |
| **PF15(2)R** | recycled | ✓ | ✓ | – | ✓ | – |
| **PF30R** | recycled | ✓ | ✓ | – | ✓ | – |
| **JF15R** | recycled | ✓ | ✓ | – | ✓ | – |
| **JF30R** | recycled | ✓ | ✓ | – | ✓ | – |
| **HYB15R** | recycled | ✓ | ✓ | – | ✓ | – |
| **HYB30R** | recycled | ✓ | ✓ | – | ✓ | – |

Table 5.1: Summary of the investigated formulations and corresponding experimental datasets.

To ensure a consistent interpretation across the dataset, results are discussed according to the following comparison axes:

- **Fiber type effect** (PF vs. JF at constant fiber content): comparisons at 15 and 30 wt%.
- **Fiber content effect** (15 vs. 30 wt% within each fiber family): reinforcement efficiency.
- **Hybridization effect** (HYB relative to single-fiber references): HYB15 and HYB30 compared with PF/JF at matched total content.
- **Recycling effect** (recycled vs. virgin): property changes after reprocessing for each formulation.

To support these comparisons, the following sections report results using consistent data-

reduction rules and reporting conventions. Detailed testing standards, specimen geometries, and experimental setups were described in Chapter 4; here, only the processing steps that directly affect the interpretation are summarized.

All plots and tables report mean values together with scatter (standard deviation), since variability is an important outcome for natural-fiber composites where performance can be sensitive to dispersion, void content, and interfacial quality. The reported metrics follow the definitions introduced in Chapter 4:

- **Density ($\rho$)**: experimental density for all materials; when referenced, deviations from theoretical density are used as an indirect indication of consolidation and potential void content.
- **Tensile tests**: elastic modulus $E$, tensile strength $\sigma_M$, and elongation at break $\varepsilon_B$; complete stress–strain curves are provided in the Appendix to support qualitative interpretation.
- **Flexural tests (virgin only)**: flexural modulus $E_f$, maximum flexural stress $\sigma_{f,M}$, and flexural strain at break $\varepsilon_{f,B}$.
- **Izod impact tests**: absorbed energy $W$ and impact toughness $a_k$ (energy normalized by ligament area at the notch).
- **Water uptake tests**: mass gain $\Delta w$ (%) vs. immersion time for PF and JF composites at 15 and 30 wt%.

For each formulation and test type, multiple specimens were tested (replicate numbers are reported in Chapter 4 and are not repeated here). Data were excluded only when clear, traceable anomalies were documented, and exclusions were kept to the minimum necessary to ensure reliability and applied consistently across material families.

## 5.2. Density results

Density is presented first because it provides a direct physical baseline for the investigated materials and an indirect indication of processing quality. In natural-fiber composites, deviations of the experimental density from expected (theoretical) values can reflect the presence of voids/porosity, incomplete impregnation, or non-uniform fiber dispersion, all of which can significantly influence mechanical behavior, especially strength and impact resistance. For this reason, density results are used throughout this chapter as supporting evidence when interpreting tensile, flexural, and impact trends.

In addition to the composite formulations, the density of neat polypropylene (PP) is

reported as a reference baseline. This allows the density increase associated with fiber addition to be quantified and provides a consistent frame of comparison across compounds.

Figure 5.1 summarizes the average experimental density values for neat PP and for all virgin and recycled composites, together with the corresponding theoretical densities, shown with the suffix "T" in the ID of the material. The theoretical density of each formulation was calculated from the nominal composition using a rule of mixtures approach based on mass fractions. In particular, the theoretical composite density was obtained as

$$\rho_t = \left(\sum_i \frac{w_i}{\rho_i}\right)^{-1},$$

where $w_i$ and $\rho_i$ are the mass fraction and density of each constituent (PP, PF, and/or JF), respectively (see Chapter 3). This reference allows deviations of the experimental density from $\rho_t$ to be interpreted as an indirect indication of processing effects such as void content and consolidation quality.

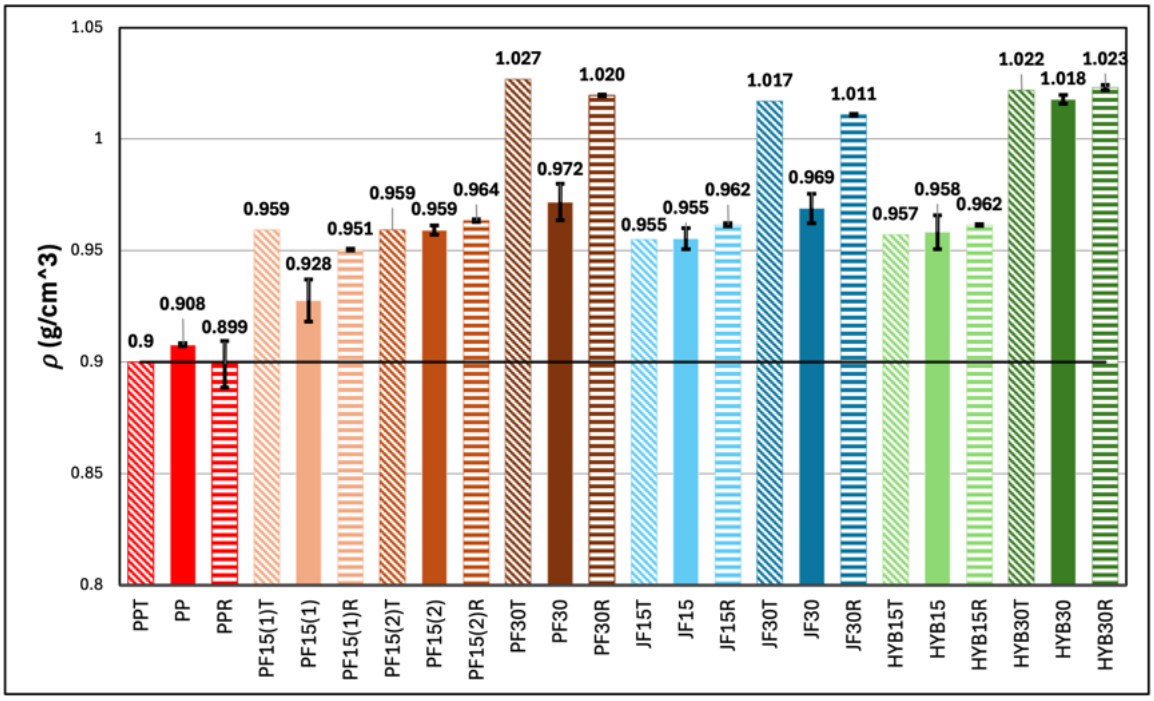


Figure 5.1: Average density of neat polypropylene (PP) and of all investigated composites. For each formulation, theoretical density (suffix "T") is shown using diagonal stripe bars, while virgin compounds are represented by fully filled bars, and recycled compounds are represented by horizontally striped bars (suffix "R"). Materials are grouped by fiber type and by fiber content, with recycled counterparts reported next to their corresponding virgin reference. The neat PP density is reported as baseline.

A lower experimental density than expected at fixed composition is commonly associ-

ated with voids and porosity, while a closer agreement with theoretical density suggests improved impregnation and reduced void volume fraction. These effects are especially relevant for high fiber content compounds, where increased melt viscosity and more challenging wetting/compaction conditions can promote air entrapment and incomplete consolidation.

To quantify the effect of recycling on consolidation quality, virgin and recycled compounds are compared formulation by formulation (PF15(1) vs. PF15(1)R, PF15(2) vs. PF15(2)R, PF30 vs. PF30R, JF15 vs. JF15R, JF30 vs. JF30R, HYB15 vs. HYB15R, HYB30 vs. HYB30R). The recycling effect on density is summarized in Figure 5.2.

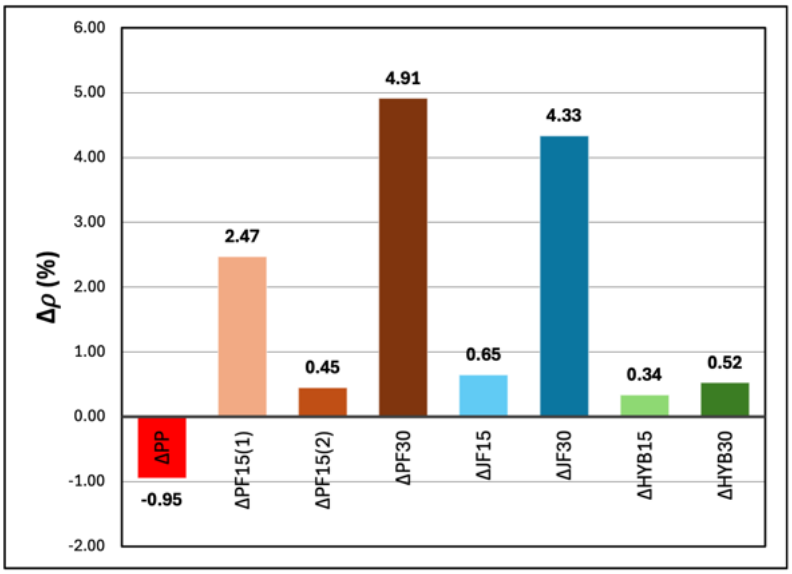


Figure 5.2: Relative density variation between recycled and virgin compounds, computed as $\Delta\rho = (\rho_R - \rho_V)/\rho_V \cdot 100\%$.

All recycled composites exhibit a positive $\Delta\rho$, indicating a systematic densification after reprocessing. The magnitude is particularly pronounced for the 30 wt% single-fiber composites (PF30 and JF30), whereas it remains below 1% for the 15 wt% compounds and for the hybrid systems. These trends are consistent with the qualitative microstructural evidence (Section 4.7), which indicates a reduction of voids and porosity after recycling.

In contrast, neat PP shows a small negative density variation after reprocessing ($\Delta\rho \approx -0.95\%$). Even for unfilled PP, repeated melting and solidification can modify the crystallization state and the final microstructure, so small density changes (positive or negative) may arise from differences in thermal history, crystallinity, and/or the presence of microvoids introduced during processing [9]. Given the limited magnitude, this variation is also considered in light of experimental scatter.

The PF15(1) vs. PF15(2) comparison provides a focused case study to quantify how the compounding feeding strategy affects consolidation quality. Although both materials were designed with the same nominal composition (15 wt% PF in PP), the experimental density results (Figure 5.1) show a clear difference: PF15(1) exhibits a lower absolute density than PF15(2). For PF15(1), the adopted feeding route may also have limited the ability to guarantee the target theoretical composition locally, in addition to producing poorer impregnation and a more heterogeneous microstructure.

The density variation supports this interpretation. As shown in Figure 5.2, PF15(1) undergoes a markedly larger densification after recycling ($\Delta\rho \approx 2.47\%$) than PF15(2) ($\Delta\rho \approx 0.45\%$). This indicates that reprocessing is particularly effective in reducing the defect population of PF15(1), whereas PF15(2) is already relatively well consolidated in the virgin state and therefore shows limited room for further densification.

## 5.3. Tensile behavior

Tensile results provide the core mechanical assessment of the investigated materials and enable a consistent comparison across virgin and recycled formulations. The discussion focuses on three key aspects: (i) stiffness, quantified by the tensile modulus E, as an indicator of reinforcement efficiency and load transfer; (ii) strength, quantified here by the ultimate tensile strength (UTS), which is strongly affected by defects and interfacial quality; and (iii) ductility, quantified by the elongation at break, which reflects the typical loss of deformation capacity. When relevant, trends are interpreted using density results and the observed porosity reduction after recycling.

### 5.3.1. Representative stress-strain response

The complete set of stress–strain curves (Appendix A.3 and A.4) provides qualitative insight into deformation mechanisms and failure behavior across the investigated systems. Neat PP exhibits a highly ductile response with large plastic deformation prior to fracture, while all fiber-reinforced composites show markedly reduced strain at break and a more abrupt fracture behavior, consistent with the introduction of rigid reinforcements and defect failure mechanisms.

Across composite families, the curves confirm the expected stiffening effect of fiber addition, visible as a steeper initial slope compared to PP, and a progressive reduction of post-yield deformation at increasing fiber content. Differences in curve shape and scatter among formulations are also informative: larger scatter typically reflects greater

microstructural heterogeneity (e.g., local fiber clustering, voids, or variable interfacial conditions), whereas more consistent curves indicate improved process repeatability and more uniform dispersion/impregnation.

Virgin and recycled curve sets further highlight that reprocessing may increase stiffness (often consistent with densification) while modifying strength and fracture strain. This indicates that recycling can simultaneously improve consolidation (reducing void-related stress concentrators) and introduce competing effects such as fiber damage/shortening or matrix degradation. These aspects are addressed quantitatively in the following subsections and interpreted consistently using density and, where relevant, impact and water uptake results.

### 5.3.2. Elastic modulus

Figure 5.3 reports the tensile modulus $E$ for neat PP and for all virgin and recycled composites.

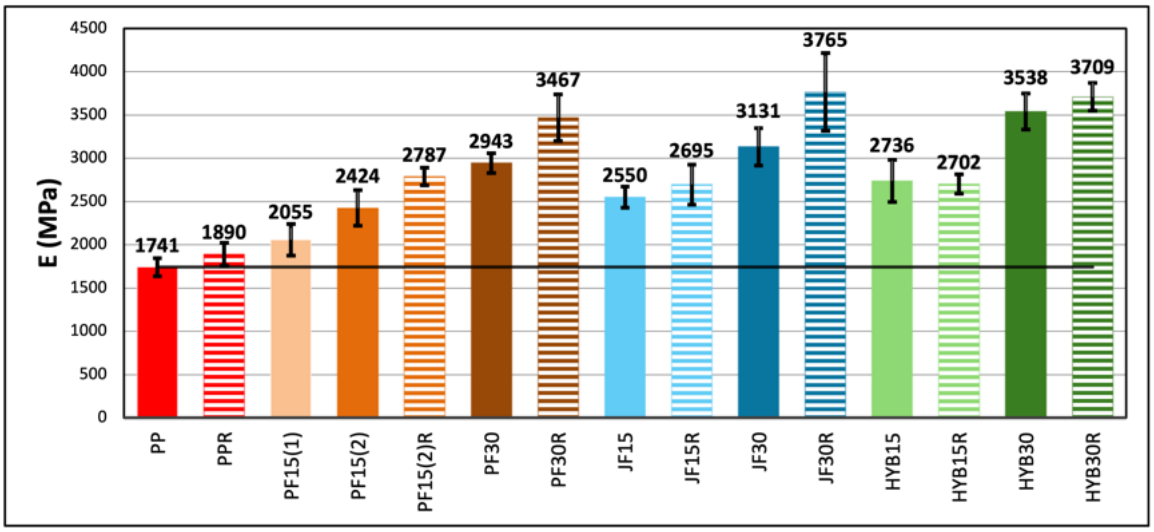


Figure 5.3: Average elastic modulus of neat polypropylene (PP) and of all investigated composites. For each formulation, virgin compounds are represented by fully filled bars and recycled compounds are represented by striped bars (suffix "R"). Materials are grouped by fiber type and by fiber content, with recycled counterparts reported next to their corresponding virgin reference. The neat PP elastic modulus is reported as baseline.

Tensile modulus increases with fiber addition, confirming the expected stiffening effect of natural-fiber reinforcement relative to neat PP. For all families, moving from 15 to 30 wt% produces a clear modulus increase, indicating a progressively more fiber-dominated elastic response.

Within the PF family, the modulus is strongly affected by the PF15 feeding strategy: PF15(2) is distinctly stiffer than PF15(1), showing that processing quality and consolidation can significantly influence reinforcement efficiency even at constant nominal composition. Increasing PF content to 30 wt% further raises stiffness. Recycling generally increases modulus, with the strongest effect observed for the high-fiber PF30 system, consistent with the densification and porosity reduction discussed in the density section.

JF composites follow the same overall behavior, with higher modulus at 30 wt% than at 15 wt%. Compared at constant content, JF-based materials tend to be slightly stiffer than PF-based ones, and the modulus increasing after recycling is particularly pronounced for JF30, again consistent with the large densification measured after reprocessing.

Hybrid composites also show high stiffness. At 15 wt%, HYB15 is comparable to the single-fiber references, whereas at 30 wt% HYB30 reaches one of the highest modulus levels in the dataset. Recycling produces a moderate modulus gain for HYB30, while changes at 15 wt% are limited, suggesting that at lower reinforcement levels stiffness is less sensitive to the consolidation improvements achieved by reprocessing.

Overall, modulus trends highlight four key points: stiffness increases with fiber content, PF15(2) outperforms PF15(1) due to the feeding strategy, JF systems are generally stiffer than PF at equal content, and the highest stiffening occurs after recycling for the 30 wt% composites.

### 5.3.3. Tensile strength

Figure 5.4 summarizes the ultimate tensile strength (UTS) of neat PP and of all investigated composites.

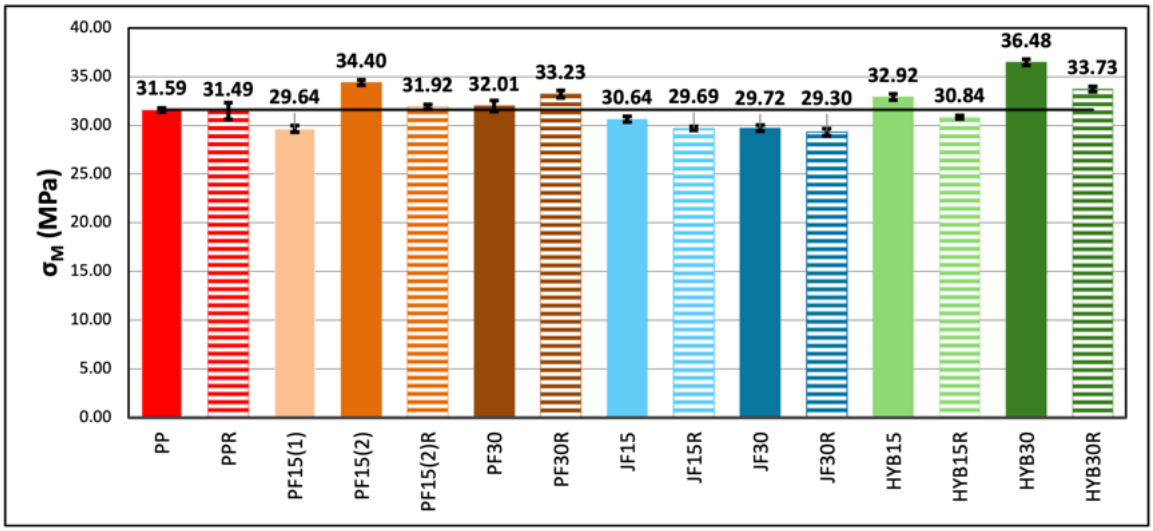


Figure 5.4: Average tensile strength of neat polypropylene (PP) and of all investigated composites. For each formulation, virgin compounds are represented by fully filled bars and recycled compounds are represented by striped bars (suffix "R"). Materials are grouped by fiber type and by fiber content, with recycled counterparts reported next to their corresponding virgin reference. The neat PP tensile strength is reported as baseline.

Unlike stiffness, strength does not increase monotonically with fiber content, reflecting the strong sensitivity of UTS to defects and interfacial quality in natural-fiber composites. A key outcome is that most composite UTS values remain relatively close to the neat PP reference, indicating that tensile strength is only weakly improved by fiber addition and remains largely controlled by matrix. In this dataset, recycling generally causes a slight reduction in UTS for most formulations, suggesting that densification benefits do not necessarily translate into higher strength when competing effects such as fiber damage and matrix or interface degradation are present. The main exception is PF30, which shows a small UTS increase after recycling. Finally, JF-based composites are the only group that stays below the neat PP baseline in both virgin and recycled conditions. This is probably a consequence of weaker adhesion of PP and JF, a factor that should be investigated in more detail in future studies.

### 5.3.4. Elongation at break

Figure 5.5 reports the elongation at break for all composites.

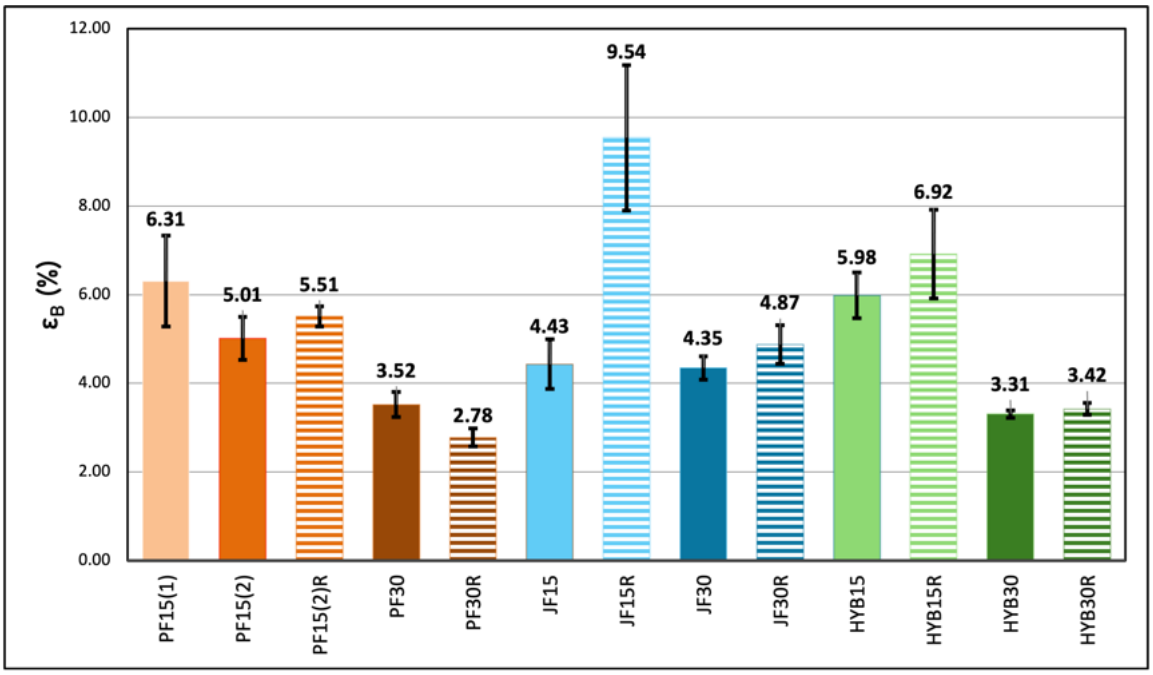


Figure 5.5: Average elongation at break of all investigated composites. For each formulation, virgin compounds are represented by fully filled bars and recycled compounds are represented by striped bars (suffix "R"). Materials are grouped by fiber type and by fiber content, with recycled counterparts reported next to their corresponding virgin reference.

As expected, adding natural fibers strongly reduces ductility compared to neat PP, indicating a shift from a highly ductile polymer response to a more brittle behavior. The elongation at break of neat PP is not reported here because several PP specimens did not reach fracture within the software limits (maximum crosshead displacement 30 mm), so a reliable $\varepsilon_B$ could not be extracted; however, it is clearly much higher than that of all composites. Moreover, the PP supplier datasheet reports an elongation at break of about 30% (see Chapter 3).

A clear overall trend is observed after recycling: elongation at break increases for most formulations, suggesting that reprocessing often allows slightly larger deformation before fracture, possibly through improved consolidation and reduced premature failure triggered by voids. The main exceptions is PF30, for which recycling is associated with a more brittle response. Although tensile toughness was not explicitly reported as a standalone metric, formulations with higher $\varepsilon_B$ at comparable strength are expected to absorb more tensile energy.

## 5.4. Flexural behavior

Flexural results are reported for the virgin compounds to complement the tensile analysis and to assess performance under bending. Since bending produces tensile and compressive stresses across the specimen thickness, flexural response is especially sensitive to surface defects, local fiber distribution, and compressive instabilities [3]. For this reason, flexural properties are discussed mainly as comparative trends across formulations rather than as values directly comparable to tensile metrics.

### 5.4.1. Flexural modulus

Figure 5.6 reports the flexural modulus $E_f$ for the virgin PF-, JF-, and hybrid composites.

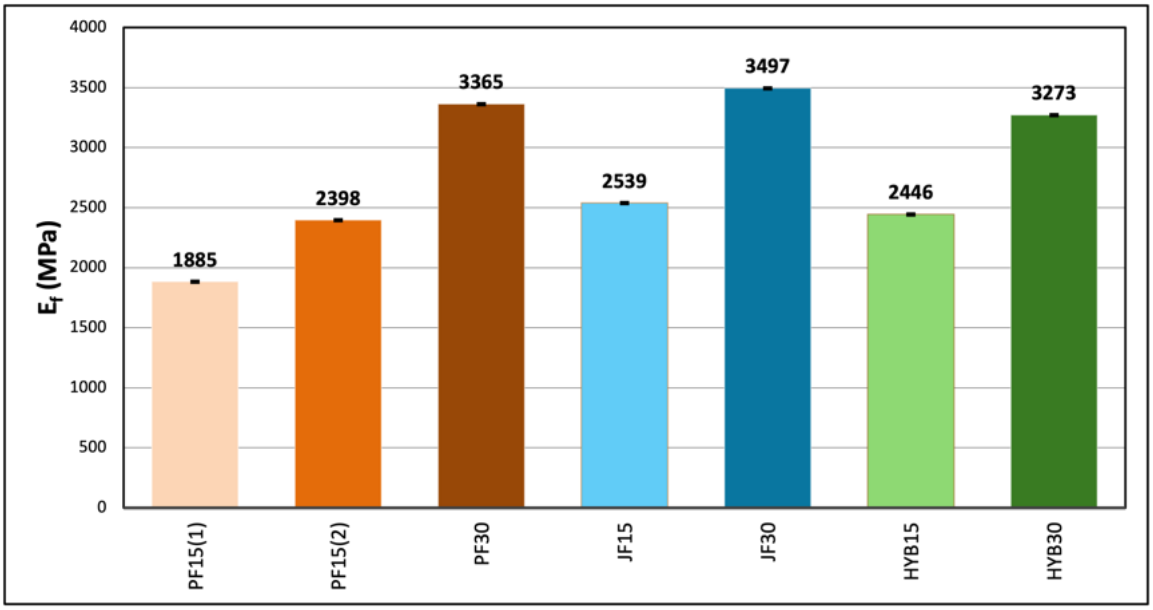


Figure 5.6: Average flexural modulus of all virgin composites, represented by fully filled bars. Materials are grouped by fiber type and by fiber content.

The dominant trend is a strong stiffness increase with fiber content for all families. For PF composites, $E_f$ increases from PF15 to PF30. A similar stiffness increase with fiber content is observed for JF systems, with JF30 showing the highest flexural modulus among the tested materials. Hybrid composites follow the same trend.

Comparing fiber types at equal fiber content, JF-based composites show slightly higher flexural modulus than PF-based composites at both 15 wt% and 30 wt%, suggesting a marginally more effective stiffness contribution under bending for the jute reinforcement in the present processing conditions. Overall, the increase of fiber content is the main

factor controlling $E_f$, while differences between PF and JF remain smaller.

Hybrid composites show intermediate behavior at 15 wt%, comparable to single-fiber 15 wt% formulations, while at 30 wt% the hybrid modulus approaches the stiffness of the 30 wt% single-fiber systems. This suggests that, in terms of flexural stiffness, hybridization does not introduce a strong synergistic effect beyond what is primarily dictated by total fiber fraction.

### 5.4.2. Flexural strength and strain at break

Figure 5.7 summarizes flexural strength $\sigma_{f,M}$ for the virgin composites.

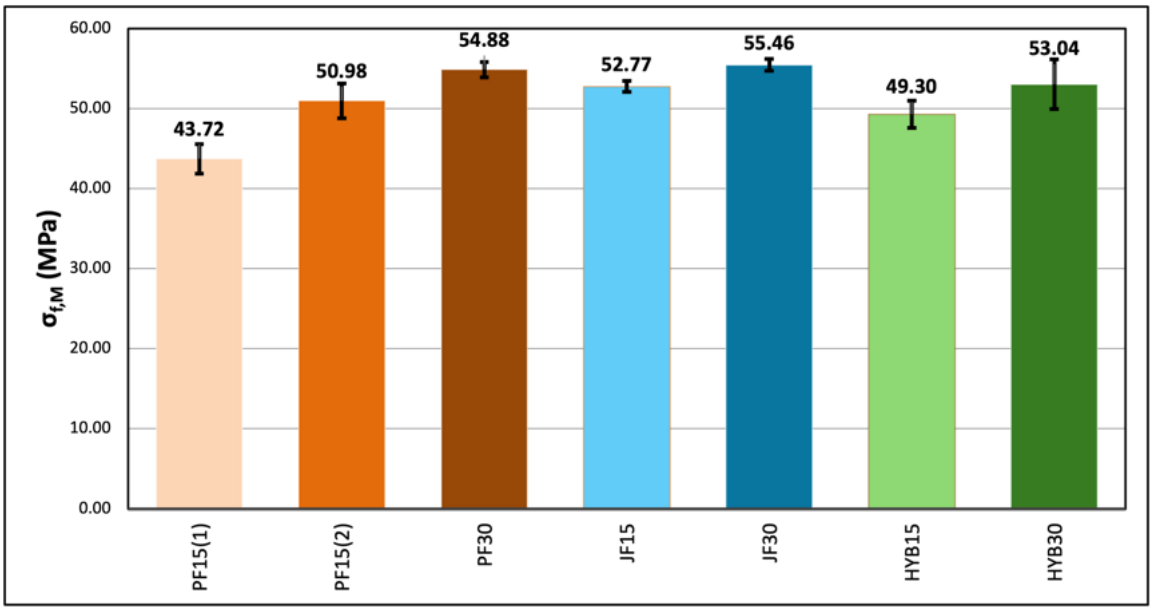


Figure 5.7: Average flexural strength of all virgin composites, represented by fully filled bars. Materials are grouped by fiber type and by fiber content.

Strength increases with fiber content within each family, with JF30 showing the highest flexural strength in the dataset. Hybrid composites follow the same increasing trend with fiber content, although their values remain comparable to single-fiber materials at the same total fiber content. At both fiber contents, JF-based systems tend to exhibit slightly higher flexural strength than PF and hybrid counterparts, indicating a modest advantage under bending in this specific test set.

Figure 5.8 reports flexural strain at break $\varepsilon_{f,B}$, which displays the opposite trend.

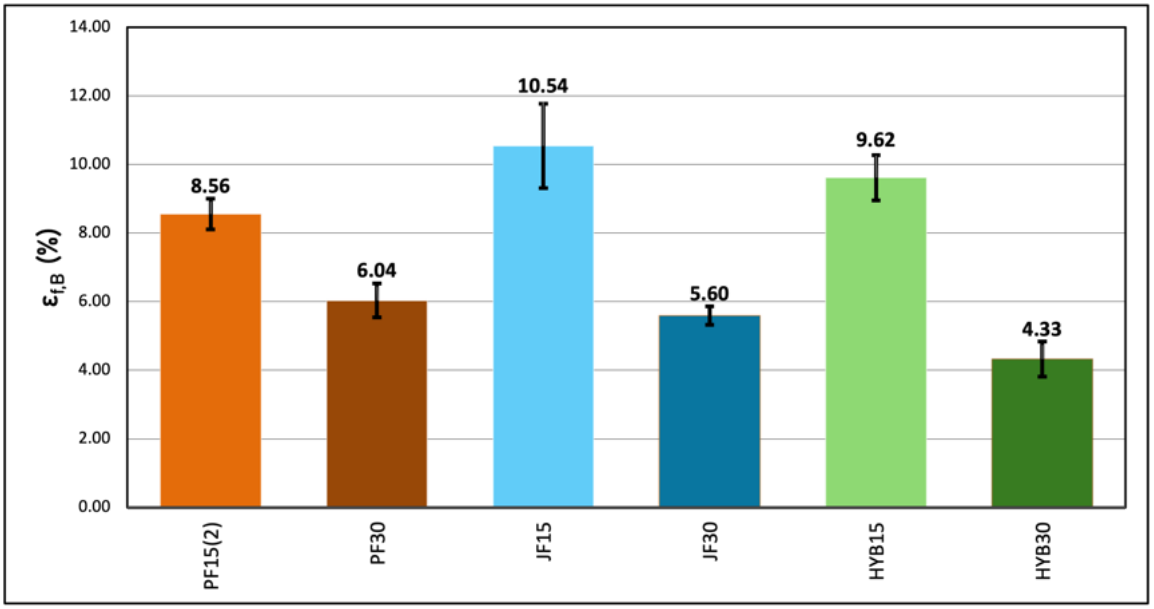


Figure 5.8: Average flexural elongation at break of all virgin composites, represented by fully filled bars. Materials are grouped by fiber type and by fiber content.

$\varepsilon_{f,B}$ decreases markedly with increasing fiber content. It should be noted that $\varepsilon_{f,B}$ could not be determined for PF15(1), because the specimen did not fracture within the imposed displacement limit set in the testing software; the test was therefore automatically stopped at the predefined threshold and the recorded value does not correspond to a true fracture strain. For all formulations, a decrease in elongation at break with increasing fiber content is evident. For JF composites, the reduction is more pronounced, than for PF composites. Hybrid composites show a similar drop, with HYB30 exhibiting the lowest value among the tested materials.

This behavior confirms the expected trend: increasing fiber fraction enhances bending stiffness and strength, but it reduces deformation capability and promotes a more brittle failure response.

## 5.5. Impact behavior (Izod)

Impact results are discussed to assess dynamic fracture resistance and notch sensitivity, which are particularly affected by microstructural defects and interfacial debonding in natural-fiber composites. In notched Izod testing, the fracture process is typically governed by crack initiation at the notch root and subsequent crack propagation through a heterogeneous microstructure. Both absorbed energy $W$ and impact toughness $a_k$ are reported; while W directly reflects the pendulum energy loss, $a_K$ normalizes the response

by the net section and is adopted here as the primary metric for comparison.

Table 5.2 and Figure 5.9 summarize the Izod results for all investigated formulations in terms of absorbed energy $W$ and impact toughness $a_k$. Overall, impact response depends on both total fiber content and formulation, and the trends are not simply proportional to the amount of reinforcement.

| **Material** | $W$ **(J)** | $a_k$ **(kJ/m$^2$)** | $\beta$ **(deg)** |
|---|---|---|---|
| **PF15(1)** | $0.273 \pm 0.011$ | $8.506 \pm 0.282$ | $139.429 \pm 0.269$ |
| **PF15(2)** | $0.236 \pm 0.014$ | $7.412 \pm 0.427$ | $140.486 \pm 0.418$ |
| **PF15(2)R** | $0.207 \pm 0.015$ | $6.484 \pm 0.530$ | $141.400 \pm 0.529$ |
| **PF30** | $0.414 \pm 0.011$ | $12.928 \pm 0.344$ | $135.371 \pm 0.304$ |
| **PF30R** | $0.220 \pm 0.010$ | $6.846 \pm 0.292$ | $141.040 \pm 0.288$ |
| **JF15** | $0.203 \pm 0.008$ | $6.339 \pm 0.207$ | $141.543 \pm 0.207$ |
| **JF15R** | $0.160 \pm 0.010$ | $5.033 \pm 0.342$ | $142.867 \pm 0.351$ |
| **JF30** | $0.300 \pm 0.006$ | $9.427 \pm 0.212$ | $138.557 \pm 0.199$ |
| **JF30R** | $0.193 \pm 0.013$ | $6.083 \pm 0.432$ | $141.800 \pm 0.432$ |
| **HYB15** | $0.207 \pm 0.010$ | $6.497 \pm 0.242$ | $141.386 \pm 0.241$ |
| **HYB15R** | $0.174 \pm 0.023$ | $5.415 \pm 0.758$ | $142.480 \pm 0.766$ |
| **HYB30** | $0.311 \pm 0.012$ | $9.748 \pm 0.356$ | $138.257 \pm 0.331$ |
| **HYB30R** | $0.258 \pm 0.004$ | $8.035 \pm 0.135$ | $139.880 \pm 0.130$ |

Table 5.2: Izod impact results for the investigated composites (mean ± SD): absorbed energy $W$, impact toughness $a_k$ (normalized by net section), and pendulum angle $\beta$.

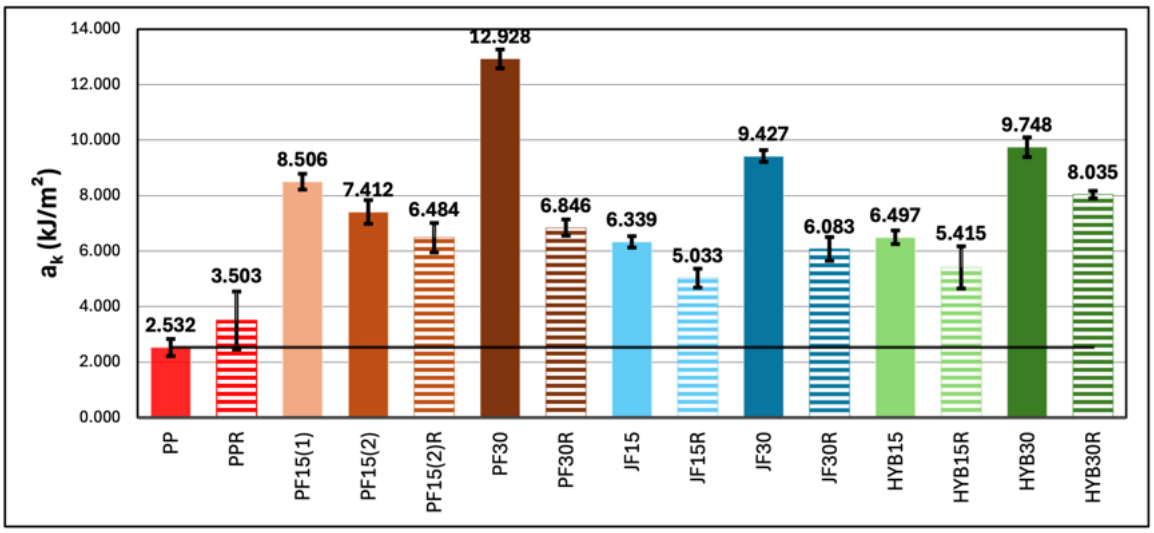


Figure 5.9: Average impact toughness of all investigated composites. For each formulation, virgin compounds are represented by fully filled bars and recycled compounds are represented by striped bars (suffix "R"). Materials are grouped by fiber type and by fiber content, with recycled counterparts reported next to their corresponding virgin reference.

Across virgin materials, impact toughness generally increases from 15 to 30 wt% for PF, JF, and HYB systems, indicating that higher fiber content can enhance dynamic energy absorption when crack propagation activates mechanisms such as crack bridging and fiber pull-out. The PF family shows the strongest content effect, with PF30 providing the highest toughness in the dataset. For JF and HYB systems, the 30 wt% formulations also outperform their 15 wt% counterparts, but they remain below PF30.

A clear additional trend is observed when comparing virgin and recycled states: impact toughness decreases after recycling for every formulation in Figure 5.9. This indicates that, even though recycling improves density (reduced porosity), reprocessing tends to penalize notch-impact resistance, likely because dynamic fracture is highly sensitive to fiber integrity (effective fiber length/aspect ratio) and to matrix embrittlement. Therefore, impact behavior is interpreted together with density and SEM evidence in the following sections.

Finally, the comparison between PF15(1) and PF15(2) shows that processing strategy can affect notch sensitivity even at constant composition: PF15(1) displays slightly higher impact toughness than PF15(2), consistent with the idea that microstructural heterogeneity and interfacial features can modify the efficiency of dissipation mechanisms.

## 5.6. Water uptake behavior

Water uptake results are presented to evaluate moisture sensitivity and to support microstructure interpretations of mechanical behavior. Since natural fibers are intrinsically hydrophilic, moisture absorption is expected to increase with fiber content and to depend on fiber type, morphology, and interfacial quality. In addition to diffusion through the polymer matrix, water can be transported through faster pathways such as fiber/matrix interfacial channels, microcracks, and interconnected voids. Therefore, the uptake kinetics provide indirect insight into defect population and interfacial integrity, which are also key drivers of strength scatter and impact performance.

In this study, water uptake was measured for PF and JF families at two fiber contents (15 and 30 wt%) and at two temperatures (20 °C and 60 °C). The results are reported as relative mass gain $\Delta w(\%)$ versus immersion time.

Figure 5.10 and Figure 5.11 show the evolution of mass gain with immersion time at 20 °C and 60 °C.

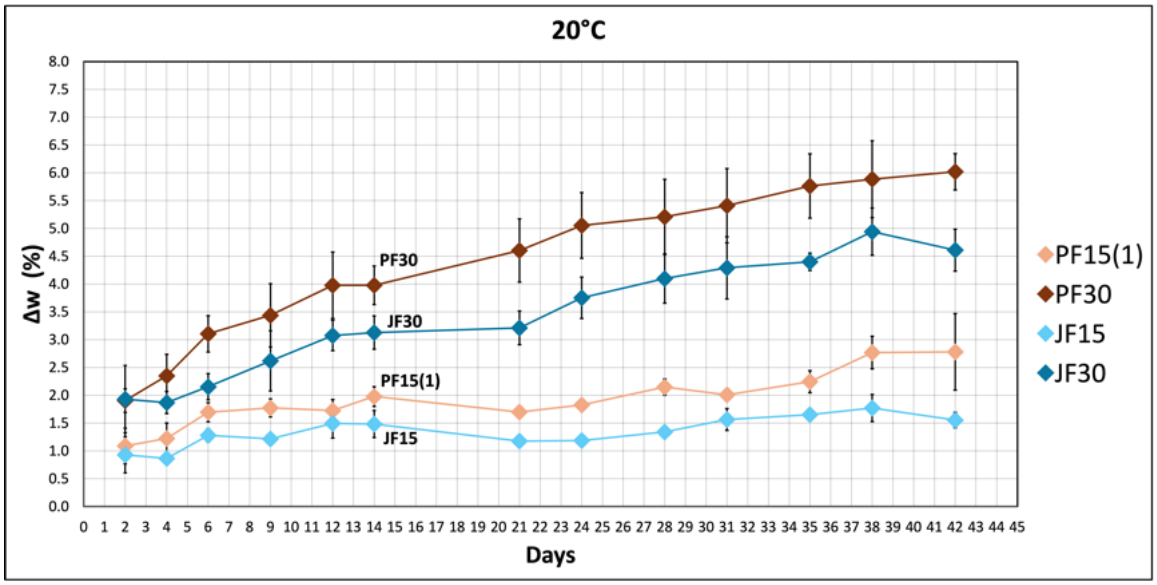


Figure 5.10: Water uptake ($\Delta w$) as a function of immersion time at 20 °C for PF- and JF-based composites (15 and 30 wt% fiber).

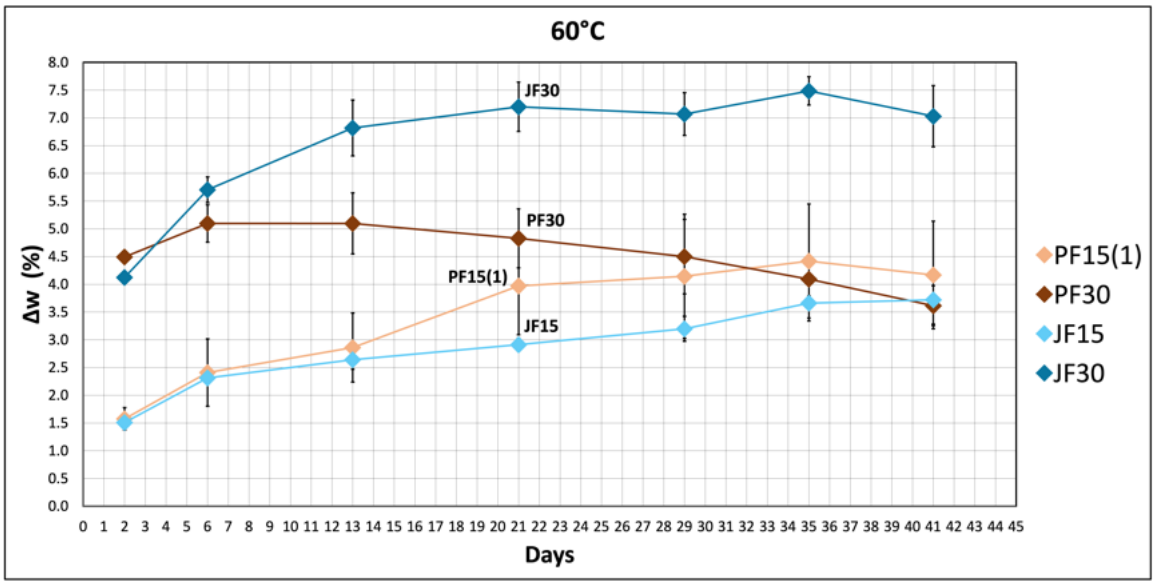


Figure 5.11: Water uptake ($\Delta w$) as a function of immersion time at 60 °C for PF- and JF-based composites (15 and 30 wt% fiber).

For all formulations, uptake increases rapidly at early times and then evolves more gradually at longer times, approaching a quasi-plateau within the exposure window. This behavior is consistent with an initial fast contribution (near-surface absorption and preferential transport paths) followed by a slower regime controlled by diffusion. Temperature strongly accelerates the kinetics: at 60 °C, all curves rise steeply within the first days and reach near-steady values earlier than at 20 °C, where uptake continues to increase more gradually over the test duration.

At 20 °C, water uptake shows a clear dependence on both fiber type and content. Increasing fiber content from 15 to 30 wt% increases the long-time mass gain for both families, consistent with a larger fraction of hydrophilic reinforcement and a more extensive fiber/matrix interfacial area that can act as a transport pathway. At long times, PF30 exhibits the highest uptake, followed by JF30, while PF15(1) remains lower and JF15 shows the lowest uptake. This indicates that, at ambient temperature, the PF-based system at 30 wt% is the most moisture sensitive in the present dataset. The relatively low uptake of JF15 suggests either a lower water-accessible fiber fraction (e.g., better wetting) or less efficient interfacial transport compared to PF15(1).

At 60 °C, uptake levels increase and the separation between curves becomes more pronounced. In this condition, JF30 shows the highest uptake, clearly exceeding the other formulations. PF15(1) and JF15 remain in an intermediate range, while PF30 displays a non-monotonic trend, with an early increase followed by a slight decrease at longer times.

While a purely absorptive process would normally increase and then level off, the slight decrease at long times may indicate competing effects during hot-water exposure, such as leaching of soluble constituents and hydrothermal damage that can promote minor material loss alongside moisture uptake [43–45].

Water uptake results can be interpreted together with density as indicators of microstructural transport pathways. Higher uptake is generally associated with a larger hydrophilic fiber fraction, a greater interfacial area, and more accessible pathways such as void networks and imperfectly sealed fiber-matrix boundaries. Although mechanical tests were conducted on dry specimens, higher moisture uptake usually indicates microstructures where fibers swell more and interfaces weaken more easily, which can increase scatter and promote crack initiation under notched loading.

Overall, these results confirm that higher fiber content increases moisture sensitivity, and that fiber type affects both the uptake level and the kinetics, especially at elevated temperature where swelling and interfacial transport become more relevant.

## 5.7. Microstructural observations (SEM)

SEM observations are used to support the interpretation of mechanical trends by providing direct evidence of microstructural features such as fiber dispersion uniformity, void population, interfacial bonding quality, and fracture morphology. For natural-fiber composites, small variations in processing and consolidation can strongly affect properties because defects act as stress concentrators and preferential crack paths. In addition, recycling can alter the microstructure through two competing effects: improved consolidation/dispersion (often reducing voids) and possible degradation mechanisms such as fiber shortening/damage and matrix embrittlement. The SEM discussion therefore follows three main comparison axes that mirror the structure of the mechanical analysis: (i) PF15 feeding strategy, (ii) fiber content (15 vs. 30 wt%), and (iii) virgin vs. recycled microstructural evolution.

SEM micrographs were acquired on fracture surfaces obtained from tensile and Izod impact tests.

The SEM analysis focuses on microstructural features that are most relevant to the mechanical response. In particular:

- **Voids and porosity:** higher void content is expected to reduce strength and impact toughness and increase scatter, consistent with density reductions and higher variability [1, 3].

- **Fiber wetting and interfacial gaps:** evidence of poor polymer impregnation around fibers and interfacial debonding gaps. Poor wetting typically reduces load transfer, penalizing strength [1, 4].
- **Pull-out length and bridging:** long pull-out traces and fiber bridging indicate energy dissipation mechanisms that can enhance impact toughness and sometimes ductility [3, 4].

These criteria are used consistently in the following subsections to rationalize why some formulations show improved stiffness but reduced impact resistance after recycling, and why PF15(1) behaves differently from PF15(2) despite identical nominal composition.

### 5.7.1. Effect of PF15 feeding strategy

PF15(1) and PF15(2) provide a controlled comparison because they share the same nominal composition (15 wt% PF in PP) while differing only in the compounding feeding strategy. SEM observations therefore help isolate processing-induced microstructural differences, which can be linked to the density results and, later in this chapter, to the mechanical response.

Figure 5.12 summarizes representative SEM micrographs of impact fracture surfaces for PF15(1) and PF15(2) at low and high magnification. The low-magnification comparison provides the clearest evidence of a processing signature: PF15(1) shows a higher defect population, including a large macroscopic cavity and extended porous regions, while PF15(2) appears more compact, with smaller and more uniformly distributed voids and a more homogeneous fracture texture. This observation is consistent with the density results, where PF15(2) exhibits a higher experimental density, indicating improved consolidation and a reduced void fraction.

At higher magnification, the micrographs are used here to illustrate representative local features of the impact fracture surfaces. The PF15(1) shows a fiber-rich region with limited matrix coverage, consistent with local bundle persistence and incomplete impregnation. The PF15(2) shows fibers, small voids, and pull-out/debonding signatures within a PP matrix background, as typically observed in natural-fiber thermoplastic composites.

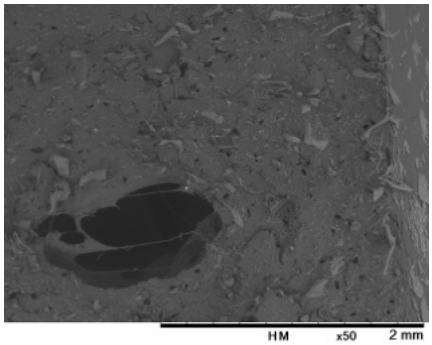


(a) PF15(1) x50, test 7 (impact).

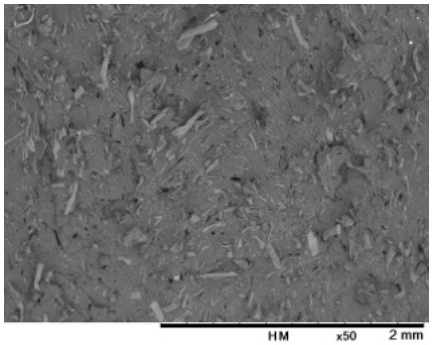


(b) PF15(2) x50, test 6 (impact).

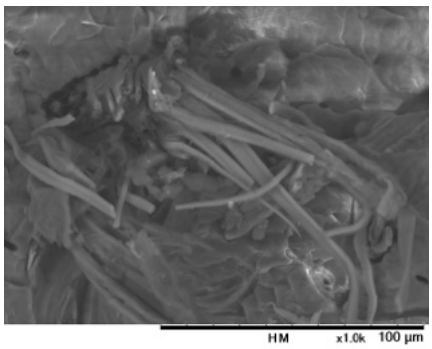


(c) PF15(1) x1.0k, test 3 (impact).

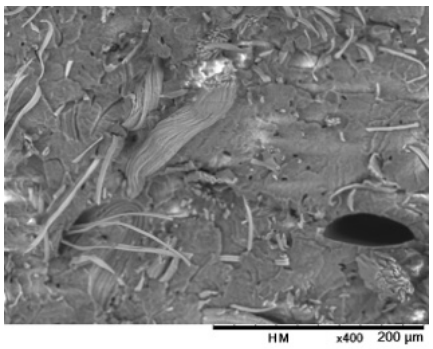


(d) PF15(2) x400, test 6 (impact).

Figure 5.12: SEM micrographs of impact fracture surfaces for PF15(1) and PF15(2) at low and high magnification.

To verify whether the same processing signature is also reflected under quasi-static loading, representative tensile fracture surfaces of PF15(1) and PF15(2) are compared in Figure 5.13. In tensile loading, cracks tend to initiate at the weakest local defects and then grow under a continuous applied load. For this reason, voids and poorly impregnated regions are especially critical, because they act as stress concentrators and promote earlier fracture.

In agreement with the impact observations, PF15(1) (Figure 5.13a) shows a more heterogeneous morphology with more pronounced porous regions and larger cavities, consistent with incomplete consolidation. PF15(2) (Figure 5.13b) appears comparatively more compact, with a more uniform texture and a reduced presence of large voids. Both materials show typical natural-fiber composite features (exposed fibers and local pull-out/debonding), but the dominant difference remains the defect population and the overall consolidation level, which is consistent with the density measurements.

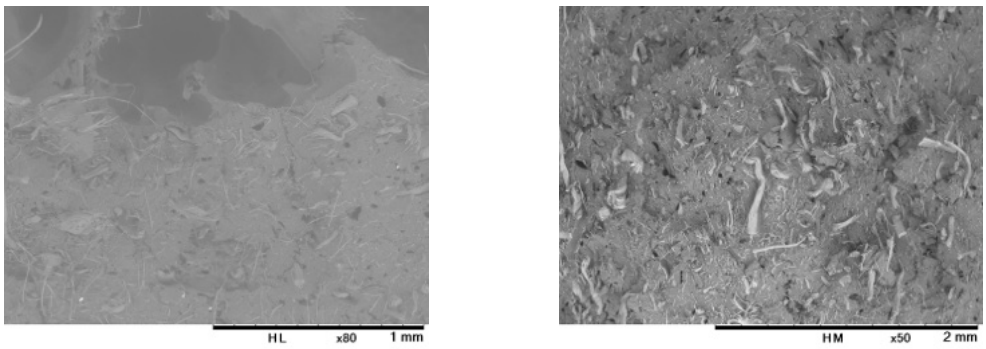


(a) PF15(1) x80, test 1 (tensile). (b) PF15(2) x50, test 7 (tensile).

Figure 5.13: SEM micrographs of tensile fracture surfaces for PF15(1) and PF15(2) at low magnification.

### 5.7.2. Effect of fiber content (15 vs. 30 wt%)

SEM comparisons were performed within each family by pairing 15 and 30 wt% composites (tensile fracture surfaces) at low and high magnification. The aim is to highlight qualitative changes in fiber crowding/dispersion and the associated fracture morphology.

- **PF-based composites.** PF-based composites show a clear content effect when comparing PF15(2) and PF30. At low magnification (Figures 5.14a and 5.14b), PF30 exhibits a more heterogeneous fracture surface, with more frequent regions densely populated by exposed fibers and a less continuous polymer background, whereas PF15(2) appears more uniform, with wider areas where the polymer phase is prevalent and a more even distribution of exposed fibers. This is consistent with a higher probability of local fiber crowding and bundle persistence at 30 wt%, which can increase local stress concentrations and favor earlier damage initiation under tensile loading.

  At higher magnification (Figures 5.14c and 5.14d), both formulations display typical natural-fiber composite fracture features (exposed fibers, pull-out/debonding signatures, and matrix tearing). However, PF30 more often shows densely packed fiber regions with reduced matrix continuity between adjacent fibers, indicating stronger fiber–fiber interactions and a local fracture process more strongly governed by fiber contact and debonding. Overall, increasing PF content shifts the tensile fracture morphology from a relatively open microstructure with a more continuous polymer phase (PF15(2)) to a more crowded and heterogeneous one (PF30).

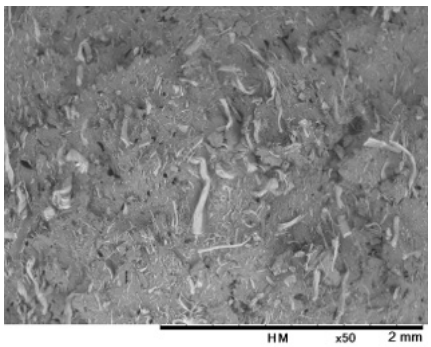


(a) PF15(2) x50, test 7 (tensile).

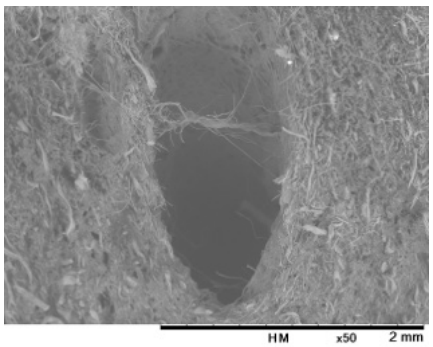


(b) PF30 x50, test 1 (tensile).

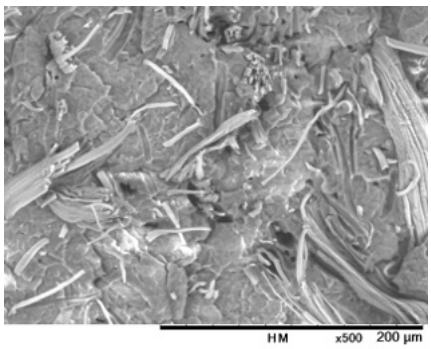


(c) PF15(2) x500, test 7 (tensile).

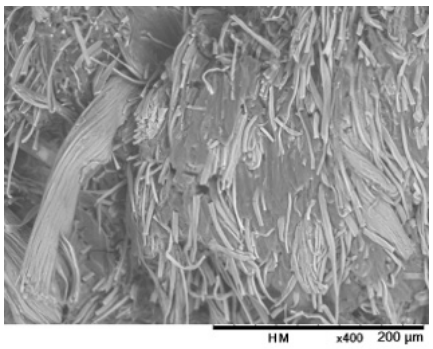


(d) PF30 x400, test 7 (tensile).

Figure 5.14: SEM micrographs of tensile fracture surfaces for PF15(2) and PF30 at low and high magnification.

- **JF-based composites.** A similar content effect is observed for the jute-based systems. At low magnification (Figures 5.15a and 5.15b), JF30 shows a fracture surface with more frequent regions densely populated by exposed fibers and a less continuous polymer background, whereas JF15 retains wider areas where the polymer phase is prevalent and the exposed fibers appear more evenly spread. This is consistent with increased fiber crowding and stronger local fiber-fiber interactions at 30 wt%, similarly to what was observed for the PF family.

  At higher magnification (Figures 5.15c and 5.15d), both formulations show typical damage signatures of natural-fiber composites, including pull-out/debonding and local matrix tearing around fibers.

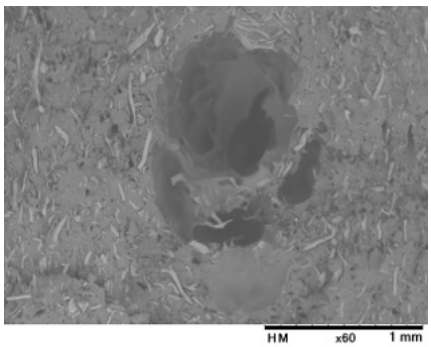


(a) JF15 x60, test 4 (tensile).

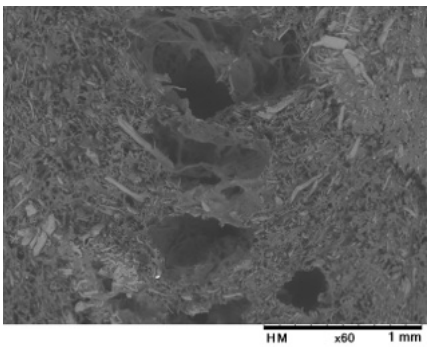


(b) JF30 x60, test 4 (tensile).

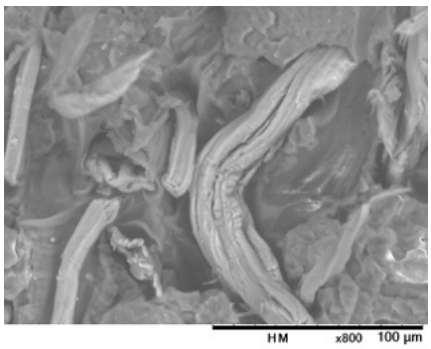


(c) JF15 x800, test 4 (tensile).

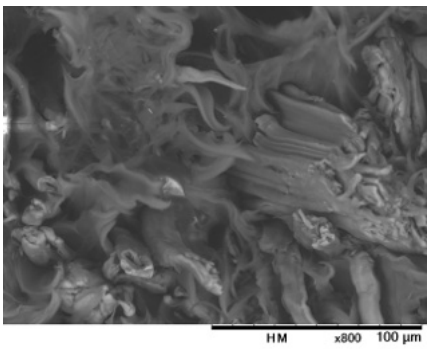


(d) JF30 x800, test 4 (tensile).

Figure 5.15: SEM micrographs of tensile fracture surfaces for JF15 and JF30 at low and high magnification.

- **HYB-based composites.** Hybrid composites show the same content effect observed for PF and JF systems. At low magnification (Figure 5.16a and 5.16b), HYB30 exhibits a more heterogeneous fracture surface, with more frequent regions densely populated by exposed fibers and a less continuous polymer background, whereas HYB15 appears more uniform, with wider areas where the polymer phase is prevalent.

  At higher magnification (Figure 5.16c and 5.16d), both materials show exposed fibers, pull-out/debonding features, and local matrix tearing.

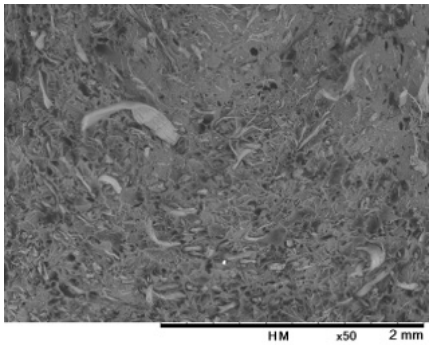


(a) HYB15 x50, test 4 (tensile).

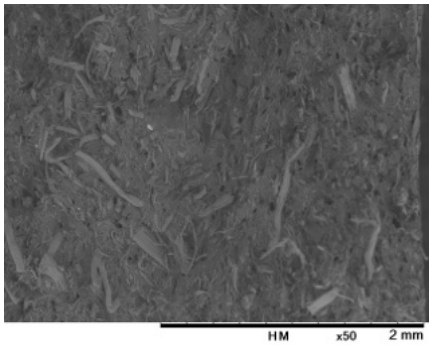


(b) HYB30 x50, test 4 (tensile).

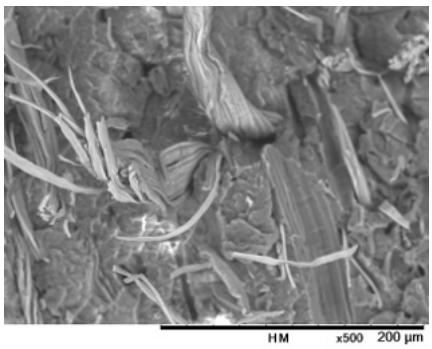


(c) HYB15 x500, test 1 (tensile).

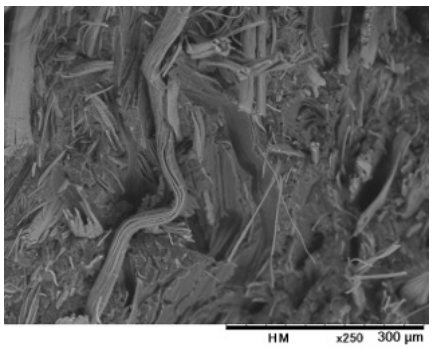


(d) HYB30 x250, test 1 (tensile).

Figure 5.16: SEM micrographs of tensile fracture surfaces for HYB15 and HYB30 at low and high magnification.

Additional SEM micrographs (including tensile, impact, and flexural specimens) for PF-, JF-, and HYB-based composites are reported in Appendix A.3. For tensile and impact, the qualitative observations are consistent with those discussed above. For flexural tests, specimens often reach failure without fully separating into two distinct pieces; therefore, it is not always possible to expose and image a clean fracture surface. The flexural SEM images in the Appendix should be interpreted as views of the cracked/damaged zone and of the surrounding surface morphology, rather than as true fracture-surface micrographs.

### 5.7.3. Virgin vs. recycled

Low-magnification SEM micrographs were used to compare each recycled compound with its corresponding virgin reference, focusing on large-scale features such as voids, porosity clusters, and fracture-surface heterogeneity. Overall, recycled materials tend to exhibit a more compact and uniform fracture surface, with fewer large cavities and fewer extended porous regions than their virgin counterparts. This qualitative trend is consistent with the density increase measured after recycling for most formulations, suggesting improved

consolidation and reduced macroscopic void content after reprocessing.

- **PF-based composites.** Within the PF family (Figure 5.17), the PF15(2)R and PF30R surfaces (Figures 5.17b and 5.17d) appear less dominated by large defect clusters than PF15(2) and PF30 (Figures 5.17a and 5.17c), indicating that reprocessing can partially reduce macroscopic voids generated during the initial compounding and injection route. In particular, PF30 shows a clear change: the virgin fracture surface contains a large cavity-like defect (Figure 5.17c), while the recycled counterpart appears more compact at the millimeter scale, without similarly large open voids (Figure 5.17d). By contrast, PF15(2) and PF15(2)R remain more comparable at low magnification (Figures 5.17a and 5.17b), suggesting that the main recycling improvement in macroscopic consolidation is more pronounced for the higher fiber-content formulation.

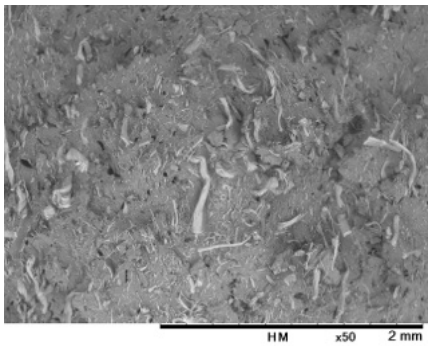


(a) PF15(2), x50 (tensile).

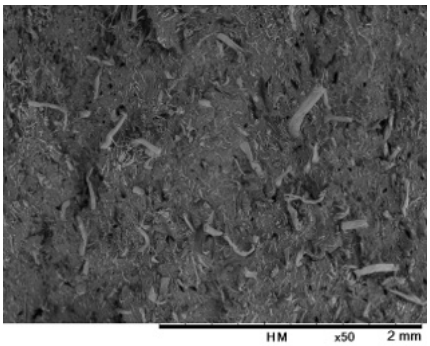


(b) PF15(2)R, x50 (tensile).

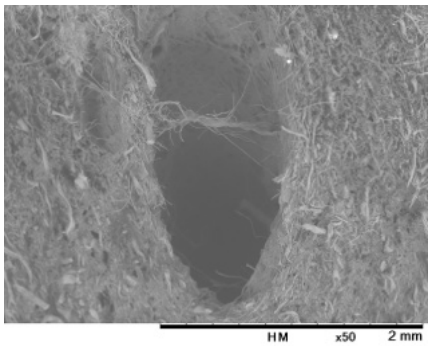


(c) PF30, x50 (tensile).

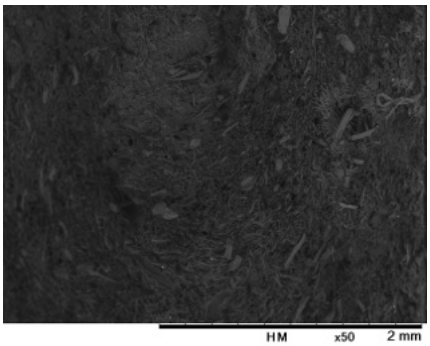


(d) PF30R, x50 (tensile).

Figure 5.17: SEM micrographs of tensile fracture surfaces comparing virgin and recycled PF-based composites at low-magnification.

- **JF-based composites.** A similar tendency is observed for the JF family (Figure 5.18), where recycled specimens generally show a more homogeneous texture at

the millimeter scale. In particular, the virgin fracture surfaces display more evident macroscopic void features and porous regions (Figures 5.18a and 5.18c), whereas the recycled counterparts appear more compact and visually more uniform, with fewer large open cavities (Figures 5.18b and 5.18d). The contrast is especially clear for JF30, where the virgin surface shows larger cavity-like defects and a more irregular porous morphology (Figure 5.18c), while JF30R appears denser and more continuous at low magnification (Figure 5.18d). Overall, these images support the view that recycling reduces the most severe, millimeter-scale defects in the JF systems.

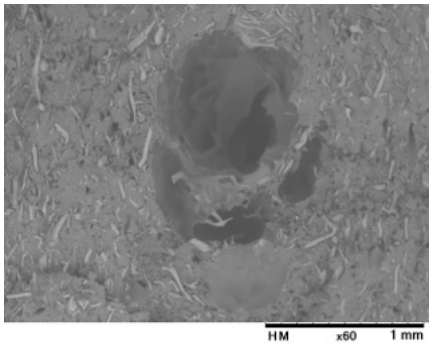


(a) JF15, x60 (tensile).

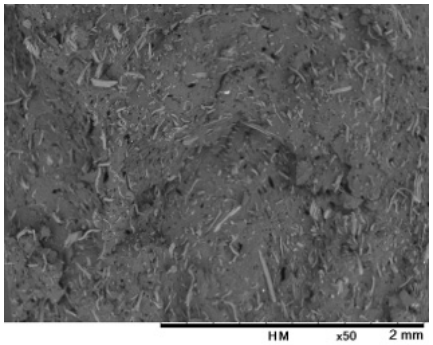


(b) JF15R, x50 (tensile).

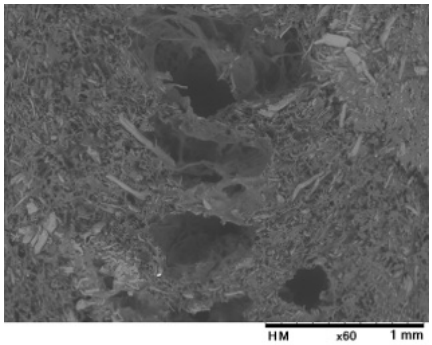


(c) JF30, x60 (tensile).

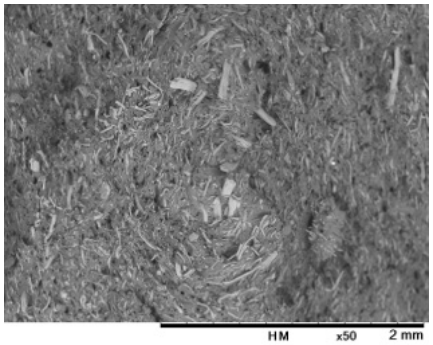


(d) JF30R, x50 (tensile).

Figure 5.18: SEM micrographs of tensile fracture surfaces comparing virgin and recycled JF-based composites at low-magnification.

- **HYB-based composites.** For the hybrid compounds, the same low magnification comparison approach was adopted (Figure 5.19). In both HYB15 and HYB30, the recycled counterparts show only minor changes in fracture-surface appearance compared with the virgin materials (Figures 5.19a, 5.19b, and 5.19c, 5.19d). At the millimeter scale, none of the hybrid pairs displays the large, cavity-like defects observed in some single-fiber formulations; instead, both virgin and recycled hybrids exhibit a relatively uniform, fiber-populated texture. For HYB30, the fracture

surface remains strongly fiber-dominated in both states (Figures 5.19c and 5.19d), consistent with the high reinforcement fraction and with the limited macroscopic densification measured after recycling for this family. Overall, the SEM comparison suggests that reprocessing does not substantially alter the macroscopic defect population of the hybrid materials, in line with the small $\Delta\rho$ observed for HYB15 and HYB30.

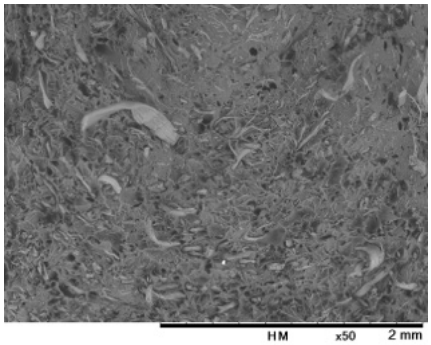


(a) HYB15, x50 (tensile).

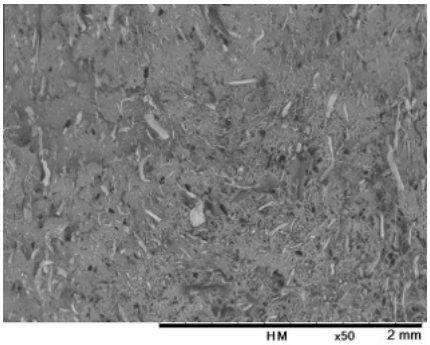


(b) HYB15R, x50 (tensile).

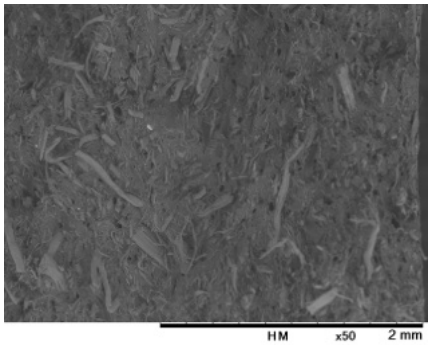


(c) HYB30, x50 (tensile).

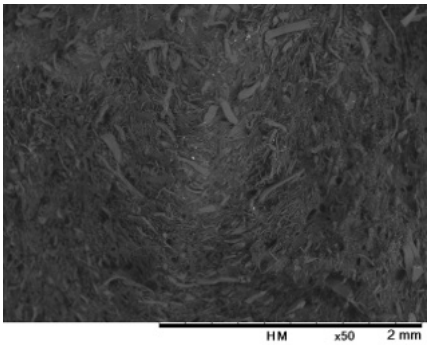


(d) HYB30R, x50 (tensile).

Figure 5.19: SEM micrographs of tensile fracture surfaces comparing virgin and recycled HYB-based composites at low-magnification.

Importantly, these observations support the interpretation that recycling can improve consolidation by reducing macroscopic porosity. However, changes in strength and impact response may still be governed by mechanisms not captured at this scale (e.g., fiber damage/shortening and matrix or interface embrittlement), which are discussed in the mechanical sections. Although the virgin vs. recycled comparison shown here is based on low-magnification tensile fracture surfaces, the Appendix A.3 also includes additional SEM micrographs at both low and high magnification for tensile and impact tested specimens, to provide a broader microstructural reference and to support the interpretation of recycling-induced changes.

## 5.8. Integrated discussion

In this section, results from density, mechanical tests, water uptake, and SEM are brought together in a single discussion. Each dataset provides complementary information: density reflects consolidation and void content; tensile and flexural results describe quasi-static performance and defect sensitivity; impact results capture notch sensitivity and energy absorption; water uptake indicates accessible moisture-transport pathways; SEM links these trends to microstructural features. Where needed, a small number of literature references is used to support the proposed mechanisms without repeating the literature review.

### 5.8.1. Fiber type effect (PF vs. JF) at constant content

PF- and JF-based compounds were compared at the same fiber contents (15 and 30 wt%) to isolate the role of reinforcement type across consolidation quality (density), quasi-static response (tensile and flexural), dynamic fracture resistance (Izod impact), and moisture sensitivity (water uptake). This comparison is particularly meaningful for natural-fiber thermoplastic composites because differences in fiber morphology and variability, intrinsic properties, and surface chemistry can modify dispersion, wetting, and crack development even at identical nominal fiber fraction. In practice, the measured response reflects not only the fiber type itself, but also how each fiber type translates into microstructure (voids, bundle formation, interfacial quality), which strongly affects strength, ductility, impact, and scatter [1, 4, 46].

To support a compact cross-test comparison, Table 5.3 summarizes PF vs. JF differences at constant fiber content across all available datasets. For consistency with the available dataset, the 20 °C water-uptake comparison at 15 wt% refers to PF15(1), while the remaining 15 wt% mechanical comparisons refer to PF15(2).

| Property | 15 wt% (PF vs. JF) | 30 wt% (PF vs. JF) |
|---|---|---|
| $\rho\,(g/cm^3)$ | **0.959** vs. 0.955 | **0.972** vs. 0.969 |
| $E\,(MPa)$ | 2424 vs. **2550** | 2943 vs. **3131** |
| $\sigma_M\,(MPa)$ | **34.40** vs. 30.64 | **32.01** vs. 29.72 |
| $\varepsilon_B\,(\%)$ | **5.01** vs. 4.43 | 3.52 vs. **4.35** |
| $E_f\,(MPa)$ | 2398 vs. **2539** | 3365 vs. **3497** |
| $\sigma_{f,M}\,(MPa)$ | 50.98 vs. **52.77** | 54.88 vs. **55.46** |
| $\varepsilon_{f,B}\,(\%)$ | 8.56 vs. **10.54** | **6.04** vs. 5.60 |
| $a_k\,(kJ/m^2)$ | **7.412** vs. 6.339 | **12.928** vs. 9.427 |
| $\Delta w\,(\%)\,at\,42\,d,\ 20°C$ | ∼**2.8** vs. ∼1.5 | ∼**6.0** vs. ∼4.6 |
| $\Delta w\,(\%)\,at\,41\,d,\ 60°C$ | ∼**4.2** vs. ∼3.7 | ∼3.6 vs. ∼**7.0** |

Table 5.3: PF vs. JF comparison at constant fiber content across density, tensile, flexural, impact, and water uptake results. Values are taken from the corresponding plots; for each PF-JF pair, the higher average value is highlighted in bold.

A consistent picture emerges when the different tests are interpreted together. In this dataset, JF-based materials show slightly higher stiffness than PF at the same fiber content (both in tension and in bending). This can be explained by differences in reinforcement stiffness and by how each fiber family disperses, wets, and transfers load at small strain, since elastic modulus is strongly affected by the continuity of the solid phase and by the effectiveness of load sharing [1, 3, 46]. A similar outcome has also been reported in comparative studies on PP composites reinforced with jute and pineapple leaf fibers, where jute can provide slightly higher stiffness depending on processing and fiber content [5, 36].

In contrast, strength does not follow the same ranking: PF-based systems reach higher UTS than JF at both 15 and 30 wt%. Since UTS is strongly affected by early crack initiation at voids and interfacial gaps, this suggests that the PF systems in this dataset achieve a more favorable balance between load transfer and resistance to premature fracture than the corresponding JF systems, despite the slightly lower modulus. Literature comparisons indicate that the strength ranking between jute and pineapple leaf fibers is not universal and can switch depending on dispersion and interfacial quality; however, high strength levels for pineapple leaf fiber reinforced PP have been reported when consolidation and

interfacial conditions are favorable, which is consistent with the higher UTS measured here for PF-based materials [5, 47].

Flexural results provide complementary support. At 15 wt%, JF15 shows higher flexural modulus and strength than PF15(2), together with higher elongation at break, suggesting a more favorable response under bending for the jute-based system at low fiber fraction. At 30 wt%, JF30 remains slightly superior in flexural modulus and strength compared to PF30, while both show reduced $\varepsilon_{f,B}$. Overall, fiber-type effects are present in bending but remain smaller than the dominant influence of fiber content, and they are consistent with bending being sensitive to surface defects and local heterogeneity through the thickness [46]. Flexural comparisons between jute and pineapple leaf fiber reinforced PP reported in the literature show similar differences caused by different processing, which supports the idea that bending performance is strongly influenced by microstructural quality rather than by fiber type alone [5, 36].

Impact toughness shows a different ranking and helps clarify why higher stiffness does not necessarily imply higher impact resistance. For both PF and JF, increasing content from 15 to 30 wt% raises $a_k$, indicating a greater contribution from mechanisms such as crack deflection and fiber pull out or bridging during dynamic fracture. At constant content, PF exhibits higher impact toughness than JF, especially at 30 wt%, suggesting that the PF microstructure promotes a more tortuous crack path and/or a larger pull out contribution under notched impact [4, 46]. Comparative studies on PP reinforced with jute and pineapple leaf fibers report that rankings related to impact results can vary with processing and interfacial conditions, which is consistent with the strong sensitivity of impact response to microstructure and fracture mechanisms observed here [5].

Water uptake trends reinforce the same microstructure and interface framework. At 20 °C, PF composites absorb more moisture than JF at both fiber contents, consistent with a larger water-accessible hydrophilic fraction and/or more effective transport pathways (interfacial channels and void networks) in the PF systems. At 60 °C the ranking changes (JF30 becomes the most moisture sensitive), indicating that at elevated temperature swelling and interfacial transport become more critical and can amplify differences between fiber families in moisture pathways.

Overall, PF vs. JF differences cannot be reduced to a single best fiber type: in this dataset, JF provides slightly higher stiffness (tension and bending), while PF shows higher UTS and higher impact toughness. Literature comparisons between jute and pineapple leaf fiber reinforced PP report similar tendencies in some cases, but also confirm that the final ranking can depend on processing, which supports interpreting the present results

primarily through consolidation, dispersion, and interfacial quality [5, 46].

### 5.8.2. Fiber content effect (15 vs. 30 wt%) within each family

This subsection isolates the effect of increasing the reinforcement fraction from 15 to 30 wt% within the PF and JF families. Higher fiber contents generally increase stiffness, but they can also amplify processing and microstructure limitations (fiber crowding, bundle formation, incomplete wetting, and sensitivity to voids and interfacial gaps), which can limit strength and reduce deformation capacity [1, 4, 46]. Table 5.4 summarizes the 15 vs. 30 wt% comparison across density, tensile, flexural, impact, and water uptake. For consistency with the available dataset, the 20 °C water-uptake value at 15 wt% for PF refers to PF15(1), while mechanical comparisons at 15 wt% refer to PF15(2).

| Property | PF (15 vs. 30 wt%) | JF (15 vs. 30 wt%) |
|---|---|---|
| $\rho\,(g/cm^3)$ | 0.959 vs. **0.972** | 0.955 vs. **0.969** |
| $E\,(MPa)$ | 2424 vs. **2943** | 2550 vs. **3131** |
| $\sigma_M\,(MPa)$ | **34.40** vs. 32.01 | **30.64** vs. 29.72 |
| $\varepsilon_B\,(\%)$ | **5.01** vs. 3.52 | **4.43** vs. 4.35 |
| $E_f\,(MPa)$ | 2398 vs. **3365** | 2539 vs. **3497** |
| $\sigma_{f,M}\,(MPa)$ | 50.98 vs. **54.88** | 52.77 vs. **55.46** |
| $\varepsilon_{f,B}\,(\%)$ | **8.56** vs. 6.04 | **10.54** vs. 5.60 |
| $a_k\,(kJ/m^2)$ | 7.412 vs. **12.928** | 6.339 vs. **9.427** |
| $\Delta w\,(\%)\,at\,42\,d,\ 20°C$ | ∼2.8 vs. ∼**6.0** | ∼1.5 vs. ∼**4.6** |
| $\Delta w\,(\%)\,at\,41\,d,\ 60°C$ | ∼**4.2** vs. ∼3.6 | ∼3.7 vs. ∼**7.0** |

Table 5.4: Effect of fiber content (15 vs. 30 wt%) within each family (PF and JF) across density, tensile, flexural, impact, and water uptake results. Values are taken from the corresponding plots; for each 15-30 wt% pair, the higher average value is highlighted in bold.

A coherent trend is observed for both PF and JF families. Increasing fiber content raises density and strongly increases stiffness in tension and bending, confirming that the elastic response becomes progressively more fiber-dominated. This behavior is consistent with comparative PP studies where higher natural-fiber content leads to clear modulus gains,

while the response becomes more sensitive to processing quality and microstructure [5].

In contrast, strength does not improve proportionally and remains close to the PP baseline, suggesting that ultimate failure is increasingly controlled by early crack initiation at voids and interfacial gaps rather than by average load transfer. This is consistent with the reduction in ductility: elongation at break decreases with fiber content, and the reduction is particularly evident in bending, where the strain at break drops markedly at 30 wt%. Since bending is especially sensitive to surface defects and local heterogeneity through the thickness, higher reinforcement levels promote earlier damage localization and reduce deformation tolerance, even though flexural stiffness and strength increase [46].

Impact toughness increases from 15 to 30 wt% in both families, indicating that at higher fiber content the fracture process under notched impact can involve more crack deflection and more fiber pull out or bridging, increasing absorbed energy even when quasi-static ductility decreases [4, 46]. Finally, water uptake increases substantially from 15 to 30 wt% in both PF and JF, consistent with the larger hydrophilic fraction and the greater availability of transport pathways; the stronger separation at 60 °C suggests that swelling and interfacial transport become more relevant at elevated temperature.

Overall, increasing fiber content mainly increases stiffness and bending strength, but reduces deformation capacity and makes failure more sensitive to voids and interfacial gaps; impact toughness can still improve because cracks are deflected and more fiber pull out and bridging can occur.

### 5.8.3. Hybridization effect

Hybrid composites combine PF and JF at the same total fiber content (15 or 30 wt%) to verify whether hybridization improves the overall property balance compared with single-fiber references. In natural-fiber thermoplastic composites, hybridization can be beneficial when the two reinforcements contribute complementary effects, but it can also lead to a compromise response if damage initiates at the weakest interface and propagates through a mixed, defect-sensitive microstructure [48–50].

Table 5.5 compares HYB15 and HYB30 with PF and JF references at matched total fiber content.

| Property | 15 wt% (PF vs. JF vs. HYB) | 30 wt% (PF vs. JF vs. HYB) |
|---|---|---|
| $\rho\,(g/cm^3)$ | **0.959** vs. 0.955 vs. 0.958 | 0.972 vs. 0.969 vs. **1.018** |
| $E\,(MPa)$ | 2424 vs. 2550 vs. **2736** | 2943 vs. 3131 vs. **3538** |
| $\sigma_M\,(MPa)$ | **34.40** vs. 30.64 vs. 32.92 | 32.01 vs. 29.72 vs. **36.48** |
| $\varepsilon_B\,(\%)$ | 5.01 vs. 4.43 vs. **5.98** | 3.52 vs. **4.35** vs. 3.31 |
| $E_f\,(MPa)$ | 2398 vs. **2539** vs. 2446 | 3365 vs. **3497** vs. 3273 |
| $\sigma_{f,M}\,(MPa)$ | 50.98 vs. **52.77** vs. 49.30 | 54.88 vs. **55.46** vs. 53.04 |
| $\varepsilon_{f,B}\,(\%)$ | 8.56 vs. **10.54** vs. 9.62 | **6.04** vs. 5.60 vs. 4.33 |
| $a_k\,(kJ/m^2)$ | **7.412** vs. 6.339 vs. 6.497 | **12.928** vs. 9.427 vs. 9.748 |

Table 5.5: HYB vs. single-fiber comparison at constant total fiber content across density, tensile, flexural, and impact results (virgin materials). Values are taken from the corresponding plots; the maximum average value within each row and fiber content is highlighted in bold.

At 15 wt%, HYB15 provides the highest tensile modulus, but it does not exceed the best single-fiber reference in strength or impact toughness. In bending, HYB15 remains comparable to the single-fiber systems but does not improve flexural strength, and its flexural modulus is intermediate, suggesting that at low content hybridization mainly affects elastic stiffening rather than properties governed by fracture and damage initiation [49, 50].

At 30 wt%, hybridization becomes more beneficial in tension: HYB30 reaches the highest tensile modulus and the highest UTS among the three 30 wt% materials. This is consistent with literature observations that hybrid architectures can improve stress redistribution and load sharing when the microstructure is sufficiently homogeneous [48, 49]. However, ductility remains low and HYB30 shows the lowest flexural strain at break, indicating that high reinforcement levels still promote early damage localization under bending [50]. In impact, both HYB15 and HYB30 remain below PF30 and are closer to the corresponding JF references, indicating that notched impact performance is not significantly enhanced by hybridization and may be governed by the limiting fiber or interface contribution.

When interpreting the hybrid results, a possible processing order effect should also be considered. HYB15 and HYB30 were manufactured at the end of the campaign (with the exception of PF15(2)), and the increased operator experience may have contributed to improved consolidation even if nominal processing conditions were unchanged. This

is consistent with the density results, where virgin hybrids, especially HYB30, show an experimental density very close to the theoretical value, with a smaller experimental deviation than PF30 and JF30.

In addition, hybridization itself may have facilitated mixing. PF tends to be more difficult to disperse because it has a stronger tendency to remain in bundles, whereas JF appears easier to mix and less prone to persistent agglomeration during pre-mixing. The coexistence of PF and JF may therefore promote a more effective breakup and redistribution of PF during compounding, leading to a more homogeneous microstructure and lower void content already in the virgin state [48]. A further contributing factor may be a more favorable packing of the mixed fiber population: combining fibers with different morphology and size distribution can reduce inter-fiber gaps and facilitate melt penetration between fibers, improving local consolidation and bringing the experimental density closer to the theoretical value [48, 49]. This provides context for why the hybrids start from a comparatively high consolidation level and why recycling produces only limited densification and only minor changes in the macroscopic appearance of fracture surfaces.

### 5.8.4. Recycling effect

Recycling effects were evaluated by directly comparing each recycled formulation to its virgin counterpart, focusing on density and on tensile and impact performance. When these datasets are interpreted together, a clear pattern emerges: experimental density increases for all recycled compounds, tensile modulus tends to increase (most clearly for the 30 wt% systems), while Izod impact toughness decreases for every formulation. This shows that reprocessing generally improves consolidation (lower macroscopic porosity), but it tends to penalize dynamic fracture resistance, which is more sensitive to fiber integrity and to matrix or interface changes than to void reduction alone [1, 10, 46, 51].

Table 5.6 provides an overview of variations across density, tensile, and impact performances after recycling. It highlights two robust trends: (i) the largest densification occurs for the 30 wt% single-fiber systems (PF30 and JF30), and these materials also show the strongest modulus increase; (ii) impact toughness decreases after recycling for all formulations, with the largest penalties again observed at 30 wt%.

| Material | $\Delta\rho$ (%) | $\Delta E$ (%) | $\Delta\sigma_M$ (%) | $\Delta\varepsilon_B$ (%) | $\Delta a_k$ (%) |
|---|---|---|---|---|---|
| **PF15(2)** | +0.45 | +14.96 | –7.21 | +9.94 | –12.52 |
| **PF30** | +4.91 | +17.77 | +3.80 | –21.08 | –47.05 |
| **JF15** | +0.65 | +5.67 | –3.09 | +115.23 | –20.61 |
| **JF30** | +4.33 | +20.25 | –1.39 | +12.13 | –35.47 |
| **HYB15** | +0.34 | –1.27 | –6.33 | +15.61 | –16.66 |
| **HYB30** | +0.52 | +4.84 | –7.53 | +3.44 | –17.58 |

Table 5.6: Cross-property effect of recycling (density, tensile, and Izod impact), computed as $\Delta X = (X_R - X_V)/X_V \cdot 100\%$. Positive values indicate an increase after recycling, while negative values indicate a decrease.

The systematic increase in experimental density indicates reduced macroscopic void content and improved consolidation after reprocessing. This naturally benefits stiffness because tensile modulus is strongly influenced by the effective solid fraction and by the continuity of the matrix phase at small strain. The effect is most evident for the 30 wt% systems, where voids and packing heterogeneity in the virgin state have a larger influence on stiffness [1, 46].

In addition to densification, a further contribution to the modulus increase after recycling may come from fiber orientation effects during the second injection-molding cycle. In injection molding, flow-induced fiber orientation can significantly affect the apparent elastic modulus measured along the loading direction, and a higher degree of alignment generally increases stiffness and anisotropy [52, 53]. Therefore, the observed post-recycling stiffening may reflect not only reduced porosity but also a slightly different orientation state of the fibers after reprocessing and re-molding. This hypothesis is also compatible with studies on injection-molded natural-fiber PP composites, where in-thickness orientation and process-induced microstructure are linked to mechanical response [54].

Impact toughness decreases for all formulations even when density increases. This is expected because notched impact resistance depends on rapid crack propagation and is therefore strongly affected by fiber integrity (effective length and aspect ratio), matrix ductility, and the balance between interfacial separation and brittle matrix cracking [4, 46]. Reprocessing can reduce voids, but it also introduces additional shear and thermal history, which can shorten or damage fibers and can promote matrix or interface embrittlement. As a result, the ability to absorb energy through mechanisms such as crack deflection and fiber pull out or bridging can be reduced, leading to lower $a_k$ even when consolidation

improves.

This opposite trend between stiffness and impact resistance is also reported in the literature: reprocessing can increase stiffness through improved dispersion and consolidation, while impact strength decreases because fiber attrition and polymer degradation reduce the effectiveness of fiber-related toughening mechanisms [10, 51].

The strongest penalties observed for PF30R and JF30R are consistent with the fact that high-fiber systems rely more on contributions from fibers during impact, making them particularly sensitive to fiber damage during recycling.

Tensile strength changes are smaller and less systematic because opposing effects compete. Void reduction and improved consolidation tend to delay early crack initiation, while fiber damage, polymer degradation, and interfacial changes tend to promote earlier failure and reduce UTS [1, 10]. Elongation at break is the most formulation-dependent metric: most recycled composites show a modest increase, but PF30 and neat PP decrease, indicating a more brittle response when polymer degradation and/or fiber damage dominates. The very large increase observed for JF15R should be interpreted with caution and is not considered a robust trend.

Overall, recycling in this study improves consolidation and often increases stiffness, but it consistently reduces impact toughness and does not systematically improve strength. This overall decoupling is coherent with a microstructure where void-related initiation sites are reduced, while the dynamic fracture resistance is limited by fiber integrity and by matrix or interface changes introduced during reprocessing. SEM observations in Section 5.7 are used to support this interpretation by linking recycled materials to reduced macroscopic porosity and to the observed fracture surface morphology.

# 6 | Conclusions and future perspectives

## 6.1. Conclusions

This Master's thesis investigated the manufacturing and characterization of sustainable natural-fiber reinforced polypropylene (PP) composites based on pineapple leaf fibers (PF), jute fibers (JF), and PF/JF hybrid systems. A systematic experimental campaign was carried out on both virgin and reprocessed materials in order to quantify how fiber type, fiber content (15 and 30 wt%), hybridization, and recycling affect consolidation quality, microstructure, and mechanical and physical performance. The experimental outcomes from density, tensile and flexural tests, Izod impact, water uptake, and SEM fracture-surface observations were interpreted consistently to identify the main mechanisms governing the observed behavior.

### 6.1.1. Processing and consolidation quality

Density measurements, combined with the comparison to theoretical density, proved to be a useful indirect indicator of consolidation quality and void content (Figure 5.1). For the composites, a lower experimental density than expected was associated with higher porosity and imperfect impregnation, especially at high fiber content where viscosity increases and compaction becomes more challenging. In contrast, recycled composites systematically showed higher density than their virgin counterparts, indicating a densification effect after reprocessing and suggesting a reduction of macroscopic voids. The densification was particularly pronounced for the 30 wt% single-fiber systems (PF30 and JF30), while it remained limited for 15 wt% systems and for the hybrids, which already exhibited relatively good consolidation in the virgin state.

A key additional outcome was the strong influence of compounding strategy on microstructure: PF15(1) and PF15(2), despite having the same nominal composition, showed different density levels in the density plot (Figure 5.1) and distinct fracture-surface features in

SEM observations (Figure 5.12). This confirms that feeding strategy and mixing efficiency can be as critical as formulation itself in natural-fiber thermoplastic composites.

### 6.1.2. Effect of fiber type

When PF- and JF-based compounds were compared at matched fiber content (Table 5.3), JF systems tended to provide slightly higher stiffness in both tension and bending, indicating a marginally more effective elastic contribution under the present processing conditions (Figures 5.3, 5.6). On the contrary, PF-based systems reached higher tensile strength than JF at both 15 and 30 wt%, suggesting that, in this dataset, PF composites achieved a more favorable balance between reinforcement efficiency and resistance to premature crack initiation (Figure 5.4).

In terms of moisture sensitivity, water uptake confirmed the expected dependence on natural-fiber reinforcement. At 20 °C, increasing fiber content increased long-time uptake for both fiber families; at 60 °C, kinetics accelerated and the differences between PF- and JF-based composites became more evident, highlighting the role of fiber swelling and interfacial transport pathways at elevated temperature (Figures 5.10, 5.11).

### 6.1.3. Effect of fiber content

Increasing fiber content from 15 to 30 wt% (Table 5.4) consistently increased density and produced a strong stiffening effect in tension and bending, confirming that the elastic response becomes progressively more fiber-dominated (Figures 5.3, 5.6). However, tensile strength did not increase proportionally and remained close to the PP baseline, indicating that ultimate failure is largely controlled by defects and interfacial quality rather than by average load transfer (Figure 5.4). Ductility decreased with fiber content, with the reduction being particularly evident in bending where strain at break dropped markedly at 30 wt% (Figure 5.5). These trends are consistent with the greater defect sensitivity and the earlier damage localization expected at high reinforcement levels.

Interestingly, notched Izod impact toughness increased from 15 to 30 wt% for PF, JF, and hybrid systems (Figure 4.9). This indicates that, under dynamic fracture, higher fiber content can promote energy dissipation mechanisms such as crack deflection and fiber pull-out/bridging, even when quasi-static ductility decreases.

### 6.1.4. Hybridization effect

Hybrid composites were investigated to assess whether combining PF and JF improves the balance of properties relative to single-fiber references (Table 5.5). At 15 wt%, the hybrid provided the highest tensile modulus among the 15 wt% materials, but no clear improvement in strength or impact toughness over the best single-fiber reference was observed. At 30 wt%, hybridization became more beneficial in tension: HYB30 reached the highest tensile modulus and the highest tensile strength among the three 30 wt% materials, suggesting that hybrid architectures can enhance stress redistribution and load sharing when the microstructure is sufficiently homogeneous (Figures 5.3, 5.4). Nevertheless, ductility remained low and flexural strain at break for HYB30 was the lowest, confirming that high reinforcement levels still promote early damage localization under bending (Figure 5.5, 5.8). In impact, hybrid materials did not exceed the best PF reference (PF30), indicating that impact performance may be governed by the limiting fiber or interface contribution rather than by synergistic hybrid effects (Figure 4.9).

The hybrid results also suggest that mixing and packing effects may contribute to the comparatively good consolidation of the hybrids already in the virgin state, consistent with the smaller density deviation from theoretical values and the minor SEM changes observed after recycling (Figure 5.1).

### 6.1.5. Recycling effect

A consistent pattern emerged when comparing virgin and recycled states (Table 5.6). Recycling improved consolidation, as indicated by increased density (Figure 5.1) and by SEM evidence of a more compact and uniform fracture surface with fewer large voids and porous regions (Chapter 5). This densification was reflected in tensile stiffness, which tended to increase after recycling, particularly for the 30 wt% compounds where void reduction most strongly improves effective load transfer (Figure 5.3).

However, recycling did not lead to a general strength improvement: tensile strength slightly decreased for most formulations (with PF30 as a notable exception showing a small increase) (Figure 5.4). The most robust mechanical penalty associated with reprocessing was the systematic reduction of Izod impact toughness for every formulation (Figure 4.9). This suggests that, while void reduction increases stiffness, impact resistance is affected by other factors, such as fiber shortening, matrix embrittlement, and changes at the fiber/matrix interface. Therefore, the present results indicate that mechanical reprocessing can be advantageous to recover or enhance stiffness and consolidation quality, but it may compromise notch-impact performance and does not guarantee strength retention.

Overall, this work confirms that processing quality and microstructure control are central to achieving reliable properties in natural-fiber PP composites. Consolidation (void content), fiber dispersion, and interfacial integrity govern the balance between stiffness, strength, ductility, impact resistance, and moisture sensitivity, and they also explain why recycling can simultaneously provide benefits (density and stiffness) and drawbacks (impact toughness).

## 6.2. Future perspectives

Based on the outcomes of this study, several research and development directions can be proposed to strengthen the industrial relevance of recyclable natural fiber-PP composites and to improve the property balance after reprocessing.

- **Interface engineering and microstructure control.** Improve strength stability and damage tolerance by enhancing fiber/matrix adhesion while preserving energy dissipation. Future work should evaluate compatibilization strategies (e.g., MAPP) and controlled surface treatments (alkali, silane, enzymatic, or plasma routes) to improve wetting and reduce interfacial gaps, while avoiding excessive embrittlement. In parallel, further optimization of compounding and feeding strategy is recommended, given the sensitivity observed between PF15(1) and PF15(2). Systematic studies on controlled feeding, screw-element configuration (balancing dispersion and fiber preservation), and processing windows (temperature and shear) would help maximize impregnation and repeatability while minimizing thermal and mechanical degradation.
- **Recycling and fiber integrity over multiple cycles.** Although recycling improved densification and stiffness, impact toughness decreased systematically, suggesting competing mechanisms such as fiber damage/shortening and changes in matrix conditions. Future work should quantify fiber length/aspect ratio distributions before and after reprocessing to separate the benefits of void reduction from the drawbacks of fiber integrity loss. In addition, multiple recycling loops should be evaluated to determine property evolution and practical recyclability limits. Blending recycled and virgin feedstock at controlled ratios represents a promising industrial strategy to stabilize performance, particularly for impact resistance, while preserving circularity benefits.
- **Durability, validation, and sustainability assessment.** Water uptake results confirm the importance of environmental conditioning, especially at high temperature. Future work should include mechanical tests after conditioning (wet, hot-wet,

freeze-thaw) to evaluate property retention, together with diffusion analyses to estimate apparent diffusion parameters and clarify the role of interfacial transport. Microstructural observations before and after conditioning would help identify the main damage mechanisms. For engineering design and material selection, further tests such as fatigue and creep, notch sensitivity evaluation and fracture mechanics characterization, and dynamic mechanical analysis (DMA) to assess the effect of temperature on mechanical behavior are recommended, together with improved statistical reporting (mean, scatter, and confidence intervals) to enable a more reliable comparison among formulations and support material selection. Finally, a preliminary life cycle assessment (LCA) screening could quantify the environmental advantage of natural fibers and mechanical reprocessing compared to conventional synthetic fiber-PP composites.

In conclusion, recyclable natural fiber-PP composites represent a promising route toward more sustainable lightweight materials. The present work shows that careful control of processing and consolidation is essential to achieve consistent properties, and that recycling can effectively improve densification and stiffness but may penalize impact resistance due to competing microstructural mechanisms. Future developments combining improved interface engineering, optimized processing, and recycling-aware design strategies can expand the application window of these materials while preserving circularity and sustainability targets.

# Bibliography

[1] V. Chauhan, T. Kärki, and J. Varis. Review of natural fiber-reinforced engineering plastic composites, their applications in the transportation sector and processing techniques. *Journal of Thermoplastic Composite Materials*, 35(8):1169–1209, 2022. doi: 10.1177/0892705719889095.

[2] B. Dev, M. A. Rahman, M. R. Alam, M. R. Repon, and Y. Nawab. Mapping the process in natural fiber reinforced composites: Preparation, mechanical properties, and applications. *Polymer Composites*, 44(6):3748–3788, 2023. doi: 10.1002/pc.27376.

[3] G. S. Mann, L. P. Singh, P. Kumar, and S. Singh. Green composites: A review of processing technologies and recent applications. *Journal of Thermoplastic Composite Materials*, 33(8):1145–1171, 2020. doi: 10.1177/0892705718816354.

[4] O. Faruk, A. K. Bledzki, H. P. Fink, and M. Sain. Biocomposites reinforced with natural fibers: 2000–2010. *Progress in Polymer Science*, 37(11):1552–1596, 2012. doi: 10.1016/j.progpolymsci.2012.04.003.

[5] M. M. A. Sayeed, A. S. M. Sayem, J. Haider, S. Akter, M. M. Habib, H. Rahman, and S. Shahinur. Assessing mechanical properties of jute, kenaf, and pineapple leaf fiber-reinforced polypropylene composites: Experiment and modelling. *Polymers*, 15 (4):830, 2023. doi: 10.3390/polym15040830.

[6] M. C. Symington, W. M. Banks, O. D. West, and R. A. Pethrick. Tensile testing of cellulose based natural fibers for structural composite applications. *Journal of Composite Materials*, 43(9):1083–1108, 2009. doi: 10.1177/0021998308097740.

[7] M. Zampaloni, F. Pourboghrat, S. A. Yankovich, B. N. Rodgers, J. Moore, L. T. Drzal, A. K. Mohanty, and M. Misra. Kenaf natural fiber reinforced polypropylene composites: A discussion on manufacturing problems and solutions. *Composites Part A: Applied Science and Manufacturing*, 38(8):1569–1580, 2007. doi: 10.1016/j.compositesa.2007.01.001.

[8] M. R. Rahman, M. M. Huque, M. N. Islam, and M. Hasan. Mechanical properties

of polypropylene composites reinforced with chemically treated abaca. *Composites Part A: Applied Science and Manufacturing*, 40(4):511–517, 2009. doi: 10.1016/j.compositesa.2009.01.013.

[9] Milene Heloisa Martins and Marco-Aurelio De Paoli. Polypropylene compounding with post-consumer material: Ii. reprocessing. *Polymer Degradation and Stability*, 78(3):491–495, 2002. doi: 10.1016/S0141-3910(02)00195-7.

[10] Alan R. Dickson, Damien Even, Jeremy M. Warnes, and Alan Fernyhough. The effect of reprocessing on the mechanical properties of polypropylene reinforced with wood pulp, flax or glass fibre. *Composites Part A: Applied Science and Manufacturing*, 2014. doi: 10.1016/j.compositesa.2014.03.010.

[11] S. Chandgude and S. Salunkhe. In state of art: Mechanical behavior of natural fiber-based hybrid polymeric composites for application of automobile components. *Polymer Composites*, 42:2678–2703, 2021. doi: 10.1002/pc.26045.

[12] S. Vigneshwaran, R. Sundarakannan, K. M. John, R. Deepak Joel Johnson, K. Arun Prasath, S. Ajith, V. Arumugaprabu, and M. Uthayakumar. Recent advancement in the natural fiber polymer composites: A comprehensive review. *Journal of Cleaner Production*, 277:124109, 2020. doi: 10.1016/j.jclepro.2020.124109.

[13] R. Ribeiro, A. T. Marques, and J. L. Alves. Sustainable composites based on pine resin and flax fibre. In R. Fangueiro and S. Rana, editors, *Advances in Natural Fibre Composites: Raw Materials, Processing and Analysis*, pages 145–158. Springer International Publishing, 2018. doi: 10.1007/978-3-319-64641-1_10.

[14] K. Immonen, P. Lahtinen, P. Isokangas, and K. Torvinen. Potential of hemp in thermoplastic biocomposites—the effect of fibre structure. In R. Fangueiro and S. Rana, editors, *Advances in Natural Fibre Composites: Raw Materials, Processing and Analysis*, pages 1–12. Springer International Publishing, 2018. doi: 10.1007/978-3-319-64641-1_1.

[15] V. Placet, C. François, A. Day, J. Beaugrand, and P. Ouagne. Industrial hemp transformation for composite applications: Influence of processing parameters on the fibre properties. In R. Fangueiro and S. Rana, editors, *Advances in Natural Fibre Composites: Raw Materials, Processing and Analysis*, pages 13–26. Springer International Publishing, 2018. doi: 10.1007/978-3-319-64641-1_2.

[16] M. Asim, N. Saba, M. Jawaid, M. Nasir, M. T. H. Sultan, and M. F. M. Alkbir. A review on pineapple leaves fibre and its composites. *International Journal of Polymer Science*, 2015:1–16, 2015. doi: 10.1155/2015/950567.

[17] L. Uma Devi, S. S. Bhagawan, and Sabu Thomas. Mechanical properties of pineapple leaf fiber-reinforced polyester composites. *Journal of Applied Polymer Science*, 64(9): 1739–1748, 1997. doi: 10.1002/(SICI)1097-4628(19970531)64:9<1739::AID-APP10>3.0.CO;2-T.

[18] I. R. Dantas, N. C. Zanini, J. P. Cipriano, M. R. Capri, and D. R. Mulinari. Influence of coupling agent on the properties of polypropylene composites reinforced with palm fibers. In R. Fangueiro and S. Rana, editors, *Advances in Natural Fibre Composites: Raw Materials, Processing and Analysis*, pages 51–60. Springer International Publishing, 2018. doi: 10.1007/978-3-319-64641-1_5.

[19] N. T. Vila, A. L. Musialak, and A. Ferreira. Use of sugar cane fibers for composites—a short review. In R. Fangueiro and S. Rana, editors, *Advances in Natural Fibre Composites: Raw Materials, Processing and Analysis*, pages 27–36. Springer International Publishing, 2018. doi: 10.1007/978-3-319-64641-1_3.

[20] Ming Cai, Yaowei Guo, Lamei Wang, Qihua Ma, Baozhong Sun, and Geoffrey I. N. Waterhouse. Recent advances in hygrothermal aging of plant fiber reinforced composites. *Applied Composite Materials*, 32:1949–1974, 2025. doi: 10.1007/s10443-024-10275-4.

[21] Safak Yildizhan, Anand Mohanam, Ranjitha Jambulingam, Vishal Gavande, and Won-Ki Lee. Experimental study on the effects of thermal cycling and moisture exposure on mechanical properties of alkali treated woven jute fiber/epoxy composites. *Applied Composite Materials*, 32:1997–2011, 2025. doi: 10.1007/s10443-025-10334-4.

[22] Maleck Massou, Noel Babu, Puxuan Zhang, Chenggao Li, and Guijun Xian. Mechanical properties and hydrothermal aging of jute-carbon epoxy hybrid composite laminates. *Journal of Composite Materials*, 0(0):1–13, 2025. doi: 10.1177/00219983251388219.

[23] M. Bar, R. Alagirusamy, and A. Das. Advances in natural fibre reinforced thermoplastic composite manufacturing: Effect of interface and hybrid yarn structure on composite properties. In R. Fangueiro and S. Rana, editors, *Advances in Natural Fibre Composites: Raw Materials, Processing and Analysis*, pages 99–118. Springer International Publishing, 2018. doi: 10.1007/978-3-319-64641-1_7.

[24] P. Russo, G. Simeoli, V. Lopresto, A. Langella, and I. Papa. Environmentally friendly thermoplastic composite laminates reinforced with jute fabric. In *Advances in Natural Fibre Composites*, pages 119–126. Springer, 2018. doi: 10.1007/978-3-319-64641-1_8.

[25] J. De Prez, A. W. Van Vuure, J. Ivens, G. Aerts, and I. Van de Voorde. Evaluation of the extraction efficiency of enzymatically treated flax fibers. In R. Fangueiro and S. Rana, editors, *Advances in Natural Fibre Composites: Raw Materials, Processing and Analysis*, pages 37–50. Springer International Publishing, 2018. doi: 10.1007/978-3-319-64641-1_4.

[26] H. M. Khanlou, P. Woodfield, W. Hall, and J. Summerscales. Effect of time-dependent process temperature variation during manufacture of natural-fibre composites. In R. Fangueiro and S. Rana, editors, *Advances in Natural Fibre Composites: Raw Materials, Processing and Analysis*, pages 61–68. Springer International Publishing, 2018. doi: 10.1007/978-3-319-64641-1_6.

[27] Arkadiusz Kloziński, Paulina Jakubowska, Adam Piasecki, and Dorota Czarnecka-Komorowska. The multiple recycling process of polypropylene composites with glass fiber in terms of grinding efficiency and selected properties of recirculated products. *Polymers*, 17(19):2625, 2025. doi: 10.3390/polym17192625. URL `https://www.mdpi.com/2073-4360/17/19/2625`.

[28] Elif Sahiner and Yasin Altin. In-process recycling of 35% glass fiber-reinforced polyamide 6,6 runners: Effects on thermomechanical properties and viability for diesel injector socket production. *Polymers*, 17(19):2569, 2025. doi: 10.3390/polym17192569. URL `https://doi.org/10.3390/polym17192569`.

[29] Xianhui Zhao, Katie Copenhaver, Lu Wang, Matthew Korey, Douglas J. Gardner, Kai Li, Meghan E. Lamm, Vidya Kishore, Samarthya Bhagia, Mehdi Tajvidi, Halil Tekinalp, Oluwafemi Oyedeji, Sanjita Wasti, Erin Webb, Arthur J. Ragauskas, Hongli Zhu, William H. Peter, and Soydan Ozcan. Recycling of natural fiber composites: Challenges and opportunities. *Resources, Conservation and Recycling*, 177:105962, 2022. doi: 10.1016/j.resconrec.2021.105962. URL `https://www.sciencedirect.com/science/article/abs/pii/S0921344921005711`.

[30] A. J. Onyianta and R. Williams. The use of sedimentation for the estimation of aspect ratios of charged cellulose nanofibrils. In R. Fangueiro and S. Rana, editors, *Advances in Natural Fibre Composites*, pages 195–204. Springer, 2018. doi: 10.1007/978-3-319-64641-1_15.

[31] C. Poilâne, F. Gehring, H. Yang, and F. Richard. About nonlinear behavior of unidirectional plant fibre composite. In R. Fangueiro and S. Rana, editors, *Advances in Natural Fibre Composites: Raw Materials, Processing and Analysis*, pages 69–80. Springer International Publishing, 2018. doi: 10.1007/978-3-319-64641-1_9.

[32] A. Jabbar, J. Militký, A. Ali, and M. U. Javed. Investigation of mechanical and thermomechanical properties of nanocellulose coated jute/green epoxy composites. In R. Fangueiro and S. Rana, editors, *Advances in Natural Fibre Composites*, pages 175–194. Springer, 2018. doi: 10.1007/978-3-319-64641-1_14.

[33] S. Quintero, A. Porras, C. Hernandez, and A. Maranon. The response of manicaria saccifera natural fabric reinforced pla composites to impact by fragment simulating projectiles. In R. Fangueiro and S. Rana, editors, *Advances in Natural Fibre Composites: Raw Materials, Processing and Analysis*, pages 89–98. Springer International Publishing, 2018. doi: 10.1007/978-3-319-64641-1_12.

[34] K. Korniejenko, M. Łach, and J. Mikuła. Mechanical properties of raffia fibres reinforced geopolymer composites. In R. Fangueiro and S. Rana, editors, *Advances in Natural Fibre Composites*, pages 135–144. Springer, 2018. doi: 10.1007/978-3-319-64641-1_11.

[35] M. Cihan, J. I. R. Blake, and A. Sobey. Investigating the transient response of hybrid composite materials reinforced with flax and glass fibres. In R. Fangueiro and S. Rana, editors, *Advances in Natural Fibre Composites: Raw Materials, Processing and Analysis*, pages 81–88. Springer International Publishing, 2018. doi: 10.1007/978-3-319-64641-1_10.

[36] Kamrun N. Keya, Nasrin A. Kona, and Ruhul Amin Khan. Comparative study of jute, okra and pineapple leaf fiber reinforced polypropylene based composite. *Advanced Materials Research*, 1155:29–40, 2019. doi: 10.4028/www.scientific.net/AMR.1155.29.

[37] S. Rana, S. Parveen, S. Pichandi, and R. Fangueiro. Development and characterization of microcrystalline cellulose based novel multi-scale biocomposites. In R. Fangueiro and S. Rana, editors, *Advances in Natural Fibre Composites: Raw Materials, Processing and Analysis*, pages 159–174. Springer International Publishing, 2018. doi: 10.1007/978-3-319-64641-1_13.

[38] M. Brümmer, M. P. Sáez-Pérez, and J. D. Suárez. Hemp-clay concretes for environmental building—features that attribute to drying, stabilization with lime, water uptake and mechanical strength. In R. Fangueiro and S. Rana, editors, *Advances in Natural Fibre Composites: Raw Materials, Processing and Analysis*, pages 249–267. Springer International Publishing, 2018. doi: 10.1007/978-3-319-64641-1_19.

[39] E. P. Montacchini, M. A. Muñoz Veloza, R. Pennacchio, L. Savio, and S. Tedesco. The use of hemp in building components for the development of a modular house in

a rural area of cauca—colombia. In R. Fangueiro and S. Rana, editors, *Advances in Natural Fibre Composites: Raw Materials, Processing and Analysis*, pages 267–289. Springer International Publishing, 2018. doi: 10.1007/978-3-319-64641-1_20.

[40] E. Stenvall, M. E. Hoque, S. Pugalendhi, and M. Murshed. Exploring 3d printed biomimetic structures using natural fiber-based biocomposites. *Materials Today: Proceedings*, 62:3699–3706, 2022. doi: 10.1016/j.matpr.2022.03.689.

[41] S. Naeem, S. Q. Z. Gilani, V. Baheti, J. Wiener, J. Militky, S. Javed, A. Ali, Z. Javed, and S. Zameer ul Hassan. Electrical conductivity of pla films reinforced with carbon nano particles from waste acrylic fibers. In R. Fangueiro and S. Rana, editors, *Advances in Natural Fibre Composites*, pages 205–230. Springer, 2018. doi: 10.1007/978-3-319-64641-1_16.

[42] Abdul Jabbar. Literature review. In *Sustainable Jute-Based Composite Materials*, SpringerBriefs in Applied Sciences and Technology, pages 5–41. Springer, Cham, 2017. doi: 10.1007/978-3-319-65457-7_2.

[43] M. Mohammed, A. J. A. M. Jawad, A. M. Mohammed, J. K. Oleiwi, T. Adam, A. F. Osman, and M. Jaafar. Challenges and advancement in water absorption of natural fiber-reinforced polymer composites. *Polymer Testing*, 124:108083, 2023. doi: 10.1016/j.polymertesting.2023.108083.

[44] Rafaela Q. C. Melo, Marcus V. Lia Fook, and Antonio G. B. Lima. Non-fickian moisture absorption in vegetable fiber reinforced polymer composites: The effect of the mass diffusivity. *Polymers*, 13(5):761, 2021. doi: 10.3390/polym13050761.

[45] Behnaz Hassanpour and Vistasp M. Karbhari. Characteristics and models of moisture uptake in fiber-reinforced composites: A topical review. *Polymers*, 16(16):2265, 2024. doi: 10.3390/polym16162265.

[46] K. L. Pickering, M. G. A. Efendy, and T. M. Le. A review of recent developments in natural fibre composites and their mechanical performance. *Composites Part A: Applied Science and Manufacturing*, 83:98–112, 2016. doi: 10.1016/j.compositesa.2015.08.038.

[47] K. Z. M. Abdul Motaleb, Md Shariful Islam, and Mohammad B. Hoque. Improvement of physicomechanical properties of pineapple leaf fiber reinforced composite. *International Journal of Biomaterials*, 2018:7384360, 2018. doi: 10.1155/2018/7384360.

[48] Sourav Saha, Sreekanta Das, and Md Zillur Rahman. Hybridization in natural fiber

composites: Enhanced performance and sustainability. *Composites Part B: Engineering*, 308:112986, 2026. doi: 10.1016/j.compositesb.2025.112986.

[49] N. M. Nurazzi, M. R. M. Asyraf, S. F. Athiyah, S. S. Shazleen, S. A. Rafiqah, M. M. Harussani, S. H. Kamarudin, M. R. Razman, M. Rahmah, E. S. Zainudin, R. A. Ilyas, et al. A review on mechanical performance of hybrid natural fiber polymer composites for structural applications. *Polymers*, 13(13):2170, 2021. doi: 10.3390/polym13132170.

[50] M. J. Suriani, R. A. Ilyas, M. Y. M. Zuhri, A. Khalina, M. T. H. Sultan, S. M. Sapuan, C. M. Ruzaidi, F. N. Wan, F. Zulkifli, M. M. Harussani, M. A. Azman, F. S. M. Radzi, and Shubham Sharma. Critical review of natural fiber reinforced hybrid composites: Processing, properties, applications and cost. *Polymers*, 13(20): 3514, 2021. doi: 10.3390/polym13203514.

[51] M. D. H. Beg and K. L. Pickering. Reprocessing of wood fibre reinforced polypropylene composites. part i: Effects on physical and mechanical properties. *Composites Part A: Applied Science and Manufacturing*, 39(7):1091–1100, 2008. doi: 10.1016/j.compositesa.2008.04.013.

[52] S. Mortazavian and A. Fatemi. Effects of fiber orientation and anisotropy on tensile strength and elastic modulus of short fiber reinforced polymer composites. *Composites Part B: Engineering*, 72:116–129, 2015. doi: 10.1016/j.compositesb.2014.11.041.

[53] A. N. Oumer and Othman Mamat. A study of fiber orientation in short fiber-reinforced composites with simultaneous mold filling and phase change effects. *Composites Part B: Engineering*, 43(3):1087–1094, 2012. doi: 10.1016/j.compositesb.2012.01.043.

[54] A. Dupuis, L. Silva, D. Geoghegan, F. Chabert, L. Gautier, and V. Bounor-Legaré. Fiber orientation and concentration in an injection-molded ethylene-propylene copolymer reinforced by hemp. *Polymers*, 12(12):2771, 2020. doi: 10.3390/polym12122771.

# A | Appendix A

## A.1. Materials

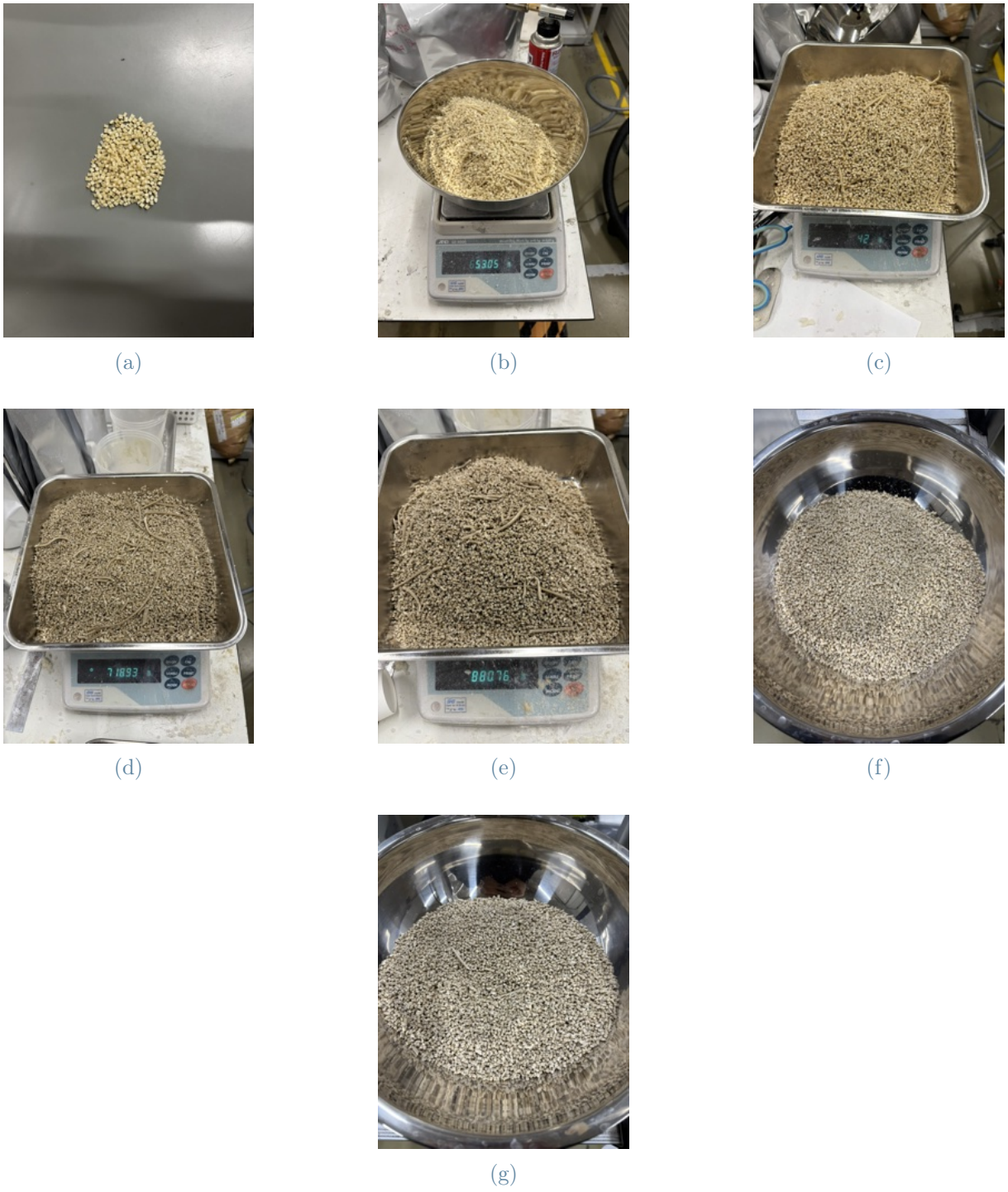

(a) (b) (c) (d) (e) (f) (g)

Figure A.1: Virgin materials pellet: (a) PF15(1); (b) PF15(2); (c) PF30; (d) JF15; (e) JF30; (f) HYB15; (g) HYB30.

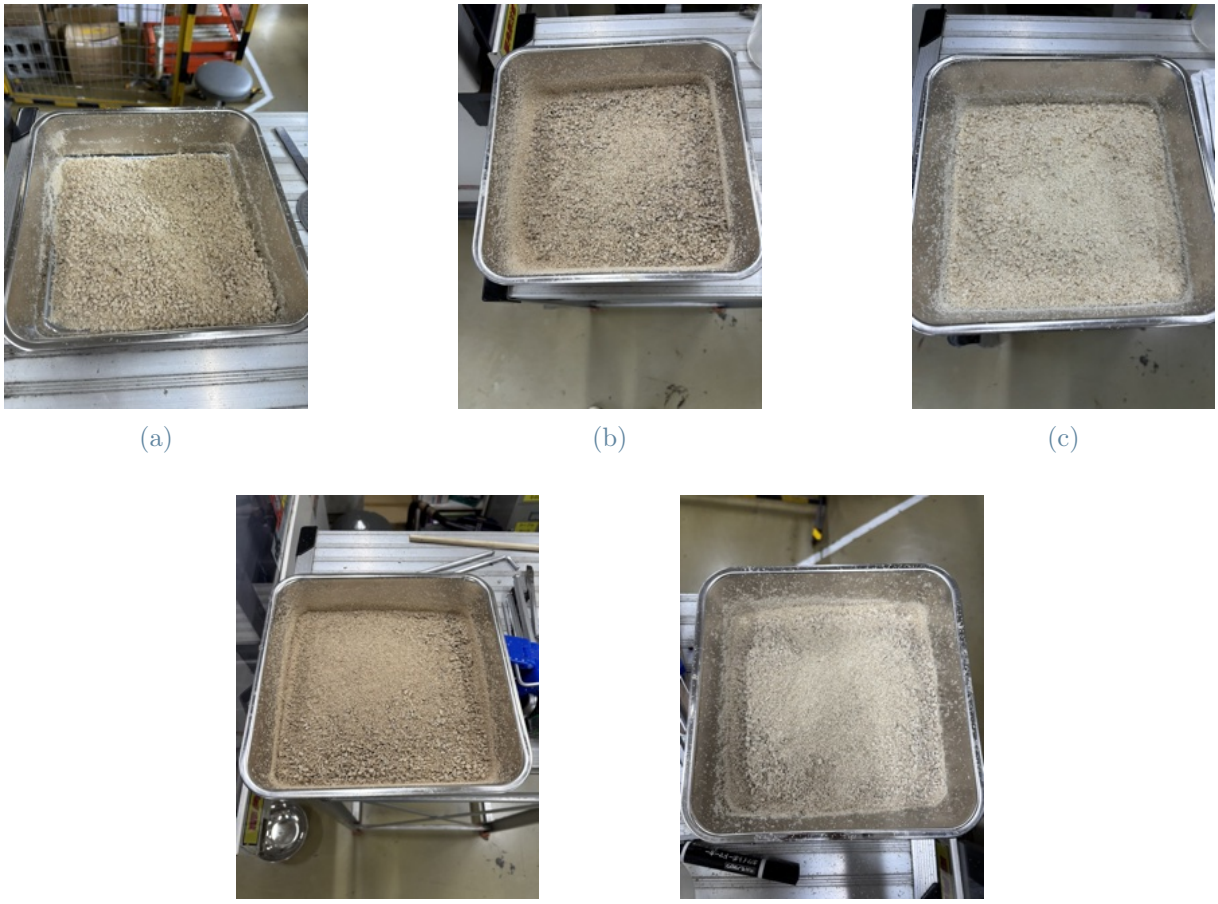

(a) (b) (c)

(d) (e)

Figure A.2: Recycled materials pellet (HYB15R not available): (a) PF15(2)R; (b) PF30R; (c) JF15R; (d) JF30R; (e) HYB30R.

## A.2. Test results

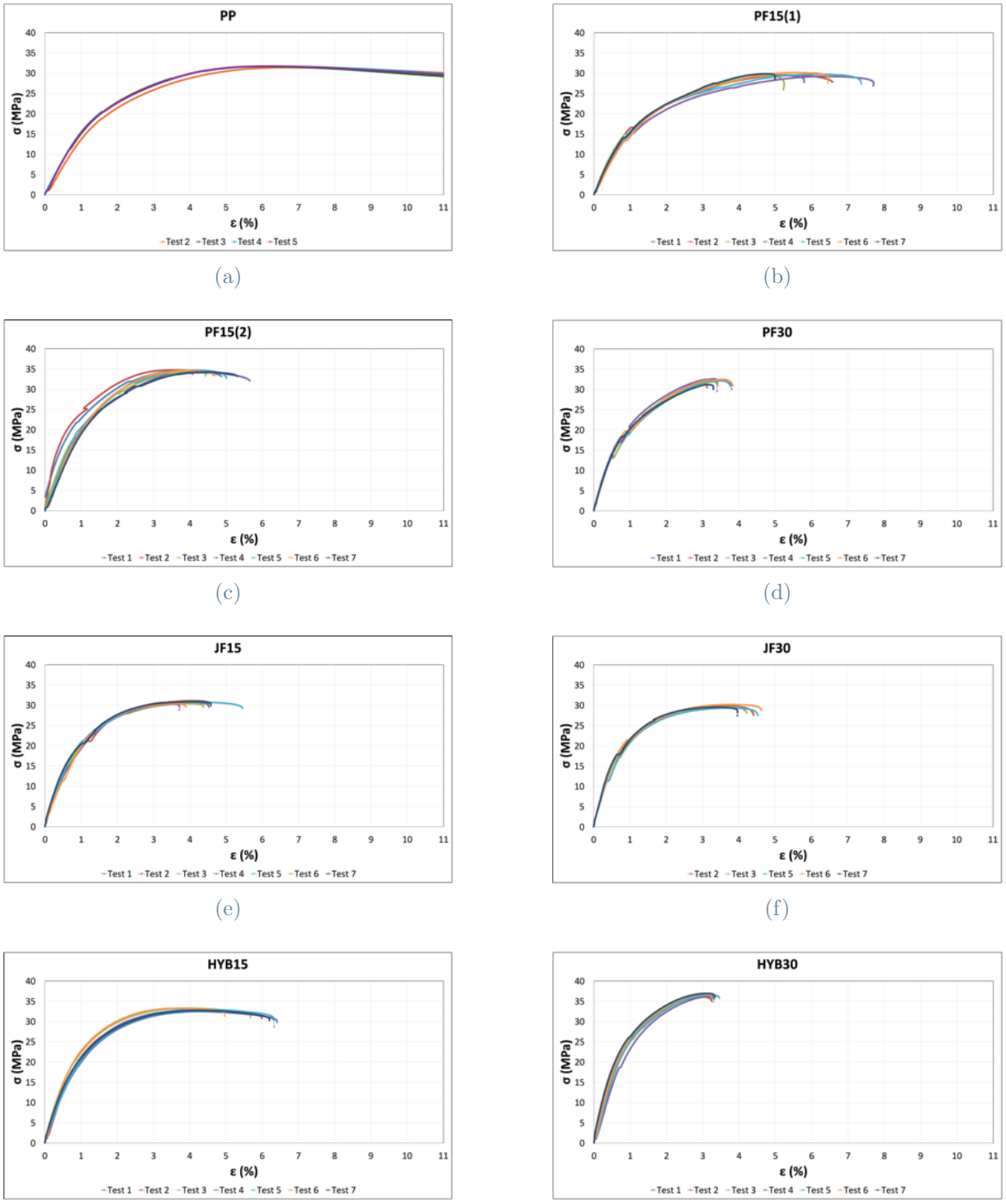


Figure A.3: Tensile stress-strain curves of virgin materials.

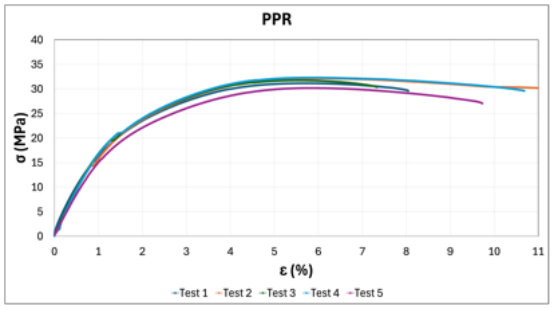


(a)

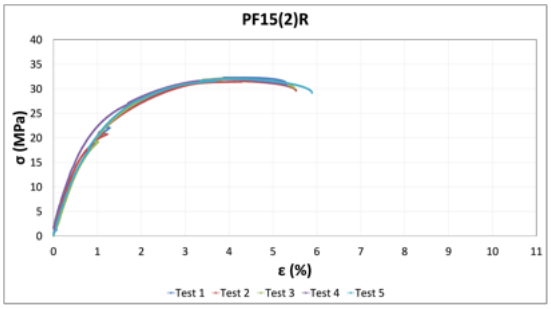


(b)

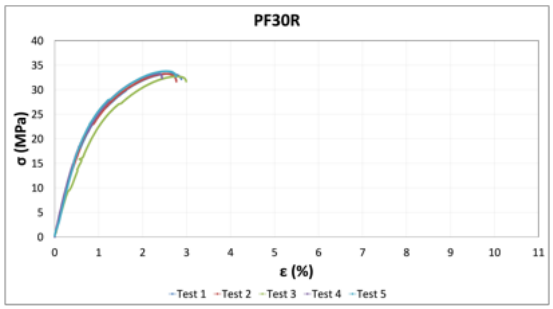


(c)

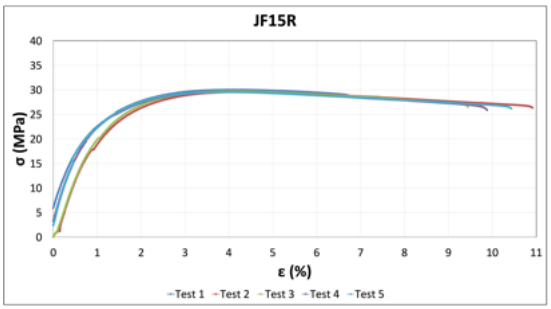


(d)

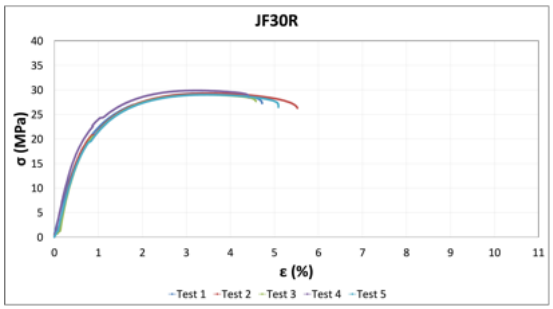


(e)

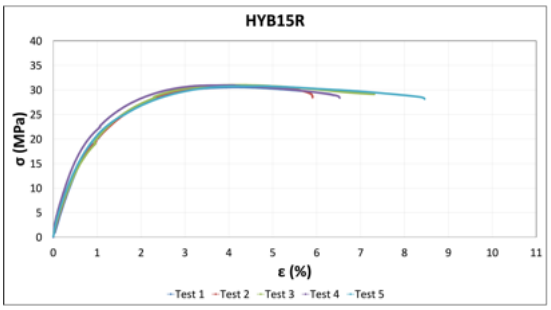


(f)

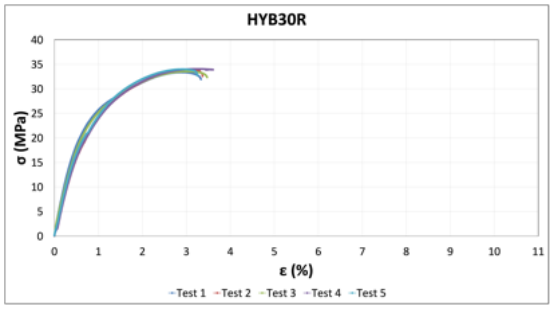


(g)

Figure A.4: Tensile stress-strain curves of recycled materials.

## A.3. SEM

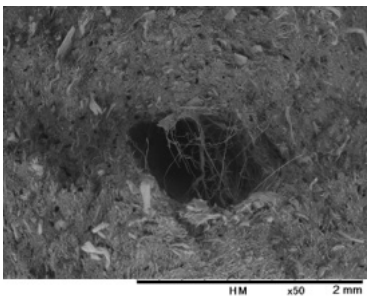


(a) PF30, impact, x50 (test 4).

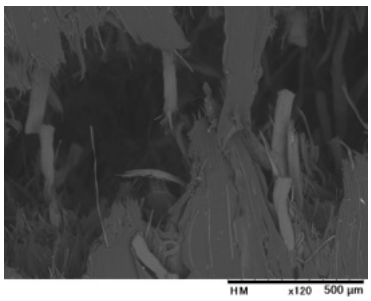


(b) PF15(2), bending, x120 (test 2).

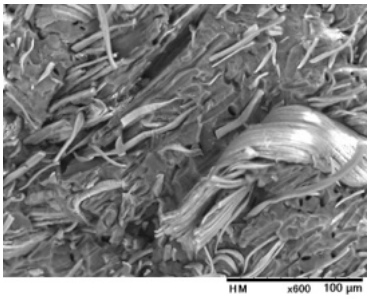


(c) PF30, impact, x600 (test 4).

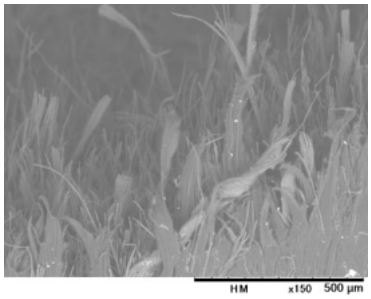


(d) PF30, bending, x800 (test 1).

Figure A.5: Appendix SEM micrographs for PF-based virgin composites (impact and bending).

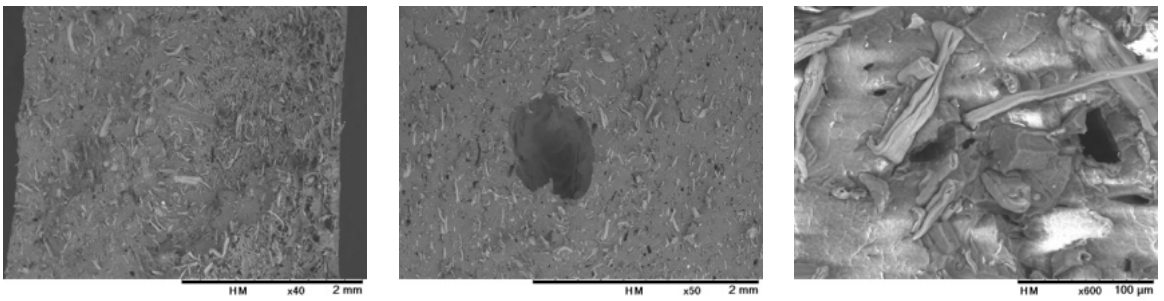


(a) JF15, bending, x40 (test 4). (b) JF15, impact, x50 (test 5). (c) JF15, impact, x600 (test 5).

(d) JF30, bending, x100 (test 2). (e) JF30, impact, x50 (test 3). (f) JF30, impact, x500 (test 3).

Figure A.6: Appendix SEM micrographs for JF-based virgin composites (impact and bending).

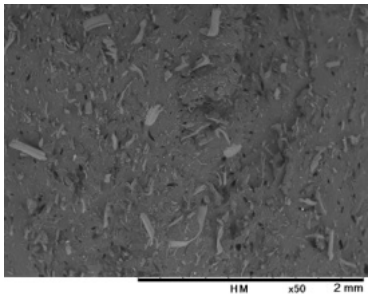


(a) HYB15, impact, x50 (test 7).

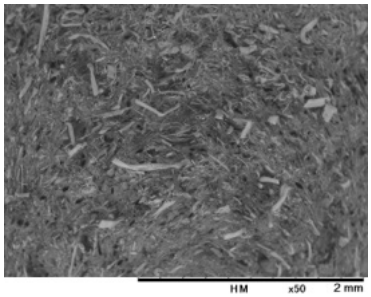


(b) HYB30, impact, x50 (test 5).

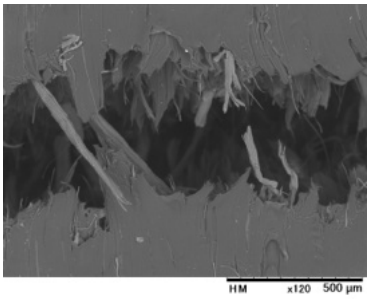


(c) HYB15, bending, x120 (test 4).

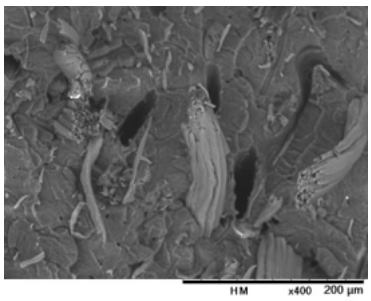


(d) HYB15, impact, x400 (test 7).

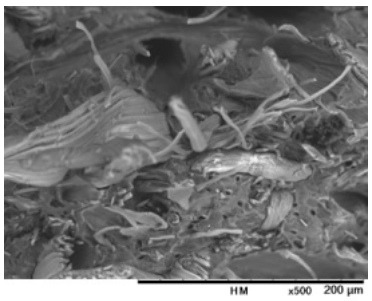


(e) HYB30, impact, x500 (test 5).

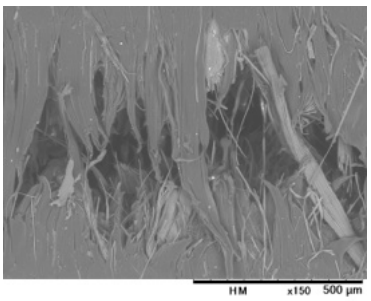


(f) HYB30, bending, x150 (test 5).

Figure A.7: Appendix SEM micrographs for HYB-based virgin composites (impact and bending).

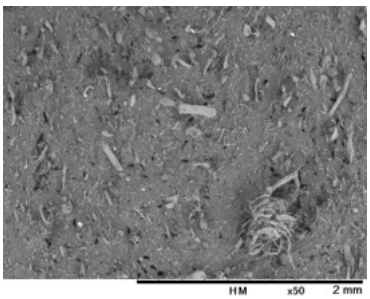


(a) PF15(2)R, impact, x50 (test 1).

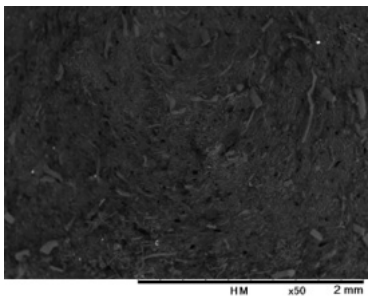


(b) PF30R, impact, x50 (test 3).

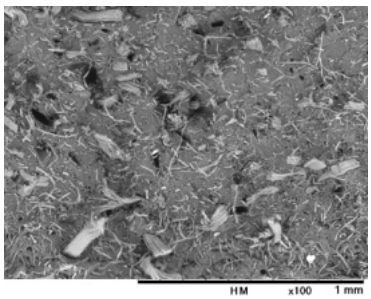


(c) PF15(2)R, impact, x100 (test 1).

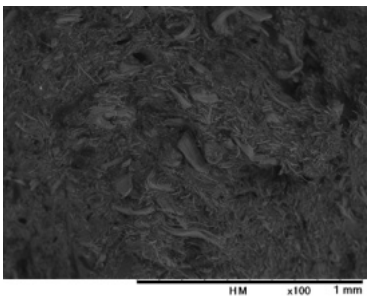


(d) PF30R, tensile, x100 (test 3).

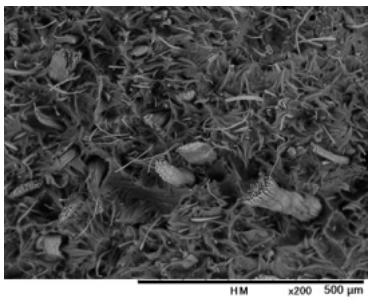


(e) PF15(2)R, tensile, x200 (test 4).

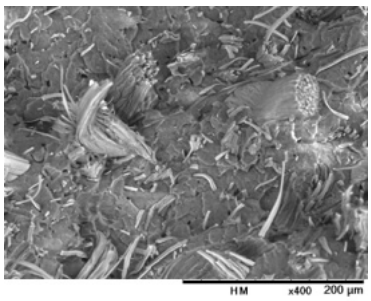


(f) PF15(2)R, impact, x400 (test 1).

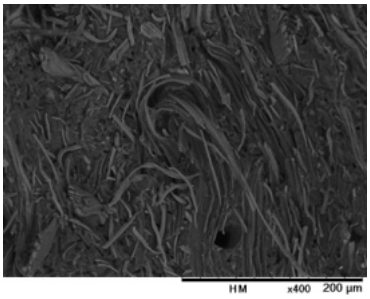


(g) PF30R, impact, x400 (test 3).

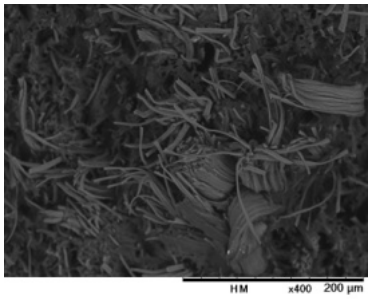


(h) PF30R, tensile, x400 (test 3).

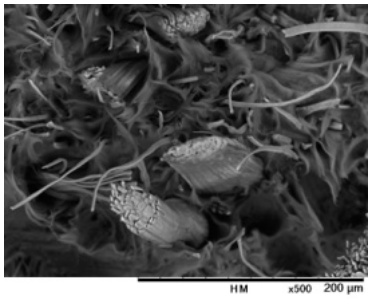


(i) PF15(2)R, tensile, x500 (test 4).

Figure A.8: Appendix SEM micrographs for PF-based recycled composites (impact and tensile).

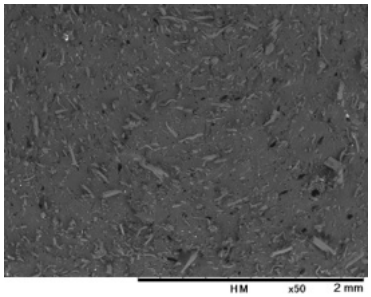


(a) JF15R, impact, x50 (test 3).

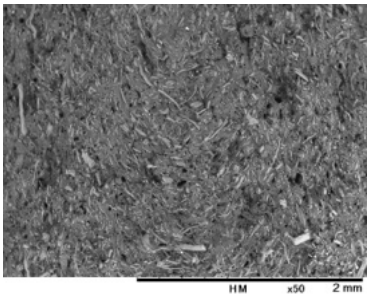


(b) JF30R, impact, x50 (test 3).

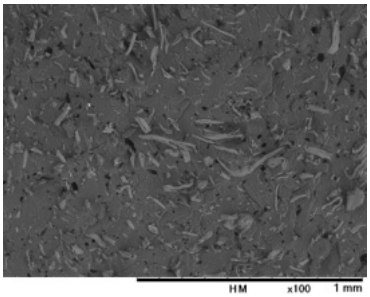


(c) JF15R, impact, x100 (test 3).

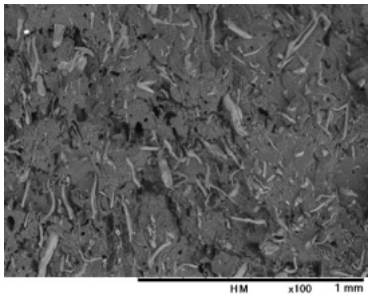


(d) JF15R, tensile, x100 (test 1).

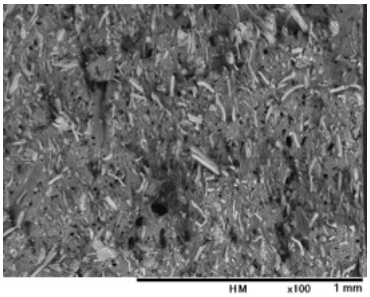


(e) JF30R, impact, x100 (test 3).

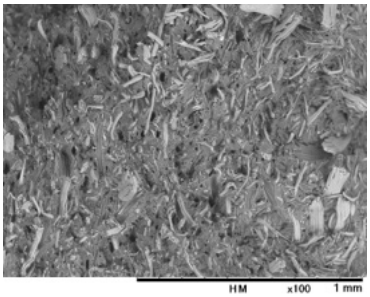


(f) JF30R, tensile, x100 (test 3).

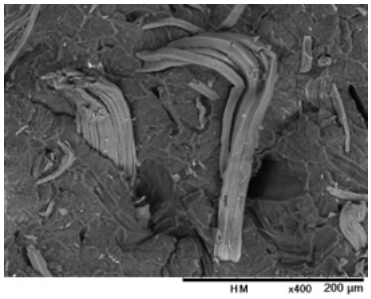


(g) JF15R, impact, x400 (test 3).

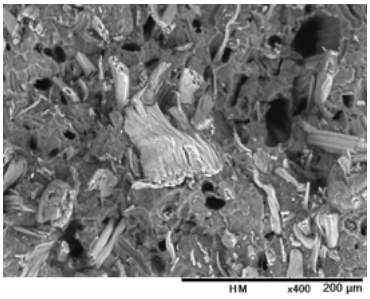


(h) JF30R, impact, x400 (test 3).

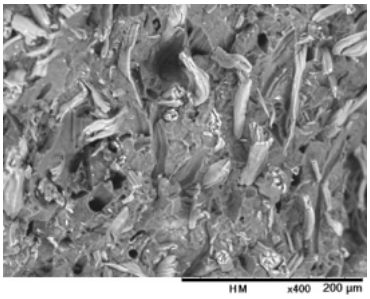


(i) JF30R, tensile, x400 (test 3).

Figure A.9: Appendix SEM micrographs for JF-based recycled composites (impact and tensile).

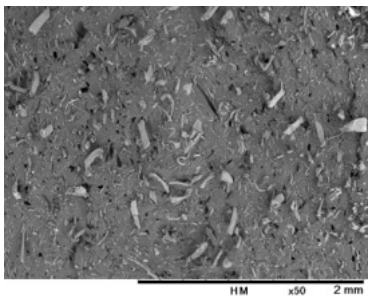


(a) HYB15R, impact, x50 (test 5).

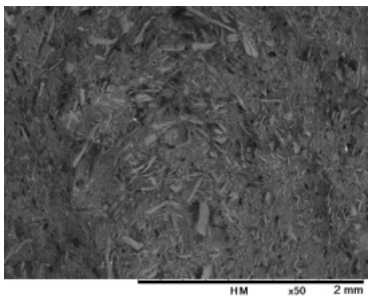


(b) HYB30R, impact, x50 (test 2).

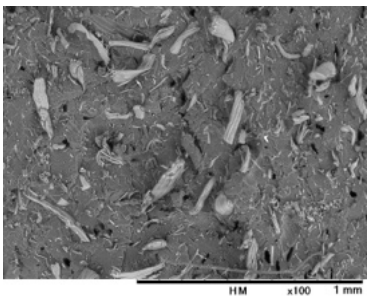


(c) HYB15R, impact, x100 (test 5).

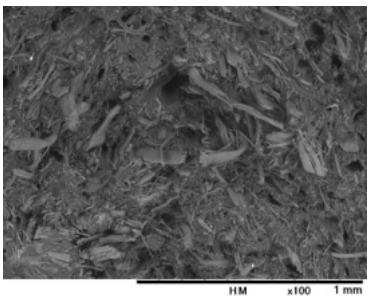


(d) HYB30R, impact, x100 (test 2).

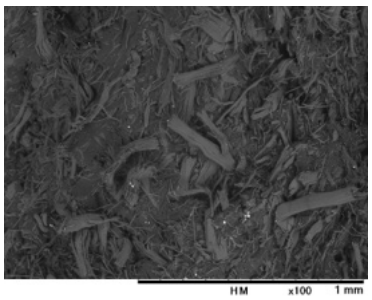


(e) HYB30R, tensile, x100 (test 5).

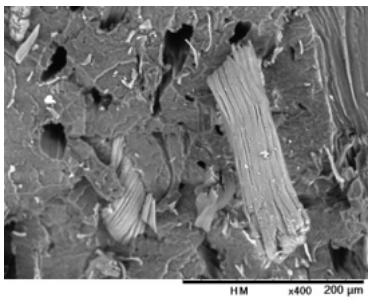


(f) HYB15R, impact, x400 (test 5).

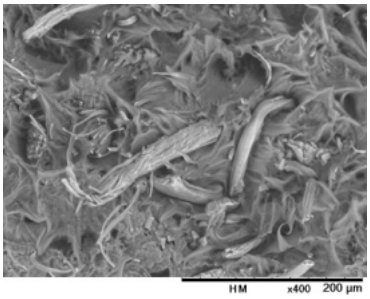


(g) HYB15R, tensile, x400 (test 4).

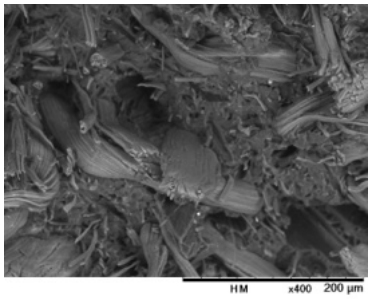


(h) HYB30R, impact, x400 (test 2).

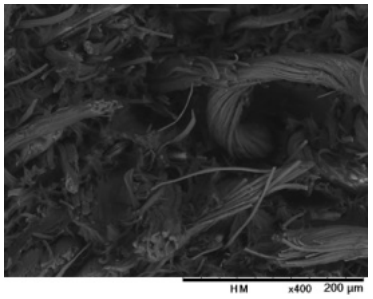


(i) HYB30R, tensile, x400 (test 5).

Figure A.10: Appendix SEM micrographs for HYB-based recycled composites (impact and tensile).

# List of Figures

# List of Tables